Concept Design of a Long Range AUV Propulsion System with an Onboard Electrical Generator

by

Jason Eric Poulin

B. Eng. Mechanical Engineering
Royal Military College of Canada, 2006

SUBMITTED TO THE DEPARTMENT OF MECHANICAL ENGINEERING IN PARTIAL FULFILLMENT OF THE REQUIREMENTS FOR THE DEGREES OF

MASTER OF SCIENCE IN NAVAL ARCHITECTURE AND MARINE ENGINEERING
AND
MASTER OF SCIENCE IN MECHANICAL ENGINEERING
AT THE
MASSACHUSETTS INSTITUTE OF TECHNOLOGY

June 2012

Signature of Author .....
Autonomous Underwater Vehicle Lab
Naval Construction & Engineering Program (2N)
May 11, 2012

Certified by .....
Chryssostomos Chryssostomidis
Doherty Professor of Ocean Science and Engineering
Department of Mechanical Engineering
Director, MIT Sea Grant College Program
Thesis Supervisor

Accepted by .....
Professor David E. Hardt
Chairman, Departmental Committee on Graduate Students
Department of Mechanical Engineering

(This page intentionally left blank)

Concept Design of a Long Range AUV Propulsion System with an Onboard Electrical Generator

by

Jason Eric Poulin

Submitted to the Department of Mechanical Engineering
on May 11, 2012, in Partial Fulfillment of the Requirements for the Degrees of Master of Science in Naval Architecture and Marine Engineering and Master of Science in Mechanical Engineering

ABSTRACT

Automated Underwater Vehicle (AUV) Technology has come a long way in the past decade. Due to advances in batteries and telecommunications, unmanned underwater vehicles no longer require a tether to a mother ship for power, command and control. AUV endurance and range, however, are still limited by the size and capacity of the onboard batteries. Attempts to overcome this limitation, with studies utilizing fuel and solar cells were developed to augment the stored energy onboard. This thesis examines the viability of utilizing an internal combustion engine as an onboard generator to recharge the batteries in during the mission in order to increase both range and endurance. Working in conjunction with the MIT Rapid Development Group, an onboard generating system was developed utilizing a gasoline generator. This system was incorporated into in a clean sheet propulsion system design of a long range AUV propulsion system. Maximum efficiency of all components was stressed at every point in the design process in order to decrease the propulsion system power requirements. Advanced lithium-ion battery systems were also investigated in order to find a system that balanced maximal energy storage with low recharge time. The study resulted in a theoretical AUV propulsion system that could traverse distances that span the Atlantic Ocean at a speed of 2 kts. It is believed that this type of AUV would be ideal for both scientific research and military applications.

Thesis Supervisor: Chryssostomos Chryssostomidis
Title: Doherty Professor of Ocean Science and Engineering
Department of Mechanical Engineering
Director, MIT Sea Grant College Program

Acknowledgements

I would like to thank Dr. Chryssostomos Chyssostomidis for his time as Thesis Supervisor. His knowledge and experience in the field of Autonomous Underwater Vehicles was a great benefit throughout the design process. I would also like to thank him for giving me the freedom to go out and develop this project on my own with little interference.

The MIT Rapid Development Team, especially Dr. Doug Hart and Dan Dorsch, for allowing me to utilize their generator system design and to allow me to interrupt their important work to ask as many questions as possible.

Brenden Epps at MIT Sea Grant for all his help in propeller design, especially teaching me the intricacies of OpenProp and having the patience to ensure I developed a reasonable propeller design.

Seth Newberg at MIT Sea Grant for his help answering AUV design questions and for his work converting drawings into different formats.

Dr. James Kirtley for teaching me the basics of Brushless DC Motors

Steve Carkner at Panacis Inc, for all his help teaching me the complexities of lithium battery theory and providing me the details of a possible battery system when no other company would answer my messages.

The Royal Canadian Navy for giving me the time and opportunity to pursue graduate studies at MIT.

Finally and most importantly, I would like to thank my wife Victoria and my daughter Sophie for their patience and understanding while I developed this thesis. Without their constant support, this project would not be completed.

Table of Contents

List of Figures

List of Tables

1 Introduction

The field of underwater vehicles has grown incredibly since the launching of the *TURTLE* by David Bushnell in 1775. A one-person, egg shaped submarine, it was used as a weapon against the British in New York Harbor during the Revolutionary War (Blidberg, 2001). Since this time, submersible vehicles, both manned and unmanned, have been developed for numerous applications.

In the field of Unmanned Underwater Vehicles (UUV), there are two different categories. The first is the Remotely Operated Vehicle (ROV), a tethered submersible connected to a mother ship used for operations that are deemed unsafe or impractical for human divers. Using this tether, the mother ship can provide power to the vehicle as well as communicate with the vehicle in real time. This set up allows for greater flexibility in design and the ability to incorporate power intensive equipment such as high-resolution cameras, saws, torches, etc. since a limited onboard power supply is not required. Since the ROV is under constant human control, difficult missions requiring judgment can be accomplished. ROVs have recently been in the spotlight during the Deepwater Horizon disaster. ROVs were used to do much of repair work on the burst oil riser and were able to cap the well. ROVs do have their drawbacks however. The reliance on a tether severely limits their range and it takes considerable coordination to use multiple ROVs for the same job in order to not tangle the tethers.

Figure 1.1: Oceaneering MILLENIUM ROV (Oceaneering, 2011)

The other major type of UUV used today is the Autonomous Underwater Vehicle (AUV). The main difference between an AUV and a ROV is that there is no tether, leading to much more autonomy for the vehicles. The lack of a tether also leads to some disadvantages for the AUV, specifically the fact that it must carry its power supply onboard and that the lack of communication with a human operator leads to the requirement for a much more complex control system onboard.

The history of Autonomous Underwater Vehicles can be traced all the way back to the development of the torpedo, specifically the Automobile "Fish" Torpedo developed by Robert Whitehead in Austria in 1866 (Vijay, n.d.). This early vehicle drove on compressed air and could travel at 3 m/s with a range of 700 m. Most experts in the field believe that the first developments of what we consider an AUV occurred in the 1970's. At this time several institutions started developing testbeds for testing and improving AUVs and related technologies. This included the University of Washington and their UARS and SPURV AUVs developed to operate in Arctic waters and the University of New Hampshire's Marine Systems Engineering Laboratory (now called the Autonomous Undersea Systems Institute or AUSI) EAVE vehicle developed in conjunction with the United States Navy (Blidberg, 2001).

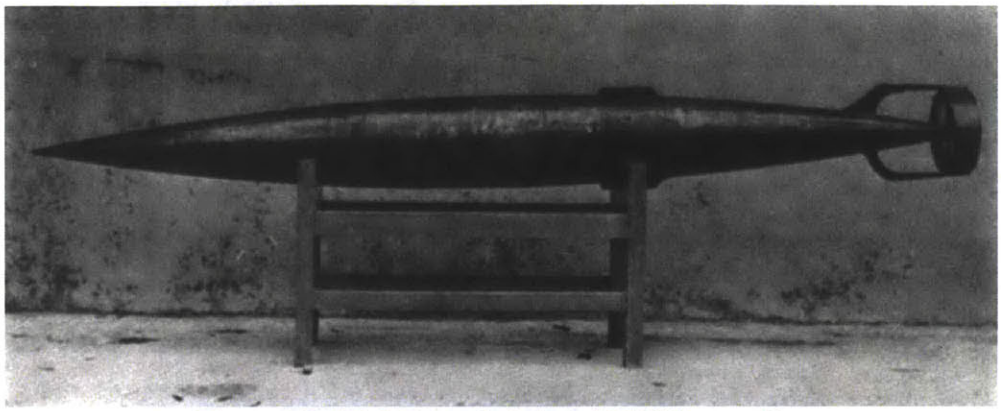

Figure 1.2: "Fish Torpedo" circa 1871(Vijay, n.d.)

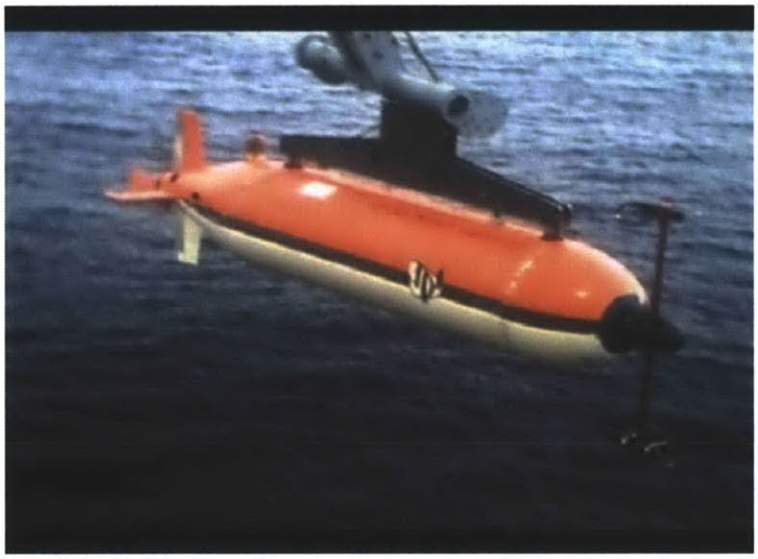

Figure 1.3: SPURV AUV developed by the University of Washington's Applied Physics Laboratory (AUVAC, 2011)

MIT has long been involved in AUV development. MIT's Sea Grant AUV Lab was started in 1989 with the goal of developing lightweight, low priced AUVs that could dive to depths of 6000 m. The lab quickly garnered acclaim for their ODYSSEY AUVs, and have subsequently developed projects with the US Navy, the National Oceanic and Atmospheric Agency (NOAA) and other academic and commercial institutions.

Due to the technology available at the time, many of these early AUVs were primitive and had limited functionality, however advances in computing and battery technology have allowed AUVs to perform varied missions. NOAA wrote a report in

2006 highlighting current and future missions for AUVs. According to this report, AUVs are currently highly used in fisheries habitat studies, underwater geological surveys and ocean exploration. In addition to a high number of defense related applications, NOAA believes that in the future AUVs will be used for the following functions (Manley, 2006):

a. Physical Oceanography;
b. Marine Sanctuary Monitoring;
c. Homeland Security; and
d. Marine Fisheries Enforcement.

One can infer from the preceding list that future AUVs will require at least one common characteristic: endurance. Many of the missions listed above require an AUV to be launched, conduct its mission by travelling or loitering in place for days or weeks at a time and then be picked up. With advancements in battery technology and the developments of low powered sensors and communication equipment, AUVs are constantly extending their operating range and endurance.

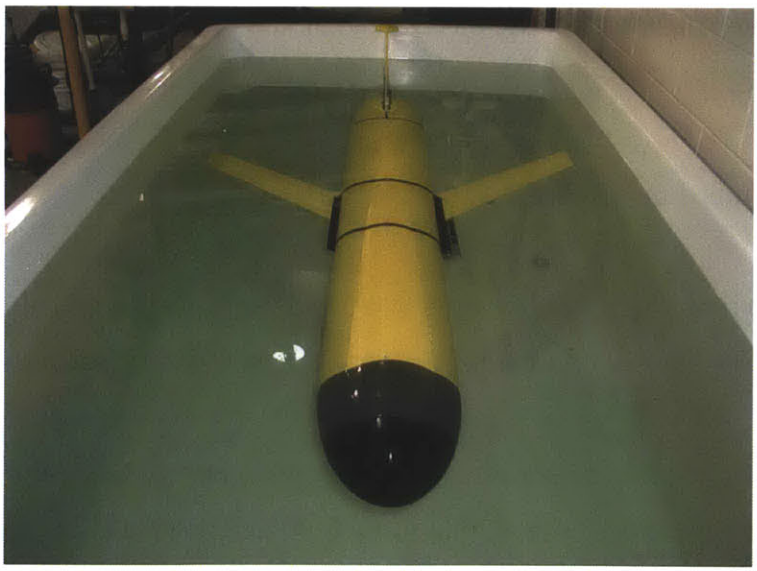

Figure 1.4: Rutgers University's SCARLET KNIGHT Glider AUV (Glenn, 2009)

One type of AUV perfectly suited for long endurance mission is the underwater glider. These vehicles do not utilize any kind of propulsion engine, but use the principles of lift to generate forward motion. This is accomplished by employing hydrofoils and a small pump in the nose of the vehicle. The pump adds or removes water from the nose of the AUV, thereby making it more or less buoyant. This raises or lowers the nose of the vehicle, thereby changing the angle of attack of the hydrofoils, creating lift and forward motion. The lack of propulsion motor allows for extremely low power consumption, thus allowing for greater range and endurance. Rutgers University's Coastal Ocean Observation Lab developed the SCARLET KNIGHT glider, which was able to conduct a transatlantic voyage in 2009. It travelled approximately 7400 km in 221 days utilizing approximately 8 kWh of battery power (Glenn, 2009). There are drawbacks to using gliders for long endurance missions. The main problem with gliders is that they are very slow vehicles. Using the numbers described above, SCARLET KNIGHT travelled on average at only 0.39 m/s (0.75 kts). The other issue is that since they have large hydrofoils, they can be subjected to undersea currents that easily take them off course.

There have been attempts in the past few years do design more standard AUVs for long endurance missions. The Monterey Bay Aquarium Research Institute developed the TETHYS AUV in 2010 for such a mission. TETHYS was designed for two separate missions (Bellingham et al., 2010):

a. Supporting a payload load of 8 W at a speed of 1 m/s for 1000 km; and
b. Supporting a payload load of 1 W at a speed of 0.5 m/s for 4000 km.

To achieve this mission, all aspects of the design were optimized for maximum efficiency and operational range, including hullform optimization and drivetrain optimization. There is one limiting factor on endurance for all of these AUVs: battery capacity. Many AUVs have found ways to minimize power consumption, but their endurance is still limited by the amount of battery power installed onboard.

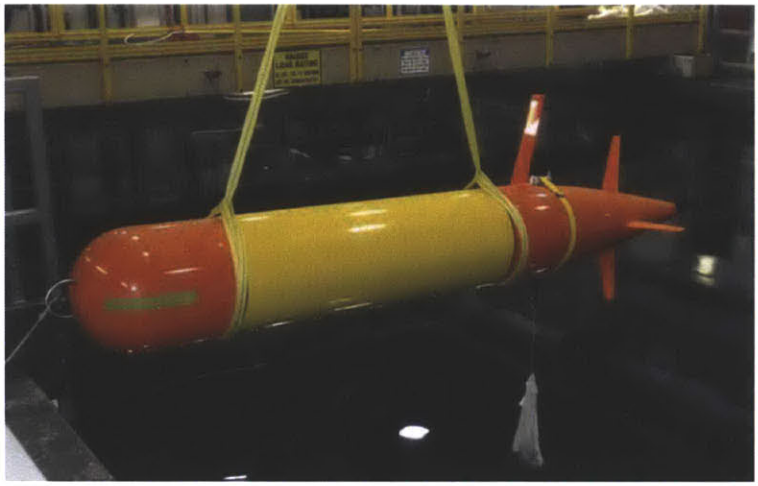

Figure 1.5: MBARI's TETHYS Long Distance AUV

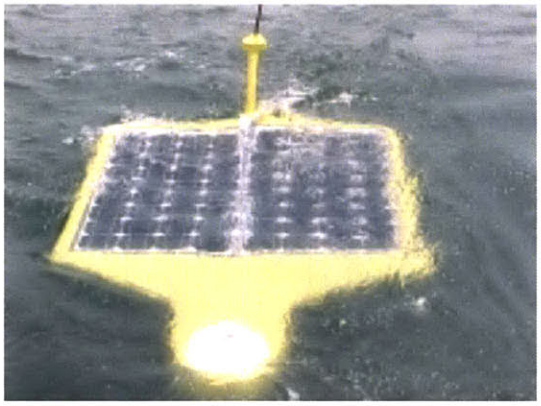

Figure 1.6: Falmouth Scentific Inc. SAUV (Jalbert et al., 2003)

In order to overcome this limitation, there have been a few different approaches. Falmouth Scientific Inc., for example, has developed the Solar Powered AUV (SAUV). SAUV carries a limited amount of onboard batteries but has the ability to charge them during the day and conduct operations at night (Jalbert et al., 2003). Though this vessel has great endurance, it cannot conduct extended missions below the ocean surface due to the requirement for regular recharging. Another strategy for long range AUV design is the use of fuel cells for Air Independent Propulsion (AIP). The Japan Agency for Marine-Earth Science and Technology (JAMSTEC) developed the URASHIMA AUV in 2004 utilizing this technology. It was able to travel over 300 km with the use of fuel cells (Yamamoto et al., 2004). The drawback to this AUV and

fuel cell technology is the size of the vessel. URASHIMA measures over 10m in length and weighs 10 tons in air, making it difficult to build, launch and recover. Fuel cells also require hydrogen as fuel, which is an extremely volatile substance.

Studies have also been undertaken into the design and development for AUV docking systems. These systems would be able to autonomously recharge AUV battery systems while at sea, increasing the AUV's endurance. One such system was the Autonomous Ocean Sampling Network (AOSN) docking system developed by the Woods Hole Oceanographic Institute (WHOI) and MIT. This docking system stretches from a buoy on the surface all the way to the ocean floor and has a dock that allows for both data and power transfer through inductive cores (Gish, 2004). The docking system was designed for use with MIT's ODYSSEY II AUV and can be seen in figure 1.7.

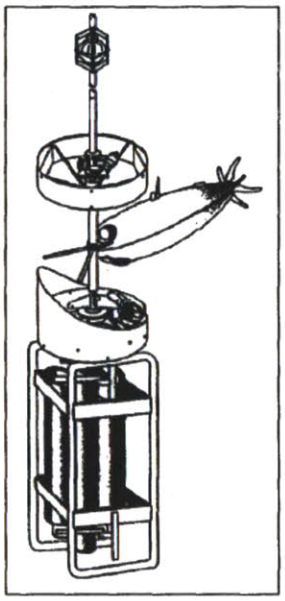

Figure 1.7: AOSN Docking System (Gish, 2004)

Universal docking stations have also been developed. The EURODOCKER, developed by the European Comission, DG XII, was one such system. It was envisioned as a garage style system where an AUV would enter a fully enclosed area for data transfer and charging.

Docking via Autonomous Surface Vehicles (ASVs) has also been investigated. The NATO Undersea Research Center (NURC) has examined the feasibility of developing a SWATH AUV that could travel at high speeds and dock with medium sized AUVs (such as FOLAGA and HYDROID) (Brizzolara, Bovio, & Federici, 2011). A concept design of such a system can be found in figure 1.8. These docking systems would have the ability to increase the endurance and range of an AUV if placed at strategic points, however each of these systems requires additional infrastructure and technology to successfully increase an AUVs range. This equates to larger funding requirements, which might not always be available.

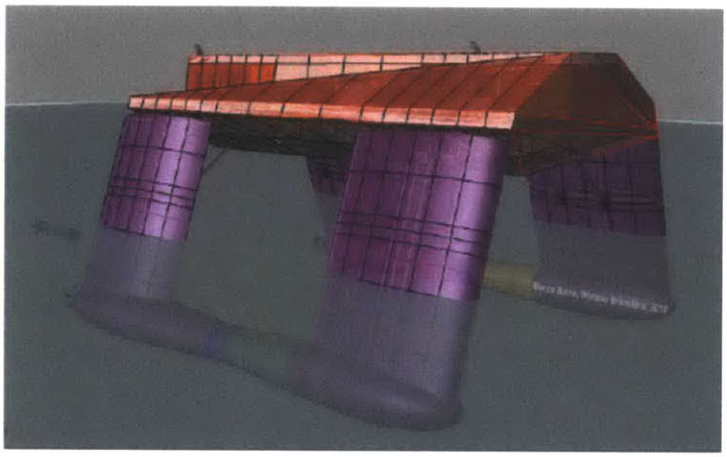

Figure 1.8: SWATH ASV designed as an AUV charging station (Brizzolara et al., 2011)

Another strategy to overcome the battery issue is to take an idea from the naval submarine world. Since almost the beginning of submarine design, an electrical generator has been installed to charge onboard batteries and to power the electric motor at the surface. With advancements in internal combustion engine design, generators are now small enough to easily fit on a small or medium sized AUV. For this project, a propulsion system for a lightweight AUV will be designed, using concepts drawn from other AUV designs and implementing an onboard internal combustion engine generator.

It was decided to name the AUV SPYROS, after Spyridon "Spyros" Louis, the winner of the first modern Olympic marathon. It seemed relevant to name a long distance AUV after a famous long distance runner and the name fits well with the tendency to use ancient Greek or Roman names for modern AUVs.

2 Design Process

Prior to commencing work on the design for a long range, rechargeable AUV, one must develop a design philosophy and strategy that will provide guidance during the design process. By developing a clear, concise approach to the process prior to starting, one has a clear path to take during the development of the design, which can avoid time-consuming mistakes. For this project, the design process as outlined in Lamb's *Ship Design and Construction* will be utilized (Lamb, 2003). Though Lamb outlines the design process for an entire complex ship, it can also be utilized smaller projects, like AUV propulsion system design.

2.1 Determination of Requirements

Prior to any design project, one must determine the customer requirements. For this project, the customer is MIT Sea Grant AUV Lab, specifically the Lab Director and thesis advisor, Dr. Chryssostomidis. After conducting meetings with Dr. Chryssostomidis, the following requirements were determined:

1. Ability to self-recharge onboard batteries;
2. Ability to travel very long distances (for this project, we will be using the requirements for the TETHYS AUV (Bellingham et al., 2010)); and
3. Minimize weight so that it could be launched with current Sea Grant assets.

2.2 Design Philosophy

According to Lamb, the Design Philosophy is "a list of desired design/ship attributes that is used in the evaluation of design alternatives" (Lamb, 2003). For this project, this list will be developed and then from this list a single overriding statement will be developed that will guide all future decisions during the design process. Utilizing

the requirements as stated earlier as well as other determined attributes, a list of ship attributes was developed below.

1. Cost effective;
2. Use of Commercial of the Shelf (COTS) material as much as possible;
3. Light Weight (Using the US Navy UUV Master Plan, wish to have SPYROS fall between the Man Portable(<100 lbs) and Light Weight (~500 lbs) (Manley, 2006));
4. Ability to recharge battery supply with onboard generator; and
5. Travel Long Distances as per TETHYS AUV Design.

Using these attributes the following Design Philosophy Statement was derived.

"Design a Cost Effective, Light Weight AUV developed with COTS Materials that will travel long distances with the use of an onboard generator to recharge onboard batteries."

2.3 Design Process

Modern Naval Vessels are extremely complex systems. The design process for these systems is not easy as there will always be many conflicting and competing requirements. Utilizing a set design process will help the designer overcome these issues and efficiently design a vessel. In the ship design industry, there are several documented methods to design a marine vehicle. In naval ship design, there are currently two methods in use, point based design and set-based design.

Point based design is the traditional method historically used by naval architects. Also known as the design spiral, it was first described in depth by MIT Professor J. Harvey Evans. The design spiral has the designer start with an initial concept of the ship design and then has the designer sequentially go through every aspect of

design in a spiral fashion. After several iterations through the cycle, the designer will have a complete ship design. An example of a design spiral can be found below.

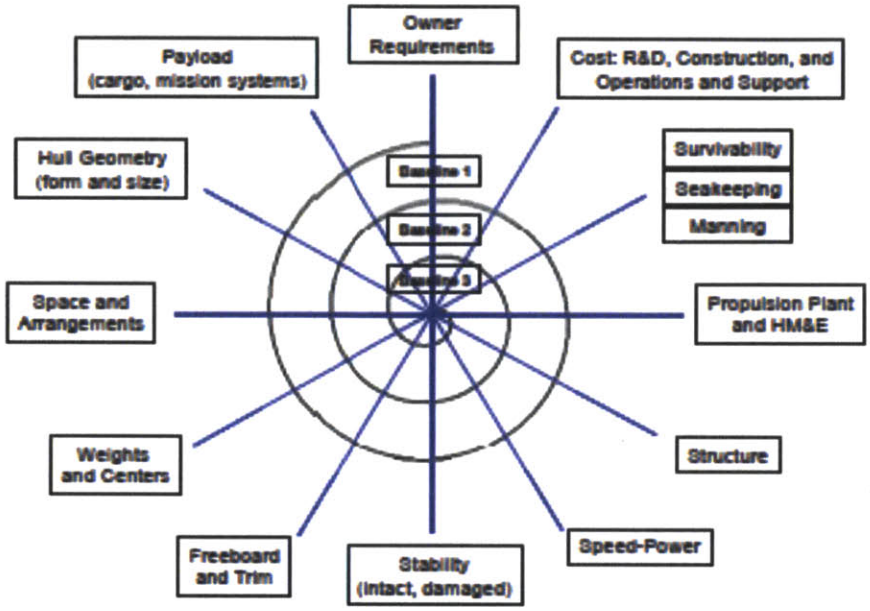

Figure 2.1 Example of Naval Ship Design Spiral (Small, 2011)

Set-based design, though not as prevalent as point based design is gaining traction amongst naval architects. Set-based design involves the use of concurrent engineering, where different groups of designers are working in different parts of the trade space. They will work independently to shrink the trade space until the different designs begin to overlap. They will continue to work until all work funnels into one design (Singer, Doerry, & Buckley, 2009). This design concept works very well with complex systems where teams work on different parts of the system independently and then come together to determine the proper solution. A illustration of this process can be found in figure 2.2.

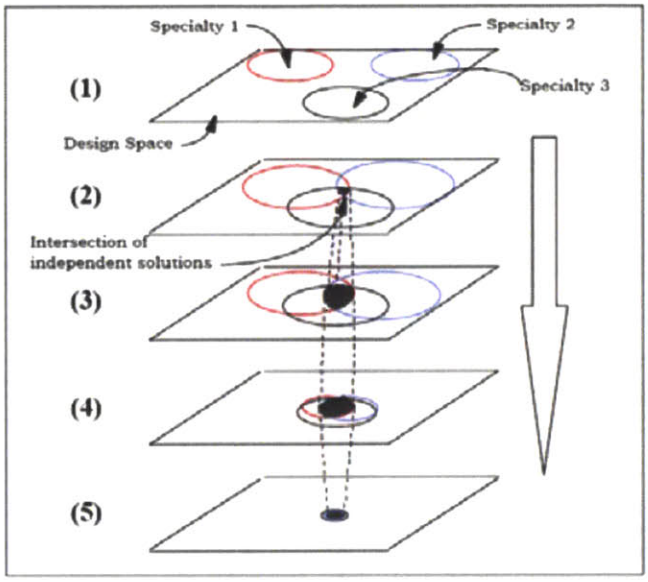

Figure 2.2: Set-Based Design Funnel (Small, 2011)

Since this project is small in nature and not a complex system, a point based design spiral will be used. The design spiral for this project was developed and can be found in the following figure.

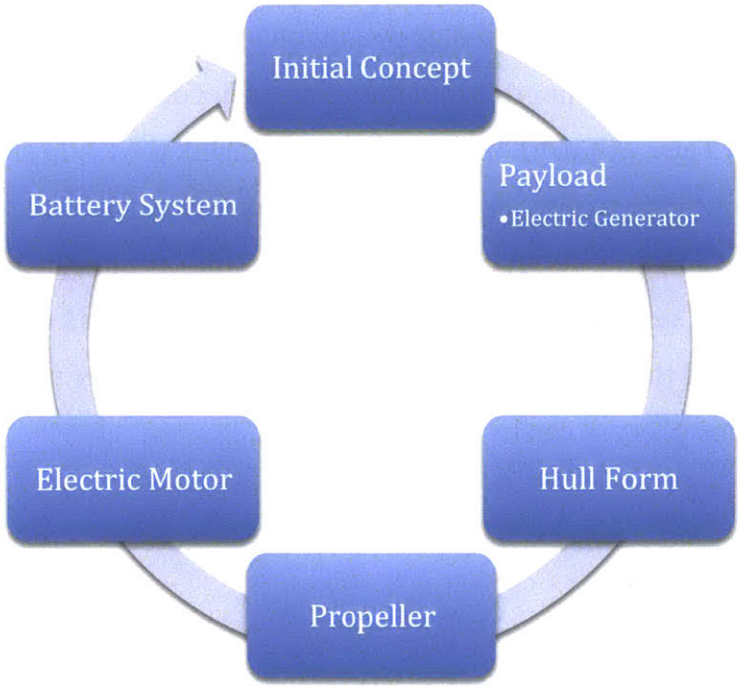

Figure 2.3: First Stage Design Spiral for AUV

The choice for the order of the design spiral mainly comes from the propulsion chain and efficiencies for a marine vehicle. A graphic of this chain can be found in figure 2.4.

The payload must be chosen first since it will determine the diameter of SPYROS. Since the electrical generator will be the largest piece of equipment onboard the vessel, it will be the driver for hull diameter. Once the hull diameter is determined, a hull form will be selected in order to minimize drag. Using the characteristics of this hull form, the drag coefficient can be ascertained. Applying the drag coefficient along with the hull diameter allows for the determination of the hydrodynamic drag. Using this value for drag, along with other variables, propeller optimization can be conducted to determine the ideal propeller for this vessel. One of the outputs of the propeller optimization will be the propeller efficiency. Utilizing this value along with the drag and power required to propel SPYROS at a desired speed, electric motor requirements can be determined and a motor can be found. Once a motor is chosen, batteries can be selected in order to effectively power the motor. Once this entire chain is complete, a possible propulsion design can be reviewed, and a further iteration of the design spiral started if the design was determined to be unsuitable. This cycle will continue until an appropriate propulsion system is developed

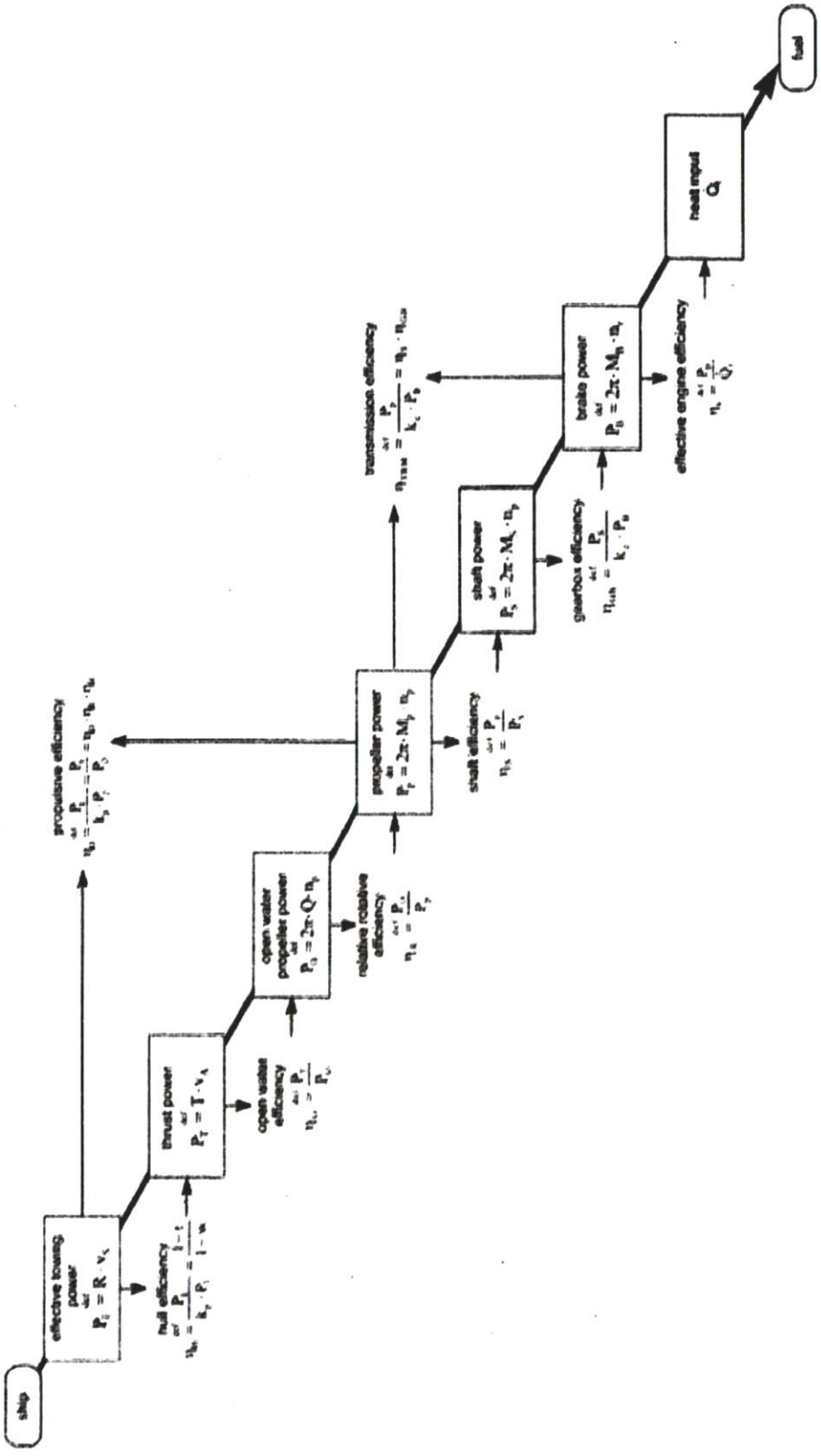

Figure 2.4: Propulsion Chain (Woud & Stapersma, 2008)

3. Generator Selection

Since the onboard generator is the largest piece of payload onboard SPYROS, it must be selected prior to any hullform or propulsion design, since the generator will drive the hull diameter. There are several different types of generators that could be used for this purpose, including:

1. Diesel Engine Generator
2. Gas Turbine Generator
3. Gasoline Engine Generator
4. Wankel Engine Generator

Since space and weight are of primary importance in the selection of an onboard generator; the space, weight and fuel consumption (needed to determine fuel space and weight requirements) was determined for a representative generator. If at all possible, engines were selected that already had matched generators. These generators would be easier to purchase

3.1 Diesel Engine Generator

A diesel engine generator would be the preferred choice for an AUV onboard generator. Diesel engines are used extensively in the maritime environment and diesel fuel is deemed safe to use at sea since it has a high flashpoint. Diesel engines are also very fuel efficient, which is important for SPYROS' design, since space is limited and onboard battery capacity needs to be maximized. Figure 3.1 shows a representative marine diesel generator, the Kubota XGen 3.5kW marine diesel, and Table 3.1 outlines its specifications.

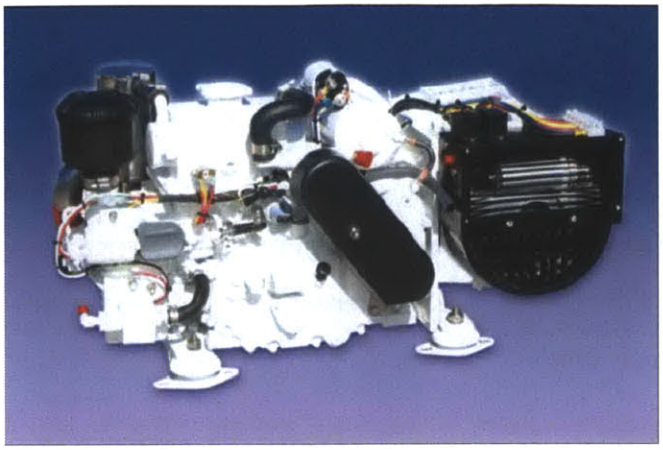

Figure 3.1: Kubota XGen 3.5kw Marine Diesel Generator

Kubota XGen 3.5kw Marine Diesel		
Generator Weight	72.6	kg
Fuel Consumption	0.013	L/min
Time Operational	540	min
Total Fuel	6.813	L
Fuel Density	0.832	kg/L
Fuel Weight	5.668	kg
Total Weight	78.268	kg
Size	0.71	m Long
	0.39	m Wide
	0.38	m Tall
Volume	0.105	m^3

Table 3-1: Kubota XGen 3.5kw Marine Diesel Specifications

From the specifications, it can be seen that the generator weight is very high. This is due to the fact that diesel engines are pressure ignition and therefore requires heavy metal components to withstand the pressures involved. Despite the fact that a diesel generator is the desirable choice, it may be too heavy to be a feasible option.

3.2 Gas Turbine Generator

On many larger vessels (especially naval warships), gas turbines are utilized for power generation. Extremely power dense, gas turbines are generally the answer for power generation when size and weight are of great importance. Gas Turbines can also run on a variety of fuels, making it desirable when used with high flashpoint fuels such as Diesel. Jaguar has recently announced that they plan on exploring the concept of gas turbine generators as range extenders on their new hybrid vehicles. Unlike traditional hybrids which use the engine and batteries for propulsion, range-extending hybrids utilize the engine (in Jaguar's case two Bladon Jets 30kw microturbines) are used only as generators to provide electrical power to recharge the onboard batteries ("JET-ENGINE MAKER AIMS TO POWER THE FUTURE," 2011).

Figure 3.2: Bladon Jets microturbine generator

It was determined that the Bladon Jets microturbine was unfeasible for this AUV project since the microturbine is still in the prototype stage and 30kW was too powerful for this application. Further investigation lead to the JetCat SPM 5 Marine Turbine as a viable option for AUV power generation ("Hobby Depot - JetCat SPM5," 2010). This turbine is designed for radio controlled model boats, but if matched with the proper generator, could generate up to 8kw of power. The SPM 5 specifications can be found in Table 3-2.

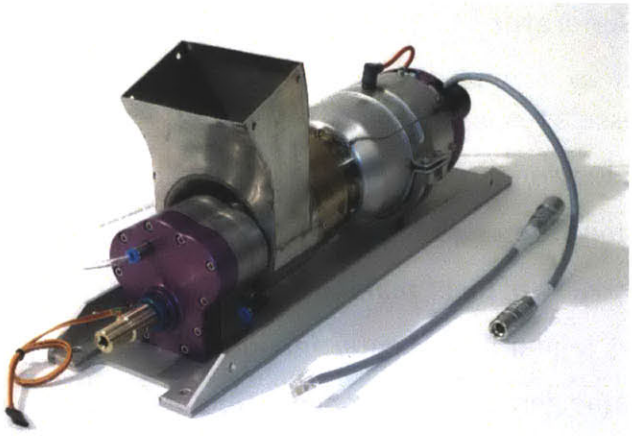

Figure 3.3: JetCat SPM5 Gas Turbine

JetCat SPM5 8kw Gas Turbine		
Generator Weight	2.93	kg*
Fuel Consumption	0.26	L/min
Time Operational	540	min
Total Fuel	140.4	L
Fuel Density	0.832	kg/L
Fuel Weight	116.813	kg
Total Weight	119.743	kg
Size	0.38	m Long
	0.10	m Wide
	0.16	m Tall
Volume	0.006	m^3

Table 3-2: JetCat SPM5 Specifications

(Note: * Only engine weight, generator would have to be matched and weight added)

Despite it's small size, the SPM5, like most gas turbines, is not fuel efficient. Utilizing the given fuel consumption, it can be seen in Table 3-2 that the fuel weight needed is

considerably higher than the weight of the engine and the required fuel tanks may pose problems in the AUV design.

3.3 Gasoline Engine Generators

Gasoline engine generators are possibly the most common electrical generator on the market. Gasoline engines of all sizes are used as a power source, from small two stroke engines used to power lawn trimmers to large 4 stroke engines in automobiles. Due to the high production and usage of these engines, gasoline engines are considered a proven technology. Gasoline generators are also very common, used primarily as a recreational generator at campsites and other locations without electricity, and as home backup generators used during blackouts.

In the marine environment, gasoline engines are primarily used as outboard motor engines in small watercraft. Most marine applications, especially in the navy, tend to stay away from utilizing gasoline engines. There are two reasons for this: gasoline engines are spark ignition engines and with any spark ignition engines there is the chance of explosion, and gasoline also has a much lower flashpoint than diesel fuel, making it much more of a fire hazard compared to diesel. However, due to the fact that it is a spark ignition engine, the components of the engine are much smaller, making the overall engine much lighter than a comparable diesel engine.

The generator selected for the comparison is a Honda EU1000i 1kw generator ("Honda EU1000i generator," n.d.). Utilizing a Honda GXH50 4 stroke engine, this generator is extremely light weight, yet capable of delivering the necessary power to recharge SPYROS' onboard batteries.

Figure 3.4: Honda EU100i 1kw Generator

Honda EU1000i Gasoline Generator		
Gen Weight	13.15	kg
Fuel Consumption	0.010	L/min
Time Operational	540	min
Total Fuel	5.348	L
Fuel Density	0.720	kg/L
Fuel Weight	3.849	kg
Total Weight	16.999	kg
Size	0.45	m Long
	0.24	m Wide
	0.38	m Tall
Volume	0.041	m^3

Table 3-3: Honda EU1000i Specifications

Upon review, the Honda gasoline generator has a much lower overall weight than the other two generators. It also has a very low volume, which can be reduced further as the generator specifications include the casing and fuel tank, which can be removed for installation in SPYROS. Despite the flammability of the fuel type, this generator would be a practical option for the AUV design.

3.4 Wankel Engine Generators

Wankel, or rotary, engines were developed by Felix Wankel in the early 20th century (Sherman, 2009). Unlike normal reciprocating engines, there are no pistons, only a rotor shaped like a reuleaux triangle that turns eccentrically inside a housing, as seen in Figure 3.5. This design allows for a much more power dense engine and has been used periodically in the automobile industry, most recently in the Mazda RX-7. Due to their small size, they are also being investigated for use as range extenders on automobiles.

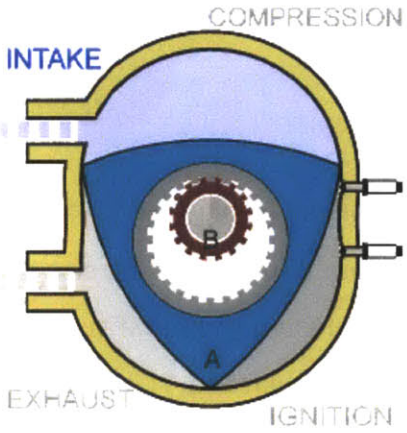

Figure 3.5: Basic Wankel Engine

There are several disadvantages to the Wankel engine. They are historically hard to seal and therefore are less fuel efficient than similar gasoline engines. They are also difficult to time, since the intake stroke is much shorter than a four stroke engine and there are no inlet or exhaust valves. Finally, by design they burn oil in order to help with the sealing process. This would require an alteration if used on an AUV, where space is limited for a lubricating oil tank.

Freedom Motors of Davis, California has been developing Wankel technology for uses outside of the automotive industry ("Rotapower 27 Series Announcement," 2010). They have developed a prototype 2 kW wankel engine which is much smaller than the gasoline equivalent (figure 3.6). They had hoped to use this engine for small motor applications, including generators, however it was found to not be economically viable and therefore not put into production.

Figure 3.6: Comparison of an equivalent Wankel and Piston Engine

This motor was the only one found of the correct size that would be feasible for the SPYROS design. All other wankel engines of that size are not designed for these types of applications are were disregarded.

3.5 Final Selection

To determine which generator is the best selection for this project, a side-by-side comparison was conducted and Table 3-4 produced. It should be noted that the volume takes into account both the volume of the generator and the volume of the fuel required.

Side by Side Comparison				
Generator	Gen. Weight (kg)	Fuel Weight (kg)	Total Weight (kg)	Volume (m^3)
Kubota XGen 3.5kw Marine Diesel	72.60	5.67	78.27	0.11
JetCat SPM5 8kw Gas Turbine	2.93	116.81	119.74	0.15
Honda EU1000i Gasoline Generator	13.15	3.85	17.00	0.05

Table 3-4: Generator Comparison

From this table, it is easy to see that the Honda gasoline generator is the best choice if overall size and weight are of the highest importance. The diesel engine itself is just too heavy, even though its fuel consumption is on par with the Honda generator. The Gas Turbine option itself is quite small, however it has such bad fuel efficiency that the amount of fuel required is so high that it becomes both the heaviest and biggest option. It cannot be forgotten that even though the Honda generator is the best option, gasoline is not the ideal fuel for use onboard an AUV. Measures will need to be taken in order to mitigate this problem.

To move forward, a hull diameter must be determined from the generator size in order to calculate SPYROS' drag. Since the MIT Rapid Development Group used the Honda Generator and were able to fit all equipment into a 0.34m diameter shell, this value will be used.

4 Hullform Selection

Once SPYROS' main payload (the generator) is determined, a hullform can be selected. For this study, the requirement of a hullform is only needed to determine the hydrodynamic drag coefficient for further drag calculations and propeller and motor selection. This process had to wait until the generator was selected in order to determine the diameter of the vessel, which is integral for drag calculations.

4.1 Hullform Geometry

Currently, there are two different types of hullform geometries used for AUV designs, Gertler Forms (Gertler, 1950) and Myring Forms (Myring, 1976). Morton Gertler developed his hullform designs while working on high speed submarine designs at the David Taylor Model Basin during the mid 20th century. His forms are exceedingly elliptical, very streamlined and produce very little drag. As can be seen in the figure below however, the form can be difficult to assemble and has little space for payload.

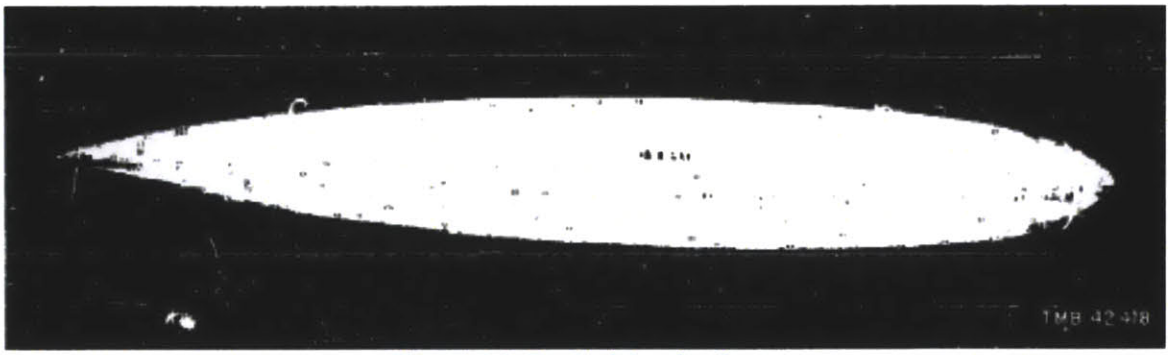

Figure 4.1: Typical Gertler form

D.F. Myring developed his body shapes while working at the University of Salford in the United Kingdom. Originally intended for aeronautical applications, Myring Forms have been heavily used in the Underwater Vehicle Community. As seen in Figure 4.2, it is not as elliptical as the Gertler form, but has a much more uniform mid-body, which would allow for easier construction and the ability to carry a larger payload. Due to this advantage, Myring forms have been used extensively in modern AUV designs, including the Remus AUV (Allen, Vorus, & Prestero, 2000) and MIT Sea

Grant AUV Lab's Didemnum Cruiser AUV (Brege, 2011). Due to these advantages, the Myring form will be used for SPYROS' drag calculations.

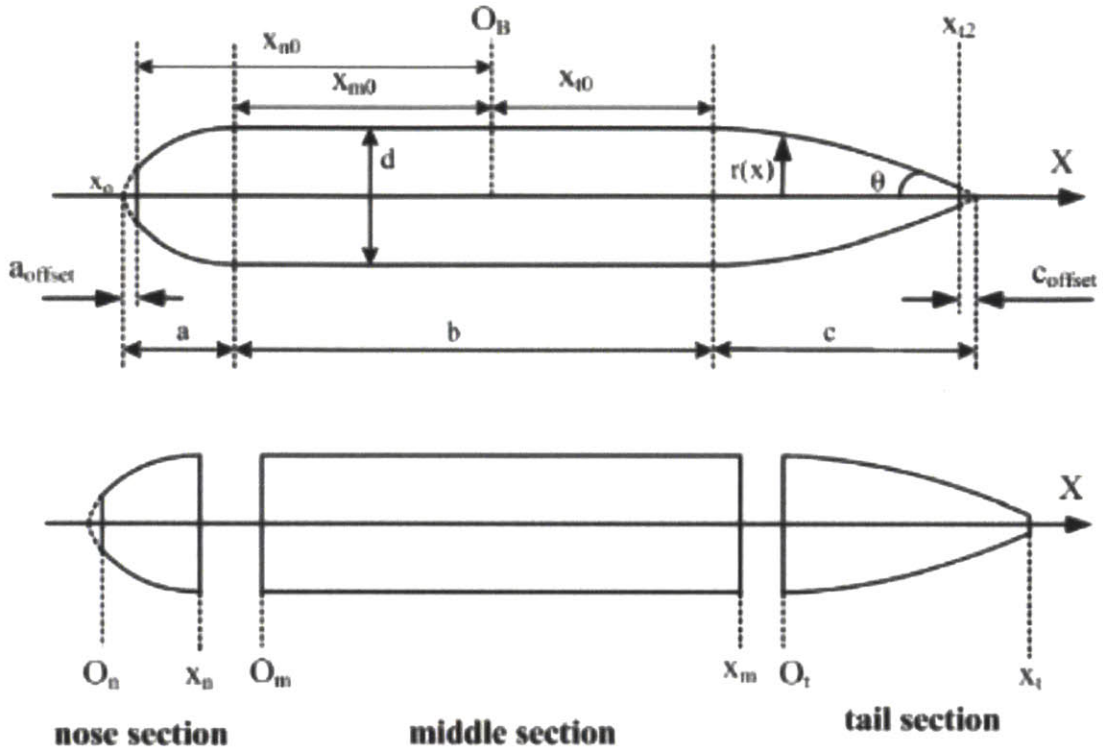

Figure 4.2: Typical Myring form (Brege, 2011)

Another advantage of the Myring form is that the body shape can be easily modeled using three simple equations; one for the nose cone, one for the mid-body and one for the nose cone.

Nose Cone Equation:

$$r1(x) = \frac{1}{2}d\left[1 - \left(\frac{x-a}{a}\right)^2\right]^{\frac{1}{n}}$$

Mid-Body Equation:

$$r2(x) = \frac{d}{2}$$

Tail Secion Equation:

$$r3(x) = \frac{1}{2}d - \left[\frac{3d}{2c^2} - \frac{\tan\theta}{c}\right](x-(a+b))^2 + \left[\frac{d}{c^3} - \frac{\tan\theta}{c^2}\right](x-(a+b))^3$$

Symbols:

a:	Nose Cone Length
b:	Mid-Body Length
c:	Tail Section Length
θ:	Tail Angle
n:	Myring Coefficient (used to determine roundness of nose cone)

4.2 Determination of Drag Coefficient

Upon obtaining the equations for a Myring Body, a MATLAB code was developed to determine the optimal shape of a Myring Body to reduce the drag coefficient. Myring originally determined the drag coefficient of by calculating the axisymmetric boundary layer. Fortunately many others have built upon Myring's original work and have developed equations to determine the drag coefficient based on the finesse ratio f (ratio of body length to maximum diameter) (Debarros, Pascoal, & Desa, 2008). The following equations are for the drag of a Myring Body with a zero degree angle of attack, a condition used extensively in SPYROS' missions as it minimizes drag and maximizes overall distance travelled. To calculate the drag coefficient, one must start by calculate the drag coefficient based on the friction drag as below.

$$C_D^* = C_f[1 + 60f^{-3} + 0.0025f]\frac{S_S}{L^2}$$

where S_S is the wetted surface area of the body and L is the length of the body. To calculate the skin friction drag C_f, the ITTC standard is utilized. For this problem the Reynolds number was calculated using a velocity of 1.29 m/s (2.5 knots) and a viscosity value of 10^{-6} m^2/s.

$$C_f = \frac{0.075}{(\log Re - 2)^2} + 0.00025$$

One must then calculate the base-drag coefficient using the following equation,

$$C_{D_b} = 0.029\left(\frac{d_b}{d}\right)^3 (C_D^*)^{-0.5}$$

where d is the maximum diameter of the body and d_b is the base diameter, which is defined as the diameter at the stern most section of the body. Finally the two drag coefficients are added together to determine the full drag coefficient of the body.

$$C_{D_O} = C_D^* + C_{D_b}$$

A MATLAB Code was generated using these equations to determine the optimal hullform of a Myring body in order to reduce the drag coefficient. The code utilized a pre-set value for body diameter d (0.34 m), finesse ratio f (10) and mid-body length b (1.87 m). The base diameter d_b (0.05 m) was also pre-determined as it was a representative value of a possible vessel propeller hub. The code then used a series of loops to vary the values of a, c, n, and θ. The MATLAB code can be found in Appendix A. After running the code through several iterations and changing the pre-set values described above, certain truths about Myring bodies were determined. It was found that at all times, the minimum size for the nose cone length and the Myring parameter n would return the lowest value for the drag coefficient. It was also determined that an increase in f causes a decrease in the drag coefficient and an increase in the base diameter will increase the drag coefficient.

After running the code it was found that the drag coefficient would always be found in the range of 1.0×10^{-3} and 2.0×10^{-3}. This value was found to be peculiar since it is much less than anticipated. However, Newman in his book *Marine Hydrodynamics* placed a curve of drag coefficient vs. angle of attack for a NACA 63-412 airfoil (Newman, 1977). His results showed that at a zero angle of attack, the drag coefficient of the airfoil are in the same range as found using the Myring drag equations. After discussions with the thesis advisor, Dr. Chryssostomidis, a more representative number is required, since any irregularity of the body's surface will lead to a large increase in the drag coefficient. Since SPYROS will require a snorkel for the propulsion engine, body irregularities are unavoidable. Sighard Hoerner conducted many tow tank tests during his career and self published a text called *Fluid-Dynamic Drag* (Hoerner, 1965). According to his research, a body with a

torpedo like shape will have a drag coefficient of 0.1. This value for the drag coefficient was utilized for this project as an assumption. Further testing must be done to determine the vessel's drag coefficient to optimize SPYROS' propulsion system.

4.3 Determination of AUV Drag

With a value for the drag coefficient, the vessel's drag can now be calculated using the following equation

$$D = C_D \frac{1}{2} \rho V^2 A$$

where ρ is the water density (1025 kg/m^3), V is the vessel speed and A is the projected area of vessel (for this case, the area of a circle with the vessel's chosen diameter of 0.34m). In order to account for fins and snorkel, an additional 20% was added to the drag (Burcher & Rydill, 1994). Using this equation, a speed/drag curve was developed.

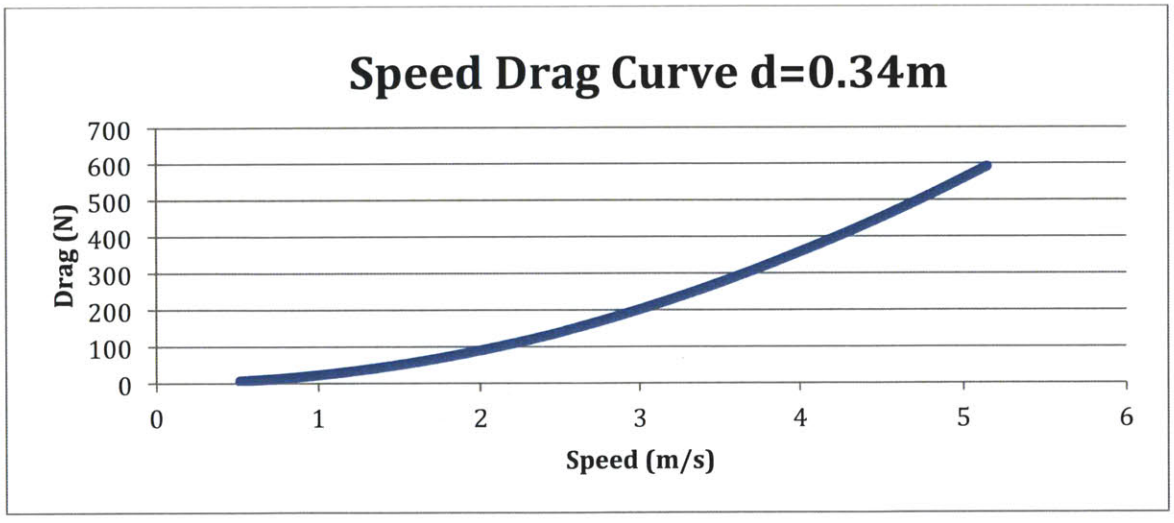

Figure 4.3: Speed/Drag Curve for AUV with diameter of 0.34m

Since power conservation is key in long range AUVs, this vessel will be travelling slowly to conserve power, since power can be calculate from drag with the following equation.

$$Power = (Drag) * (Speed)$$

To check the lower end of the curve in Figure 4.3, a second curve was developed. Since the TETHYS AUV was designed to travel at 1m/s as per the MBARI requirements (Bellingham et al., 2010), it makes sense to design to this speed as well to allow for good comparisons. From this curve, it can be seen that the chosen speed of 1 m/s corresponds to a drag of 22.3 N. This value can now be used to optimize a propeller and match the optimized propeller to an electric motor.

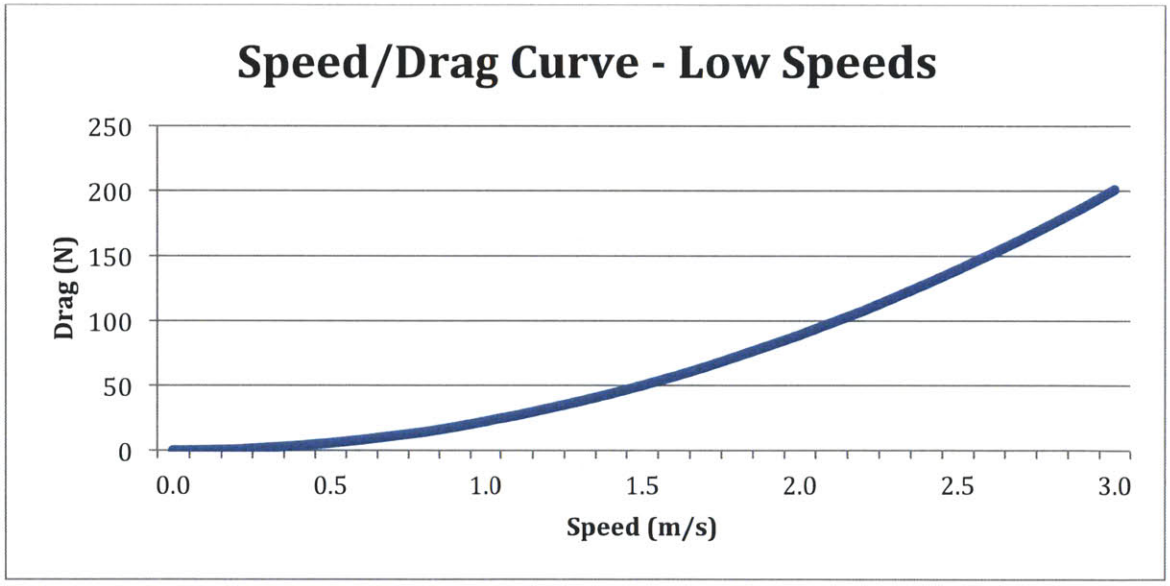

Figure 4.4: Speed/Drag Curve - Low Speeds

5 Propeller Design

Once SPYROS' resistance through the water is determined, a suitable propeller can be designed to propel the vessel through the water. For this project, two options were evaluated for SPYROS' propeller:

1. Utilize a commercial propeller, or
2. Design a propeller using available software.

5.1 Commercial Thruster Systems

An online search was conducted to find a suitable commercial propeller. Most commercial producers build a self contained thruster system, complete with gearbox and propeller duct. Unfortunately most companies produce thrusters that are too power-intensive for long range AUVs. There was one option, however, that met the appropriate power requirements. This was the "High Flow" 600HF UROV thruster developed by CrustCrawler (CrustCrawler, n.d.). This thruster system is able to deliver as little as 18 N of thrust (with 6V being delivered to the thruster). However, the propeller rotates at a very high speed (9000 rpm max) and the seal life is only 7 million revolutions, which translates to only about 13 hours of operations Even if the propeller rotates at 1000 rpm, this provides power for only 116 hours (or a little under 5 days of operation). Since the seals could not be replaced during a mission, this thruster would be unsuitable for long distance missions.

Figure 5.1: CrustCrawler "High Flow" 600HF UROV Thruster

5.2 OpenProp Theory

Since a commercial thruster system could not be found that would be suitable for long distance missions, it was decided that a propeller would be designed using available software. The choice was made too utilize OpenProp, an open-source code developed at MIT(Kimball & Epps, 2010). OpenProp is a MATLAB based program, which utilizes lifting line theory to develop propeller designs. This method is used extensively by both military and commercial designers when developing propellers.

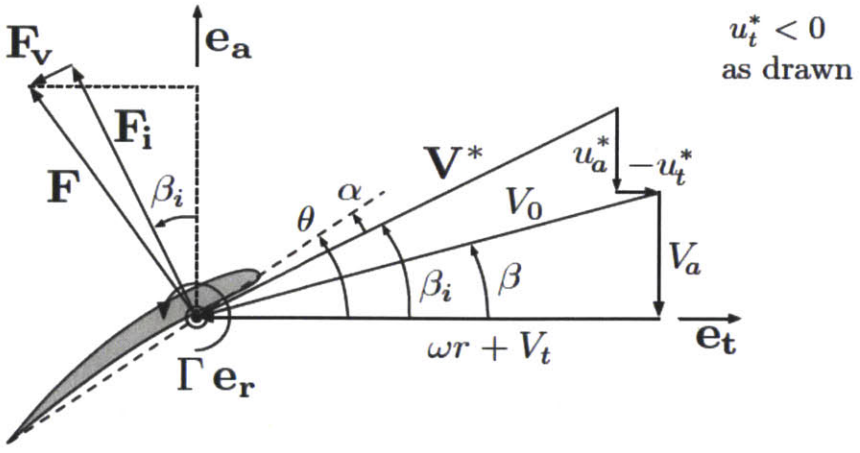

Figure 5.2: Propeller velocity/force diagram (Epps, 2010)

In lifting line theory, the propeller blade is modeled as a two dimensional lifting line (Epps, 2010). Figure 5.2 shows the velocities and forces on a section of a propeller blade in both the axial (e_a) and tangential (e_t) directions. In the axial direction, there is the axial inflow velocity V_a and the axial induced velocity u_a^*. In the tangential direction there is the swirl inflow developed by the shaft rotation (ωr), as well as the tangential inflow velocity V_t and the tangential induced velocity u_t^*. OpenProp calculates the induced velocities by using a standard propeller vortex lattice model, where the induced velocities are determined by summing the product of the induced velocities and the circulation at regular control points along the length of the blade.

The total inflow velocity, V*, can be calculated from the following equation:

$$V^* = \sqrt{(V_a + u_a^*)^2 + (\omega r + V_t + u_t^*)^2}$$

and this velocity acts at angle β_i to the e_t axis, which is determined with the following equation:

$$\beta_i = \tan^{-1}\left(\frac{V_a + u_a^*}{\omega r + V_t + u_t^*}\right)$$

On figure 5.2, one can also see the circulation Γ, the blades angle of attack α and the pitch angle θ. The loads on the blades are also illustrated, including the inviscid Kutta-Joukowski F_i and viscous drag force F_v, which is shown aligned with the total inflow velocity. As stated earlier, this model is two dimensional, so the total loads on the propeller can be determined by integrating the loads over the span of the blade. Assuming there are Z blades on a propeller, the total thrust on the propeller can be calculated.

$$T = Z\int_{r_h}^{R}[F_i\cos\beta_i - F_v\sin\beta_i]dr$$

In the previous equation, r_h is the radius at the hub and R is the radius at the tip. Similarly, the torque on the propeller can be calculated.

$$Q = Z \int_{r_h}^{R} [F_i \cos \beta_i - F_v \sin \beta_i] r dr$$

For this design, it is important to determine the power consumed by the propeller. This can be calculated by the equation below.

$$P = Q\omega$$

The useful power of the propeller is also important and this is determined by the following equation, where V_s is the vessel's speed.

$$P = TV_s$$

From these equations, the efficiency of the propeller can be determined.

$$\eta = \frac{TV_s}{Q\omega}$$

OpenProp will also optimize the given propeller by determining the circulation distribution of a propeller that will minimize the torque for a given thrust. This is accomplished by utilizing a Lagrange multiplier and Newtonian Solver to solve the differential equations that are produced in this process. For a full explanation of the procedure, refer to the OpenProp v2.4 Theory Document (Epps, 2010).

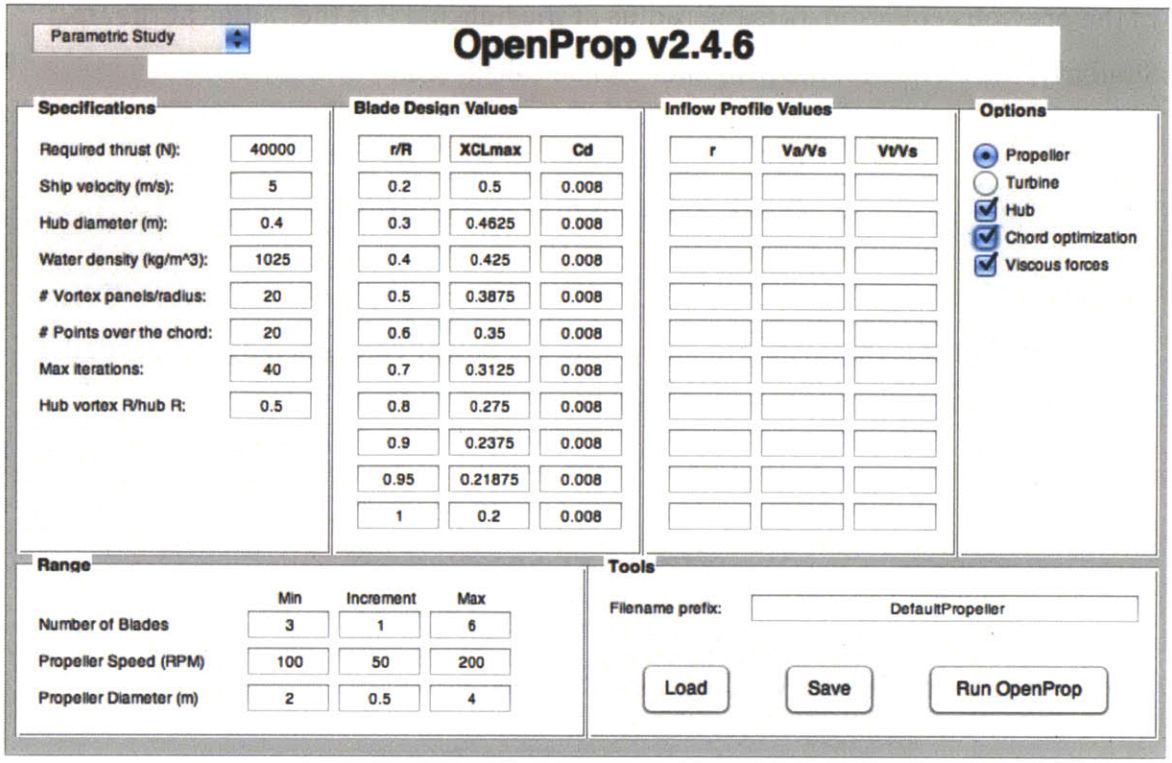

Figure 5.3: OpenProp Parametric Study User Interface

5.3 OpenProp Parametric Study Tool

In order to design the most efficient propeller possible, it was determined that the parametric study tool should be used first to determine the basic properties of the required propeller before utilizing the propeller single design tool. As seen in Figure 5.3, the user inputs the required thrust, velocity and hub diameter of the propeller, and then can input a range of blade numbers, propeller rotation speed and propeller diameter. To ensure a high efficiency, the chord optimization routine was utilized.

By minimizing the chord length *c*, the torque can be further minimized. However, the chord length cannot be too small, as it would negatively the Lift Coefficient of the propeller.

$$C_L = \frac{\Gamma}{\frac{1}{2}V^* c}$$

OpenProp therefore chooses a maximum Lift Coefficient $C_{L\,max}$ and from this the optimum chord can be determined.

$$\hat{c} = \frac{|\Gamma|}{\frac{1}{2}V^* C_{L_{max}}}$$

OpenProp will also specify an Expanded Area Ratio for the propeller in this routine (EAR_{spec}). The expanded area ratio can be defined as

$$EAR = Z \int_{r_h}^{R} \hat{c}\,(r)dr$$

From this specified EAR, the chord length distribution can be properly scaled, as per the equation below.

$$c(r) = \hat{c}(r)\frac{EAR_{spec}}{EAR}$$

Once all the inputs are entered and the program is run, the efficiencies of all the different combinations of propellers within the given ranges are calculated. The output is a series of graphs, each graph corresponding to propellers with the same number of blades. For each graph, the propeller diameter is plotted along the x-axis and the propeller efficiency is plotted along the y-axis. Each graph will have multiple curves, each corresponding to a different rotational speed for the propeller. From these graphs, the propeller characteristics with the highest efficiency can be determined.

For this study, it was determined that the best way to find the most efficient propeller was to find the most efficient combination of propeller diameter and

number of blades for several propeller speeds. Therefore a parametric study was conducted with the following inputs:

Parameter		Value	
Thrust		22.33 N	
Ship Speed		1.00 m/s	
Hub Size		0.07 m	
Variables	**Min**	**Increment**	**Max**
Number of Blades	2	1	4
Propeller Speed	100 rpm	50 rpm	500 rpm
Propeller Diameter	0.2 m	0.01 m	0.34 m

Table 5-1: OpenProp Parametric Study Inputs - First Run

The range for blade numbers was chosen arbitrarily, however it was determined that since this will be a very small propeller, any blade number above four would be very difficult to manufacture. The maximum propeller diameter was chosen to be 0.34 m since this was the diameter of the vessel. Upon investigation, the data becomes scattered at low diameters and it was found that the program would operate correctly for diameters greater than 0.2 m. Normally the ratio of the hub diameter to propeller diameter is 0.2 and therefore a hub size of 0.07 m was chosen, since this corresponds to the maximum diameter. If a different hub diameter is required, the appropriate change will be made in the Single Design Tool. Figure 5.4 show the results of this trial. From this trial, it was found that in all cases the maximum efficiency was found at the maximum diameter with 4 blades, as seen in Figure 5.5.

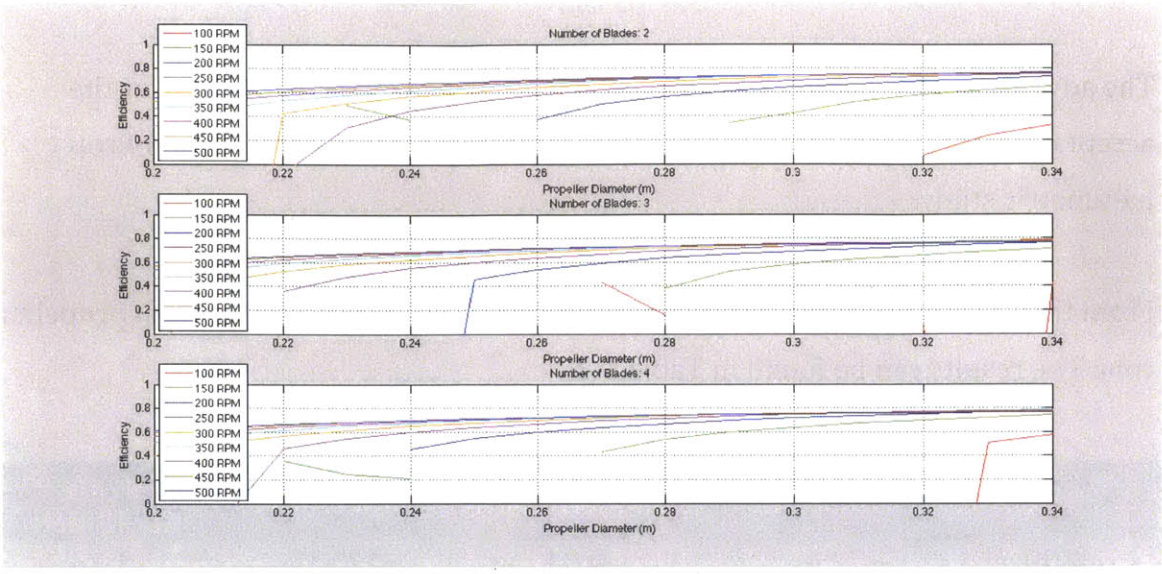

Figure 5.4: OpenProp Parametric Study - Results

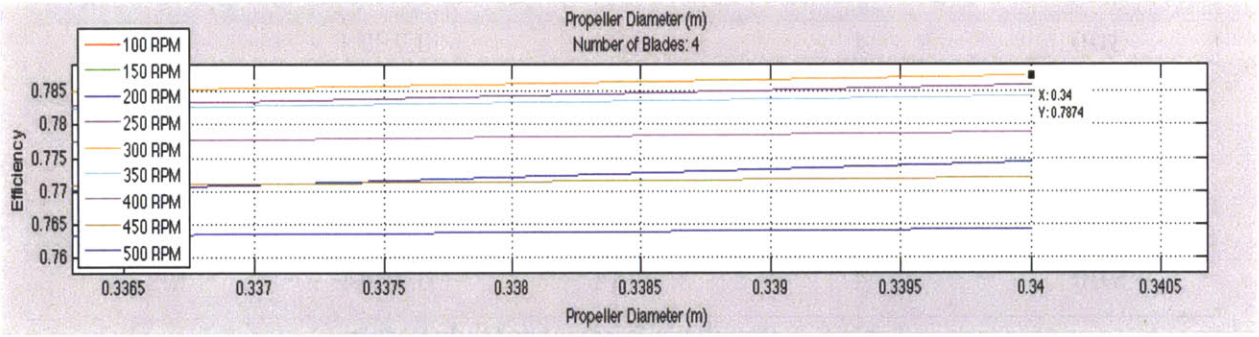

Figure 5.5: OpenProp Parametric Study - Zoomed in Results

From these results, it was determined that 100 rpm could not be used, since only scattered results were given from the parametric study. The possible reason for this is that the advance coefficient range for this propeller at the tested diameters. The advance coefficient, *J*, is extremely important as it describes the angle between the incoming fluid velocity and the angular velocity of the propeller blades. To calculate the advance coefficient the following equation is utilized, where V_s is the speed of the vessel in m/s, n is the rotational speed in rps and D is the diameter of the propeller in m.

$$J = \frac{V_s}{nD}$$

The advance coefficient for the 100 rpm is in the range of 1.8 to 3, well over the acceptable range of 0.5 to 1, leading to the scattered results from the OpenProp parametric study.

From the parametric study, the highest efficiency was determined for each propeller rpm. The results can be found in Table 5-2.

RPM	# of Blades	Diameter (m)	Efficiency	Advance Coefficient
150	4	0.34	0.7371	1.18
200	4	0.34	0.7745	0.882
250	4	0.34	0.7859	0.706
300	4	0.34	0.7874	0.588
350	4	0.34	0.7844	0.504
400	4	0.34	0.7789	0.441
450	4	0.34	0.7720	0.392
500	4	0.34	0.7644	0.353

Table 5-2: OpenProp Parametric Study Results

The results of the parametric study show that there is a maximum efficiency at a speed of 300 rpm. Furthermore, using the acceptable range of Advance Coefficients stated earlier, it is safe to assume that the propellers for 200 through 350 rpm will be the only viable results. Despite this, all propellers were evaluated with the OpenProp single design tool.

5.4 OpenProp Single Design Tool

The OpenProp Single Design Tool allows the user to take the selected results from the parametric study and fully design a propeller, including performance curves and two and three-dimensional geometry. The user interface can be seen in Figure 5.8.

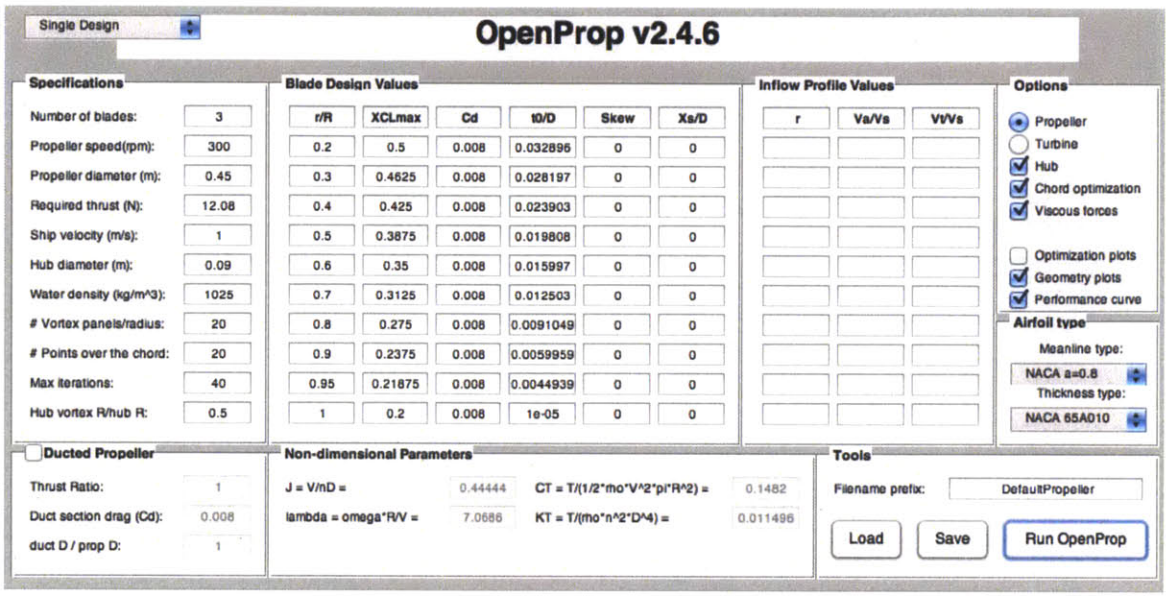

Figure 5.6: Single Design Tool User Interface

As stated earlier, this tool uses a complex optimization routine in order to develop a propeller, which minimizes torque for a given thrust. It must also be remembered that efficiency can be calculated with the following equation:

$$\eta = \frac{TV_s}{Q\omega}$$

The airfoil type was maintained as seen in Figure 5.6. The reason for this is that it was found that other airfoil types would crash the program without giving any proper output.

From Table 5-2, the maximum efficiency was determined for a given rotational speed. Using the above equation, it is safe to assume that using the info from Table

5-2 will give us a propeller with minimum torque. Figure 5.7 shows the output from the OpenProp single design tool, with the torque value highlighted.

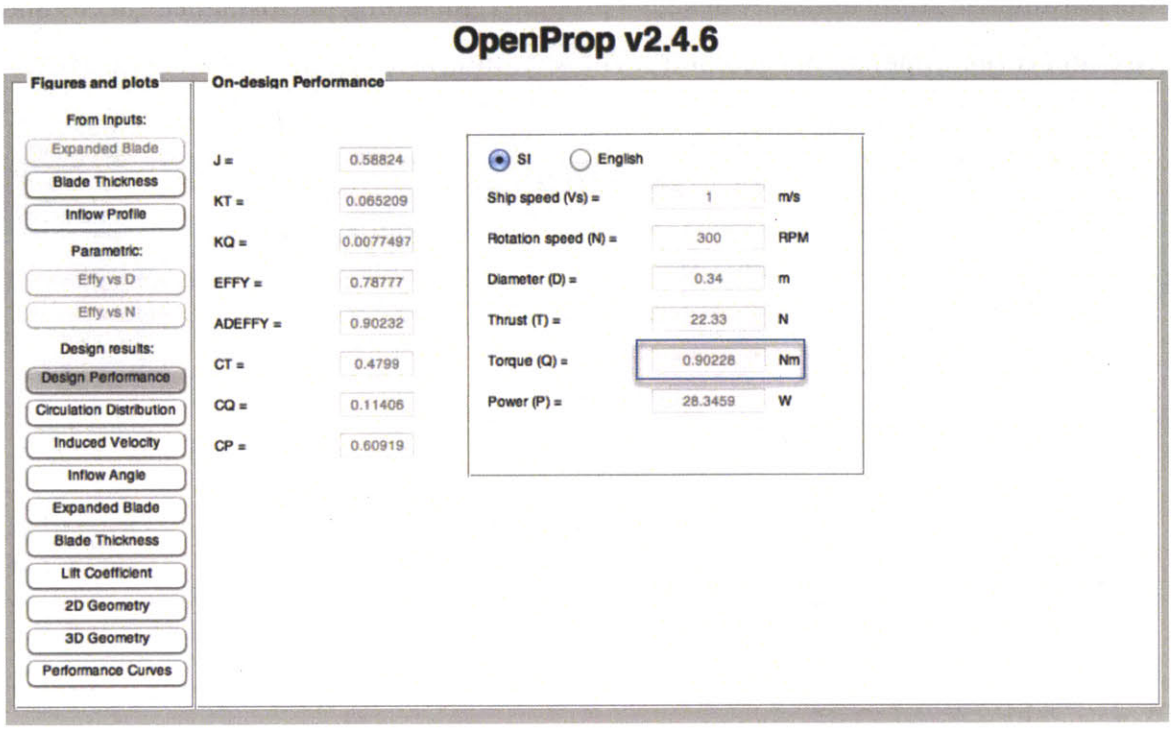

Figure 5.7: Single Design Tool Results with Torque Value Highlighted

Using the data from Table 5-2, the torque was determined for each of the propellers. In order to try to improve efficiency, each the single design tool was utilized twice, once with a duct and once without. This data can be found in Table 5-3.

Propeller Speed (rpm)	Torque (mNm)	Duct Used?
150	1837.7	Yes
200	1361.1	Yes
250	1084.6	No
300	902.28	No
350	776.51	No
400	684.27	No
450	613.63	No
500	557.78	No

Table 5-3: Torque Required for each Propeller Speed

As described in Chapter 6, a MATLAB script was developed which takes the propeller speed and torque as inputs and attempts to match the propeller with the speed/torque curves of a database of Brushless DC Motors. From this script, the 300-rpm propeller was chosen, since it best balanced a realistic propeller design with low electrical power requirement to effectively propel SPYROS. The propeller performance curves can be found in figure 5.8, and all other propeller information can be found in Appendix B.

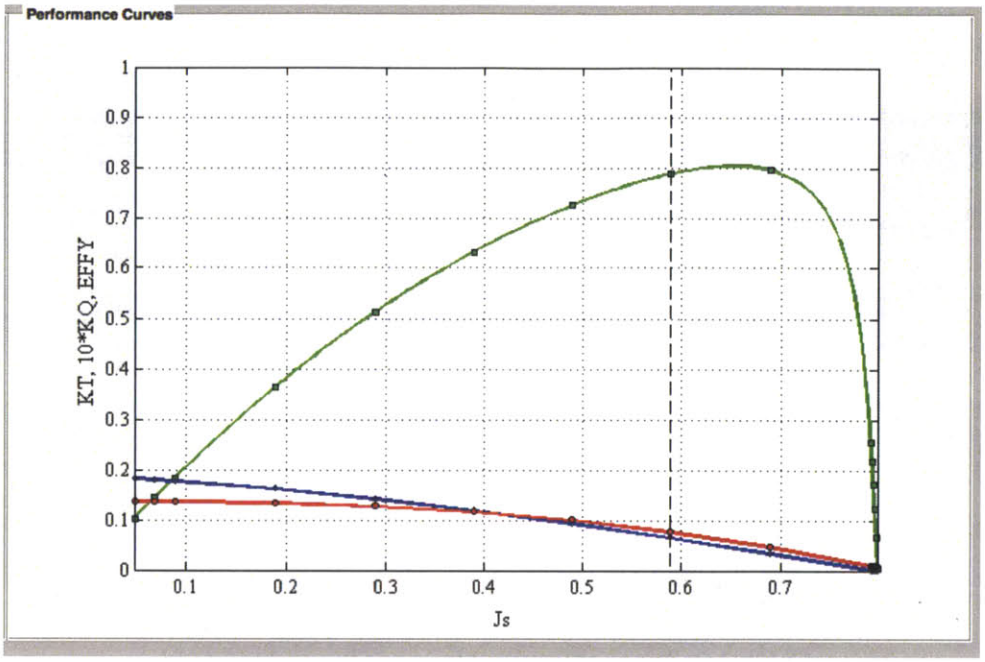

Figure 5.8: 300-rpm Propeller Performance Curves

It is worth noting that OpenProp did not choose a propeller with a maximum efficiency (as outlined in green in Figure 5.8). If the maximum efficiency from this curve was utilized, the propeller rotational would have to be changed in order to meet the required advance coefficient (since both ship's speed and propeller diameter must remain constant). Using this new information, along with the equation for propeller efficiency would give a Torque that would be greater then at the determined point.

5.5 Propeller Strength Analysis

As can be seen in Figure 5.9, one worry of the developed propeller is that of strength. The propeller blades are very thin, which may lead to yield after extended use of the propeller.

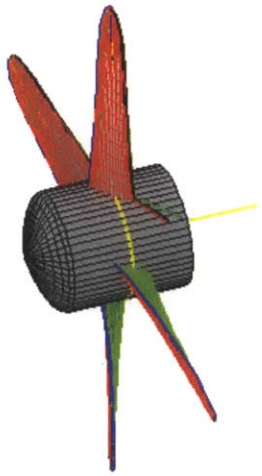

Figure 5.9: Initial 3D Propeller

Upon discussing the proper thickness with Brenden Epps, one of the developers of OpenProp, a linear fit of the thickness to diameter (t0/d) values was utilized in the Single Design Tool input, using a value of 0.02 at the root and the current value at r/R=0.95. To ensure that the On-Design Performance Values were not affected, the program was run for a second time with the new t0/d values. These were found to be identical to the previous single design.

To determine the yield stress (σ_y), a single propeller blade was modeled as a cantilever beam, with the required thrust acting at a single point at r/R=0.8, as seen in Figure 5.10.

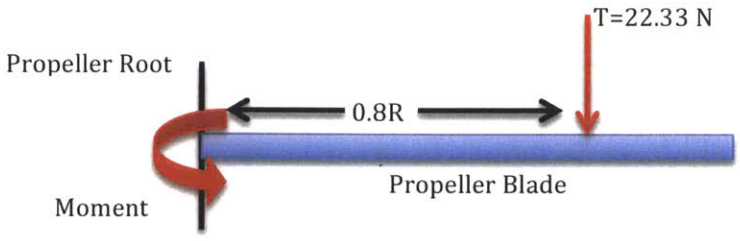

Figure 5.10: Propeller Blade as Cantilever Beam

In order to determine the moment at the root of the propeller, the following equation must be used, where R is the radius of the propeller blade (0.17 m) and T is the required Thrust (22.33 N).

$$M = 0.8RT$$

Using the above values, the moment is calculated to be 3.04 Nm. Before calculating the yield stress, the Area Moment of Inertia, *I*, must be calculated. If the propeller blade was modeled after a rectangular beam with the thickness, t_o, being equivalent to the height of a rectangular beam and the camber, *c*, of the blade being equivalent to the width of the beam, *I* can be calculated as follows.

$$I = \frac{1}{12} c t_o^3$$

To determine the camber and thickness at the root, the expanded blade and blade thickness curves from OpenProp must be utilized. Using these curves c=0.0272 m and t_o=0.0068 m at the root. Using this data in the above equation gives an Area Moment of Inertia value of 7.127×10^{-10} m^4. Finally, the yield stress at the root can be calculated by the following equation.

$$\sigma_y = \frac{M t_o}{I}$$

Using this equation gives a yield stress value of 29 MPa. An online search found that the yield stress of Nickel-Aluminum Bronze (the most common material used in propeller manufacturing) was in the range of 241-296 MPa ("Properties of Bronze for Marine Propellers," n.d.), giving the propeller a minimum safety factor of 8.3. This shows that the output of OpenProp will definitely be strong enough for the given thrust.

6 DC Motor Selection

As part of the Propeller Selection as outlined in Chapter 5, a motor was matched with the selected propeller using a MATLAB Script. Prior to discussing the results of this script, the decisions behind the DC motor selection will be outlined.

6.1 Drivetrain Selection

Prior to the matching of propeller and DC motor the type of drivetrain, or the way the motor is connected to the propeller, must be selected. For this design, two different drivetrains were considered:

1. Gearbox Transmission; and
2. Direct Drive Transmission.

There are advantages and disadvantages to either drivetrain. The gearbox transmission would allow a larger range of motors to be selected, as the motor speed does not need to be matched directly to the propeller speed, but can be modified to meet requirements. This is especially important with brushless DC motors, as they are normally small and rotate at a speed much too fast for effective AUV propulsion. However, for high speed/low torque drivetrains there is a fear of significant losses due to parasitic friction (Bellingham et al., 2010). According to Bellingham, AUV's that utilize gearbox drivetrains are flooded with a pressure compensating oil in order to prevent any large pressure differentials across the shaft seal. This is an issue with low torque drivetrains since the frictional torque of running in oil could conceivably be much higher than the original torque, leading to a very inefficient powertrain.

Utilizing a direct drive transmission would remove the possibility of inefficiencies due to requirement for pressure compensating oil. In this type of drivetrain, the motor is matched directly to the speed and torque requirements of the propeller, as the two components will be directly coupled. This makes the matching easier as

there are less components, however it does drastically reduce the number of possible motors that could be possible matches. Some form of coupling would be required in order to dissipate any misalignments between the propeller and motor due to transient forces. This does reduce the overall efficiency of the drivetrain, but it is a very minimal loss. Due to the disadvantages of a gearbox as stated above, a direct drive will be utilized for this design.

6.2 Brushed vs. Brushless DC Motors

There are many different types of motors that could be investigated for use onboard an AUV. Firstly, it must be noted that onboard batteries, which output DC power, will power the motor. Therefore unless an inverter was utilized, AC motors should not be investigated. Therefore for the purposes of this design, a DC motor will power SPYROS. There are two different types of DC motors available: Brushed and Brushless DC Motors.

Brushed and Brushless DC Motors have many similarities. As with all electric motors, they operate in accordance with Faraday's Law of Induction, which states that the generated electromotive force is directly proportional to the change in magnetic flux. This is accomplished with a rotor/stator assembly. The stator is constructed of either a permanent magnet assembly or electromagnet and the rotor is composed of a series of coils around some form of ferromagnetic material, as seen in Figure 6.1.

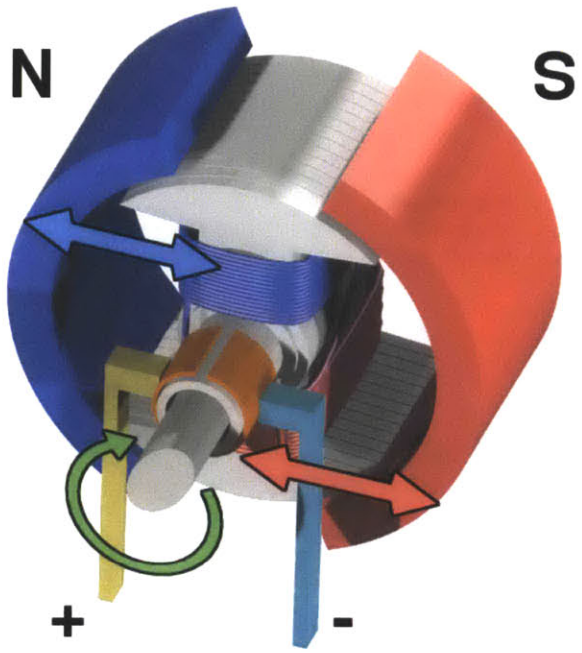

Figure 6.1: Basic 2 Pole Brushed DC Motor Assembly

An electric current is applied to the rotor, which creates a magnetic field within the rotor. Now that the motor is magnetized, it attempts to align itself with the magnetized stator. Just prior to alignment however, the current changes direction within the rotor, causing a change in rotor polarity and causing the rotor to rotate so that it will align itself with the stator in the opposite direction. If the current direction is changed at a set time rate, then rotation of the rotor (and therefore rotation of the motor) is achieved. This changing of current direction is called commutation.

The difference between Brushed and Brushless DC Motors is in the method utilized to commutate the current. In a brushed system, the current is applied to the rotor using brushes, and as the rotor turns the brushes provide current to the different poles of the rotor, thereby changing the direction of the current. There are some disadvantages to this system, especially in the fact that the brushes tend to wear,

leading to friction and sparking of the motor. Brushed motors also tend to be less efficient, especially when the brushes begin to wear.

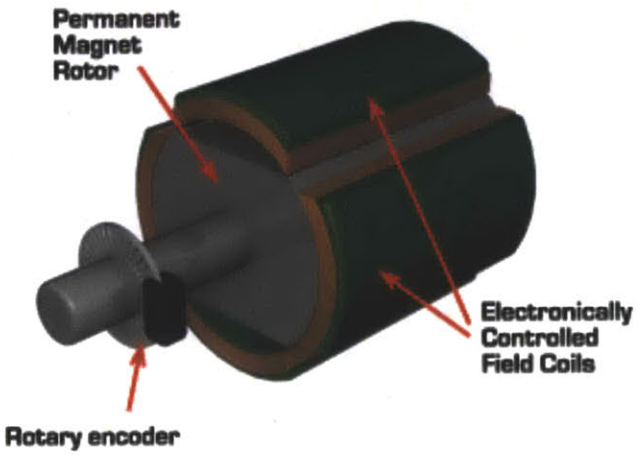

Figure 6.2: Brushless DC Motor ("EV Works Pty Ltd," n.d.)

Brushless Motors commutate in a different fashion. Instead of an electromagnetic rotor, the rotor is composed of permanent magnets with an electromagnetic stator as seen in Figure 6.2. The principle is still the same, but the electric current is applied to the stator. Commutation occurs using a switching circuit that changes the current direction and is timed for the required motor rotation. This removes many of the physical inefficiencies of the brushed DC motor. Do to the increased efficiency and lower maintenance requirement; a brushless DC motor will be utilized in the AUV design.

6.3 Brushless DC Motor Selection

Currently there are numerous brushless DC motors on the market. Unfortunately, most of them are very small and not suitable for use as an AUV motor. Since a direct drive transmission will be utilized, a low speed/high torque motor must be utilized. Most common brushless DC motors are very small and turn at high speeds with low torque. Therefore, the search turned to looking at larger, multi-pole motors, since

the mechanical speed of the motor is indirectly proportional to the number of poles by the following equation (Kirtley, 2010):

$$\Omega = \frac{\omega}{p}$$

In this equation, Ω is the mechanical speed of the motor, ω is the electrical speed (frequency of the switching circuit for brushless DC motors) and p is the number of pole pairs.

Another problem arose when looking at larger, multi-pole motors. These motors are normally used for larger, industrial applications and operate with very high power demands. Since power must be conserved as much as possible for the SPYROS design, high power motors at their design condition should not be considered.

In order to use commercial multi-pole motors, an off-design analysis of the motors was required. This proved to be very difficult as many of the manufacturers of brushless DC motors were not forthcoming with the necessary information. One company, SL Montevideo Technology, Inc. (SL-MTI), gives the consumer the ability on their website to customize the motor and determine the winding data and speed/torque curves when the customizable parameters are changed ("SL Montevideo Technology," n.d.).

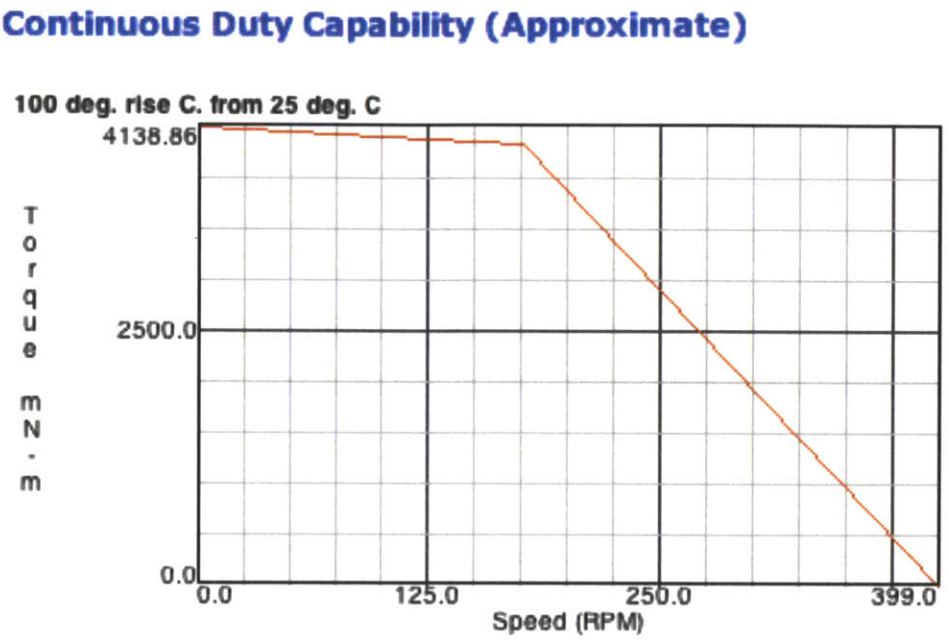

Figure 6.3: Sample Speed/Torque Curve from SL-MTI

Speed/Torque Curves for motors normally act as a linear curve from the no-load speed where there is zero torque on the motor (399 rpm in Figure 6.3) to the max torque point where the speed is zero. However, above a certain torque, continuous operation is not possible due to thermal constraints on the motor. In Figure 6.3, the max continuous torque can be seen as the "knee" in the curve. Continuous operation of this motor can be obtained at any point in the lower curve. The upper portion of the curve is the thermal limit of the motor. The motor will not operate on this point of the curve (the motor will continue to operate linearly from the lower curve), but the motor can only operate intermittently at any speed on the upper curve.

In order to correctly match the propeller to the electric motor, the designed speed and torque of the propeller must lie along a motor's speed torque curve. Another parameter that is required for propeller/motor matching is the motor's torque coefficient (K_t), which is given with SI units of mNm/A. This coefficient determines how much current is required to obtain the necessary torque, since the two are directly related. Given that battery capacity is measured in Ampere-Hours (Ah), the amount of current draw necessary to obtain the required torque must be minimized in order to extend the endurance of the batteries. At the SLM-TI website it is

possible to modify the motor's voltage, no load speed and temperature parameters in order to change the speed/torque curve and the torque coefficient. This allows a greater number of motor configurations to compare with the propeller and a greater chance to obtain the lowest possible current requirement.

To match the propellers developed in OpenProp to motors, an Excel database and a MATLAB script were developed. The Excel database was manually built utilizing data from the SLM-TI website. For the analysis, the voltage was maintained at 11 V (which is the nominal voltage for the battery system) and the default temperature parameters were preserved since the actual values are unknown. Only the no load speed parameter was changed, ranging from 600 rpm and lowered to as low as the website will allow at 50 rpm increments. At each rpm value, the speed and torque values at both no load speed and at the knee of the curve were retrieved and from these points the speed/torque curve equation of the motor at this condition was developed. The torque coefficient at each condition was also retrieved so that the required current can be calculated. This database contains 207 different speed/torque curve equations based off of the winding characteristics of 36 different motors.

This Excel file was then imported into a MATLAB script. The design speed and torque of the designed propellers are also inputted into the script. The script then compares the speed torque curve equations to the propeller speed and torque. If the results are within 5% of a specific motor, then the current draw to obtain the correct torque for a given speed is calculated and outputted. Upon completion of the script, the user can see all the motors that would be compatible for a specific propeller, as well as the current requirement for the propeller. The user can now choose which motor would be best for the given propeller. For this application, the motor that requires the least current was chosen. The Excel database, MATLAB script and the output can be found in Appendix C.

6.4 Selected Brushless DC Motor

After running the MATLAB script with the inputs outlined in Table 5-3, it was found that the lowest operating current was 3.07A. This was obtained by matching the 450 rpm propeller with the SL-MTI model BLHP-29-07-12P motor running at a no load speed of 523 rpm. Unfortunately, the propeller has an advance coefficient less than the minimum allowable value of 0.5. Therefore, it was decided to utilize the 300 rpm propeller matched with the SL-MTI model BLOV-29-13-12P motor. This motor would operate with a no load speed of 375 rpm and a torque constant K_t of 280.28mNm/A, giving a required current of 3.19A. Below is the approximate speed/torque curve of this motor overlaid with a portion of the propeller speed/torque curve.

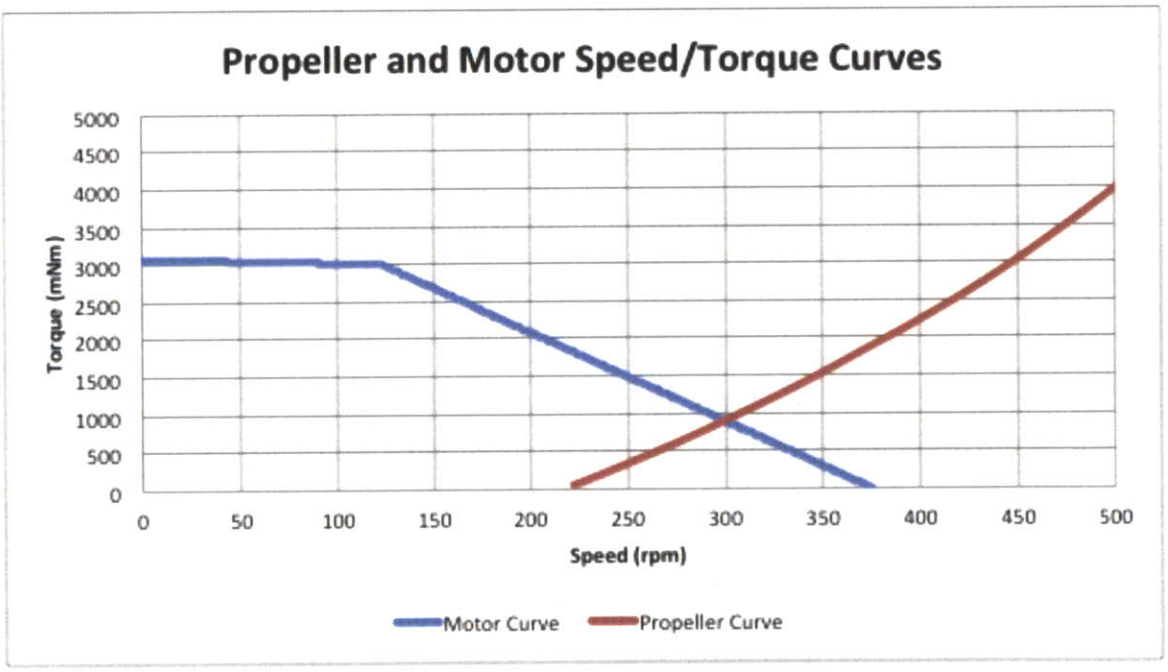

Figure 6.4: Propeller and Motor Speed/Torque Curves

To determine the Propeller Speed/Torque Curve, the torque coefficient (K_Q) values at different advance coefficients were taken from the propeller's performance curve (Figure 5.8). The propeller speed was determined using the equation for the advance coefficient as outlined in Chapter 5. To determine the torque, the following

equation was utilized, where ρ is the density of seawater (1025 kg/m^3), n is the propeller speed in rps and D is the propeller diameter in m.

$$Q = K_Q \rho n^2 D^5$$

It can be seen that at approximately 300 rpm, the two curves overlap. To be exact, at 300 rpm the motor has a torque of 892.9 mNm and the propeller has a torque of 902.3 mNm.

The SL-MTI BLOV-29-13-12P motor is small and will easily fit in SPYROS' hull. The full specifications of the motor can be found in Appendix D. The weight of the fully housed motor is 3115.6 g, has a diameter of 0.07861 m and a length of 0.17079 m ("SL Montevideo Technology," n.d.). It is a 12-pole motor, which allows for low speed/high torque operation, which as stated earlier in the chapter is a desirable attribute. The motor is also highly efficient, with an efficiency of 87%. The motor efficiency can be calculated by the following equation.

$$\eta_m = \frac{VI}{VI + R_m I^2} \times 100\%$$

In the above equation, the numerator represents the power output of the motor and is calculated by multiplying the voltage by the current. The denominator is the power input, which adds the power required to overcome the internal resistance of the motor R_m, which has a value of 0.5 Ohm for this motor.

7 Battery Selection

Once the electric motor is selected, the power requirements for propulsion are now known. For the SPYROS design, 11 V and 3.19 A (equating to 35.1 W of power) is required to provide the necessary electrical power to propel SPYROS through the water. Since the electrical generator requires air for combustion, it would only be able to provide direct electrical power when the AUV is near or at the water surface. Therefore batteries will be required for power when SPYROS is submerged.

7.1 Battery Types

Prior to commencing with further discussion on batteries, one must outline the difference between a battery and a cell. A cell is a single voltage-producing unit, while a battery is composed of two or more cells. There are currently many different types of cells on the market. These cells can be separated into two different categories; primary and secondary cells. Primary cells have only one charge and cannot be recharged. These types of cells include alkaline cells such as AA, AAA, C and D cells used in many electronics. Secondary cells can be recharged. Research into this industry has increased considerably with the advances in portable electronics such as laptops, tablets and mobile telephones. Since the battery onboard SPYROS will be recharged by the onboard generator, a secondary cell must be chosen.

There are currently many different secondary cells on the market. They range from the large Sealed Lead Acid (SLA) batteries used in automobiles to small Lithium Polymer pouches used in cell phones. They all have many different characteristics, from recharging method to energy density. Since space and weight onboard SPYROS is limited, energy density is the primary driver in battery selection. Figure 7.1 shows a typical energy density chart, showing the operating regions of different forms of secondary cells.

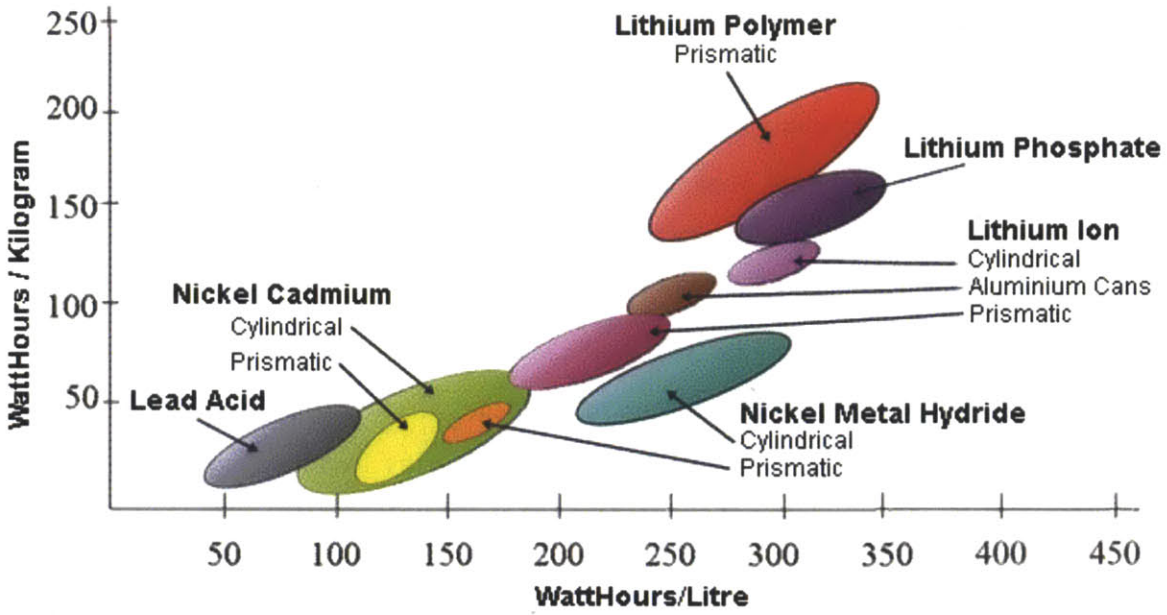

Figure 7.1: Relative Energy Densities of Common Secondary Cells ("Battery and Cell Chemistries. Battery primer.," 2005)

From the above figure, it can be seen that the primary point of investigation for AUV applications would be Lithium Polymer cells. They boast both the highest Specific Energy (Wh/kg) and Energy Density (Wh/L).

7.2 Battery Cell Options

Current AUVs typically use batteries built from 18650 Lithium Ion cells. This is the choice of cell for both the TETHYS and ODYSSEY IV AUV's (Morash, Polidoro, & Hover, 2007). They are cylindrical shaped cells typically used as a power source for laptop computers. According to Morash, 18650 cells can have an energy density of 182 Wh/kg. These cells are also very small and can be configured in a variety of ways to obtain the required power output. However, the energy density is based on the volume of a cylinder, when the cells are arranged to make a square battery pack, a significant amount of volume is lost between the cells resulting in a typical "finished pack" energy density that is significantly lower. Since they are widely used, they also are inexpensive compared to other cells. However, since the cells are small and do not have easily attachable leads the cells become increasingly complex as the

battery becomes larger. Another disadvantage of 18650 cells is the requirement for a battery management system. All Lithium battery systems require some form of management system to ensure that the batteries do not exceed voltage and thermal limits, and monitor charging operations. Anecdotal evidence shows that battery monitoring systems for 18650 cells do not scale well for large batteries, therefore leading to possible safety issues.

There are Lithium battery packs on the market that already pre arrange lithium cells for a greater output power. Traditionally these batteries are more expensive than 18650 or similar cells, but are designed for easy scalability and are matched with a proper battery management system for increased safety. Below is a table of 18650 cells compared to two different lithium battery packs currently on the market, the Corvus Energy AT3300-250-12-SB ("Corvus Energy," n.d.) and the Panacis Modular Lithium Battery System (*Modular Lithium Battery System*, 2012).

Name	Voltage (V)	Capacity (Ah)	Weight (kg)	Specific Energy (Wh/kg)
18650 cell	3.6	2.35	0.0465	182
Corvus Energy AT3300-250-12-SB	11	300	41	81
Panacis Modular Lithium Battery System	11.1	90	6	167

Table 7-1: Lithium Battery Comparison

Figure 7.2: From Left: 18650 cells (Buchmann, 2012), **Corvus Energy AT3300-250-12-SB battery and Panacis Modular Lithium Battery System**

It must be noted that to calculate the specific energy of a battery the casing and wiring to connect the battery must be taken into account. This is the reason why the Corvus and Panacis batteries have a lower specific energy than the single 18650 cell. What makes the Panacis battery even close to the individual cell is that it has a soft case and starts with cells that have a very high energy density. Most advanced battery systems have a hard case, as seen with the Corvus Energy battery in Figure 7.2. This case provides additional protection for the battery, but significantly increases the battery weight, which lowers its specific energy. The Panacis battery only has a soft case, which provides less protection but greatly reduces the battery weight. Since weight and size are of great importance to SPYROS propulsion system design, the Panacis battery will be utilized.

7.3 Battery Modification and Arrangement

Of great importance when working with any lithium cell battery system is the battery performance over its cycle life. A cycle is defined as the period starting with the battery fully charged, then discharging and then full recharging again. Figure 7.3 is a graph of the cycle performance of an actual Panacis battery. The three different curves represent different Depths of Discharge (DOD), which characterizes how much of the battery's charge is utilized when being discharged. A 100% DOD means that the entire battery is discharged before being recharged, while a 20% DOD means only 20% of the battery's charge is utilized prior to recharging. As illustrated on the graph, battery life (number of cycles) can be extended by limiting the amount of discharge during each cycle. However, since battery capacity must be maximized for long distance AUV propulsion, and so maximum DOD will be utilized while reducing overall battery life.

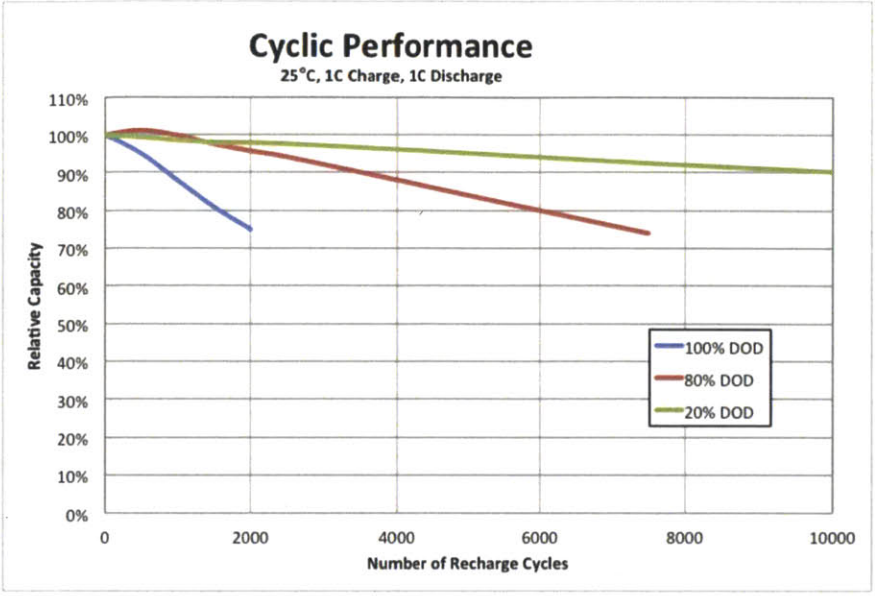

Figure 7.3: Cycle Performance of an actual Panacis Battery

Since overall battery life is not a priority in the AUV design, there are methods to increase the capacity of a lithium battery. The drawback is further degradation of the effective number of cycles. Currently, most advanced lithium cells utilize a mix of Nickel, Cobalt and Manganese as the cathode material for the lithium cells (NCM cells). By changing the NCM mixture, one can increase the capacity of the cell. This increase in capacity is coupled with a decrease in stability (cycle life), as seen in Figure 7.4.

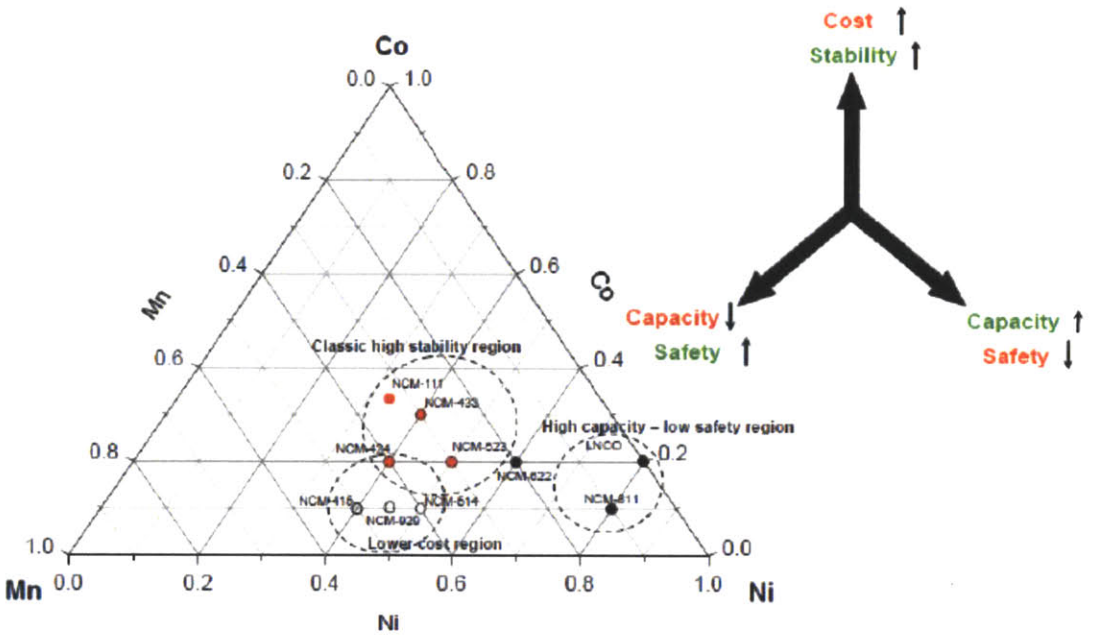

Figure 7.4: NCM cell mixture triangle (Tichy & Friel, 2012)

The cells in the Panacis Modular Lithium Battery System are comprised of NCM-111 cathodes. By changing the cathode to a NCM-622 mixture, the capacity can be increased, but with a lower stability (cycle life). There are other advanced methods that can increase the capacity of a lithium cell, including thinning the electrode material and changing the makeup and geometry inside the cell. By making these changes, Panacis can increase the capacity of the battery from 75 Ah to 90 Ah while maintaining the same dimensions and weight of the battery. By doing this, however, the maximum cycle life at 100% DOD falls from 2000 cycles to approximately 500 cycles.

Now that the batteries have been modified to maximize capacity, one must determine the correct configuration of the batteries to power the propulsion system's electrical motor. There are two ways to connect batteries together, in series and in parallel. These configurations are illustrated in the following figures.

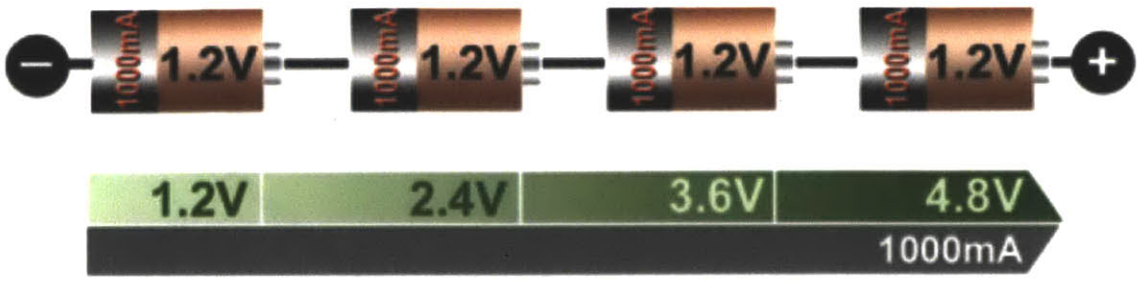

Figure 7.5: Batteries in Series (Buchmann, 2012)

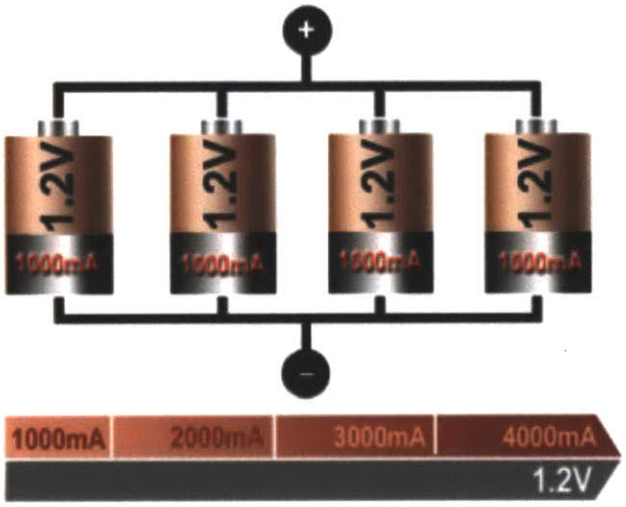

Figure 7.6: Batteries in Parallel (Buchmann, 2012)

As the figures demonstrate, if identical batteries are connected in series, the voltage increases by NV, where N is the number of batteries and V is the individual battery voltage. The current of the batteries remains constant throughout in a series connection. Parallel connection offers the opposite result. The voltage of the system remains constant, however the current increases with the number of batteries in the system.

These two methods can be combined to create a battery with the required voltage and current. This can be seen in Figure 7.7. In this figure, by connecting two batteries in series with two batteries in parallel, both the voltage and current was doubled.

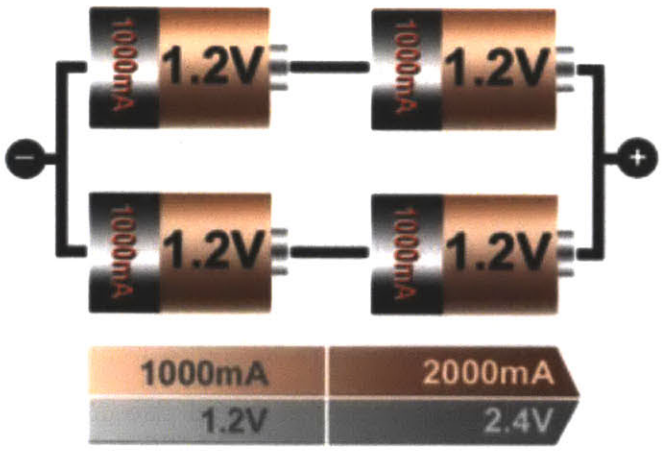

Figure 7.7: Batteries in Series/Parallel Configuration (Buchmann, 2012)

Series/Parallel configuration is used extensively in AUV battery design. Morash describes using 24 supercells with 27 18650 cells with a current capability of 4.6 A and voltage capability of 3.6 V connected in parallel to achieve a current of 120 A (27 x 4.6 A). These supercells are then connected in series to achieve a voltage of 90 V (24 x 3.6 V) (Morash et al., 2007).

The battery systems selected (Corvus and Panacis) were chosen primarily due to their low nominal voltages. This allowed for only a parallel configuration requirement of the battery as the voltage (11 V) can be matched directly to the motor. Utilizing only the parallel configuration also reduces the number of batteries required. As seen in Figure 7.7, four batteries are required to double the voltage and the current. If this figure were to be expanded, four more batteries would be required to double the current while maintaining the same voltage. If the voltage were also to be doubled, eight further batteries would be required. It is therefore advantageous to match the voltage directly and only add batteries in parallel to increase the current (and therefore the capacity) of the overall battery system.

Placing large batteries in series or in parallel creates safety issues. In series batteries, it is possible to hook up too many batteries in series, therefore increasing the voltage to a level above which the protection circuitry can handle, leading to

possible fires. In parallel, it is possible to have batteries connected together with different voltages, which could lead to fire and other damage since this could lead to extremely high currents running between the different batteries. It is therefore highly important to ensure all batteries in parallel have the same voltage. Certain battery manufacturers do not recommend connecting batteries in parallel for this reason. Panacis, however, has incorporated a balancing circuit in the battery management system that allows batteries to be connected in parallel regardless of their state of charge. This speeds up installation and also increases safety in the event the installer accidentally mixes charged and discharged batteries together.

7.4 Battery Charging

There are two stages to charging a lithium battery: constant current charge and saturation charge, as seen in figure 7.8. In this drawing, there are two other stages, but they can be ignored as they deal with having the battery in standby after its been fully charged.

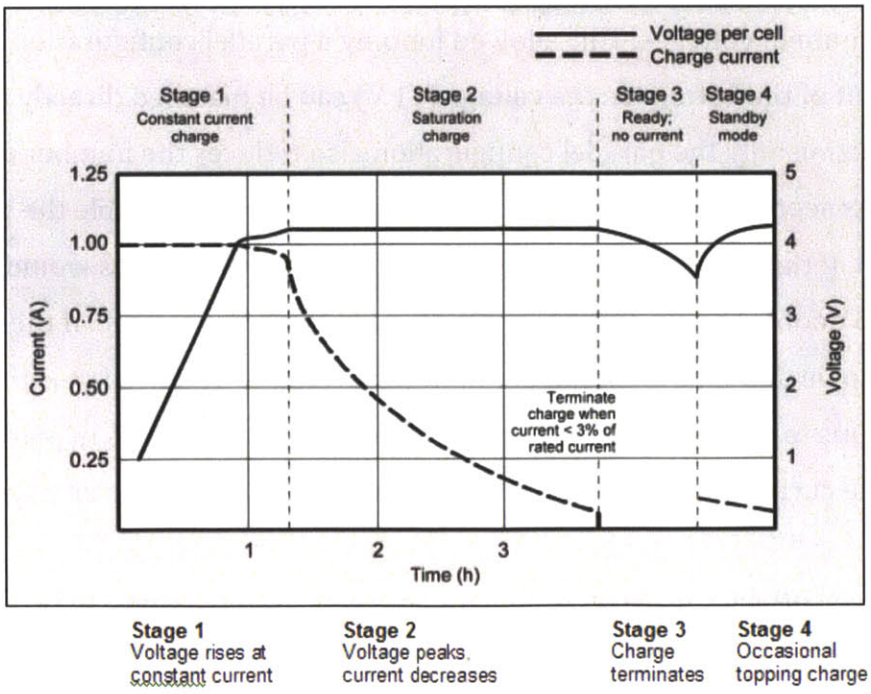

Figure 7.8: Charging States of Lithium Batteries (Buchmann, 2012)

In a traditional lithium battery charger, a constant current is fed to the batteries. When this occurs, the battery's voltage will increase until it reaches the maximum battery voltage (in the case of figure 7.8, this will be 4.2 V). Once this voltage is reached, the saturation charge begins, where the charger's current is slowly decreased until the battery is at 100% capacity. From figure 7.8, this takes about 4 hours to complete for a standard lithium battery.

There are ways to decrease the charge time of a lithium battery. In figure 7.8 at the end of stage 1, the battery is at the proper voltage and at 80% capacity in about 1.25 hours. It is common to complete the charge at this point and continue operating the battery. This is called a "fast charge".

One must remember that the length of the saturation charge changes with the amount of current being used by the charger. The higher the charge, the greater the saturation time, however this normally is not important, as the fast charge will be complete at a quicker rate. The reverse is also true. If the charger is using a low charge rate, the constant current charge will take longer, but the saturation charge will be shorter. This can reach the point to where the battery is essentially 100% charged by the end of the constant current charging. This point occurs with lithium batteries if a charge rate of less then 1C is utilized (Tichy & Friel, 2012).

This poses some issues with respect to the SPYROS design. It was decided early in the process to utilize a 1 kW generator for charger for the onboard batteries. The Panacis batteries charge at a voltage of 12.6 V, which means the maximum available current is 79.4 A. Therefore, if this were to be used as a 1C charge, then the battery would have to be a 79.4 Ah battery. This is equivalent to only one Panacis Modular Lithium Battery System battery. Therefore, the charge rate of the battery system in the case of SPYROS is limited by the generator's available output energy, not by the batteries.

Developments are currently underway with new battery chemistries that will charge much quicker then conventional lithium batteries. These batteries are currently still in the design and prototype phase and therefore not available for use onboard SPYROS.

8 Onboard Generator System

During the research phase of this thesis, it was discovered that another group at MIT, under the tutelage of Dr. Doug Hart, had been working on a similar problem. They wished to build a generator to put onboard a REMUS AUV to increase its range and endurance. Their solution was very similar to the one under development for SPYROS and therefore the author decided to work in conjunction with Dr. Hart's group in order to develop an AUV onboard recharging system. The following chapter details the results of the group's study (Dorsch et al., 2012).

Figure 8.1: 3D Model of Recharging System

8.1 Rail Support System

In order to minimize any changes to the hull of the REMUS AUV, a rail system was designed to provide support to all generator system components. Like a clamp, the rail system has two end plates that apply force on the ends of the hull. These end plates are held in place within the hull by friction in order to reduce the number of penetrations into the hull. There are two rails running the length of the support system, which all of the generator systems are connected for support. The full assembly can be seen in figure 8.2.

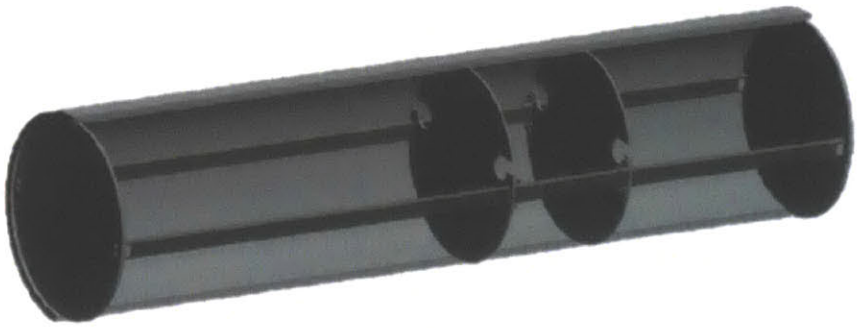

Figure 8.2: AUV Generator Rail Support System

8.2 Generator Engine

As stated in Chapter 3, the generator that was used in the design was the Honda EU1000i generator, which uses a Honda GXH50 engine as the prime mover. This engine was selected primarily due to the fact that it was readily accessible and that published specifications of the engine were easily available.

Since space within the AUV is of primary importance and fuel tanks will take up a large volume of interior space, the fuel consumption of the engine must be determined in order to calculate fuel requirements. In order to determine the correct value, both published values and engine tests were compared. From this, it was determined that the fuel consumption at full load is 0.01 L/min. The air flow rate was also determined to be 1.5 L/s by utilizing the stoichiometric air/fuel ratio of 14.7.

Figure 8.3: Honda GXH50 Engine ("Honda Engines - Small Engines Models, Manuals, Parts & Resources," n.d.)

Since this engine is normally designed for stationary use, the designers had to ensure it would be able to withstand the motions imparted onto the engine by ocean waves. To do this, the engine was placed on a rig, started and then rotated in both roll and pitch. It was found that the engine operated normally in pitch motion (40° forward with the generator facing upwards and 13° backwards with the generator facing down). In roll motions, however, it was found that the engine would stop running if excessive roll motion were encountered. The testers found that the engine would stop at roll angles greater than 40°. To mitigate the problem, an analysis of the REMUS AUV was conducted to determine at which WMO Sea State would cause a 40° angle of roll. It was found that the engine would be able to run on REMUS at a sea state of four. Since both SPYROS and REMUS use a Myring Body as the basic hull geometry, it can be assumed that SPYROS' results would be similar to REMUS.

One of the main drawbacks to using the GHX50 engine is that it is a recoil start engine. Since there is no way to pull the recoil line while at sea, another method of starting the engine was determined. The method used requires applying a high current voltage to a specially designed generator in order to turn the generator into a motor. Since the generator is directly coupled to the engine, the generator will turn the engine and allow for ignition. To calculate the power required to turn the

generator, the torque required to turn the engine at idle speed of 3000 rpm was determined to 2.75 Nm. To get the generator to apply this torque, a peak power of 865 W is briefly required. This is applied to the generator utilizing a high current stand-alone battery pack. Also fitted are stepper motors on the engine throttle and choke. These motors are automatically controlled by the onboard control system to allow for proper conditions for engine startup and operation.

Another required modification of the engine is the cooling system. The stock engine is air cooled with an onboard fan, which would not provide cooling inside the enclosed AUV. Extensive study into replacement cooling methods was conducted. Firstly, a study of the heat production of the engine was conducted. It was found that the exhaust system produced the highest heat, with temperatures ranging from 144°C to 190°C. Since this is dangerously high, these sections will be insulated for safety.

It was then determined that for effective cooling of the engine, 3 kW of heat will need to be dissipated from the engine to the ocean. It was determined that the best course of action was to utilize an open cooling system, where water is pumped from the ocean into a cooling block attached to the engine, as seen in figure 8.4. Using a pumping rate of approximately 0.15 L/s, this block will effectively remove the 3 kW of heat to maintain a temperature of approximately 70°C in the engine compartment.

Figure 8.4: Model of GXH50 Engine with Cooling Block Attached

This temperature may be low enough to ensure proper engine operation, but is still too high for all the electronic components inside the AUV. To ensure the safety of the electronics, a thermal barrier was designed to isolate the engine from the rest of the AUV. Figure 8.5 shows the thermal barrier, which is made of 3/16" aluminum sealed with a neoprene cork ring. As seen in the figure, there are two cut outs which are designed for the passage of fuel, oil and electronic lines, which would be fitted with neoprene grommets in order to restrict the airflow in and out of the engine compartment. Figure 8.6 shows the difference in the average air temperature within the AUV with and without the thermal barrier. A significant difference can be seen outside of the engine compartment, which would allow for proper operation of electronic components in the AUV.

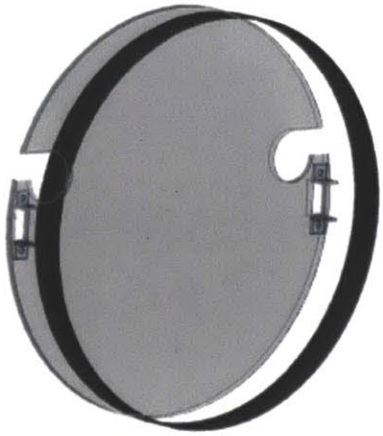

Figure 8.5: Proposed Thermal Barrier to Isolate Engine

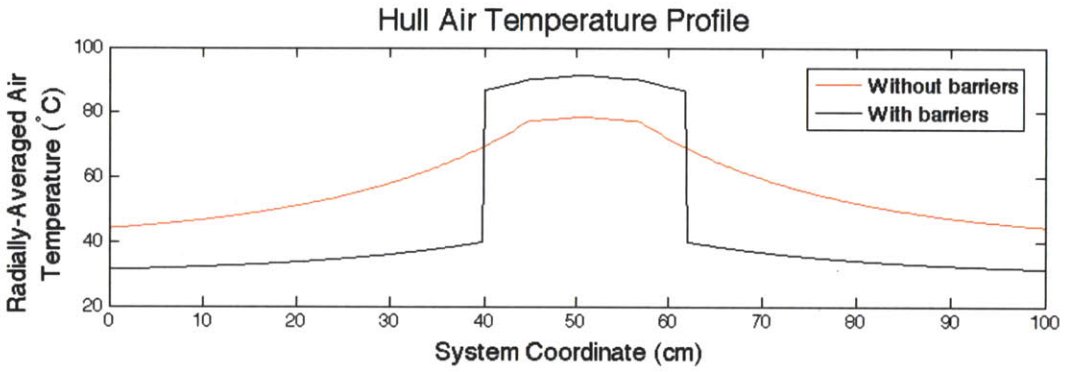

Figure 8.6: Hull Air Temperature Profile inside the AUV with and without Thermal Barriers

Lastly, the engine vibration was investigated. The vibration of the engine was measured at both full load and no load conditions. Figure 8.7 illustrates the Fourier analysis done for both tests. From these figures, it can be seen that a conservative vibration range would be between 80 and 95 Hz.

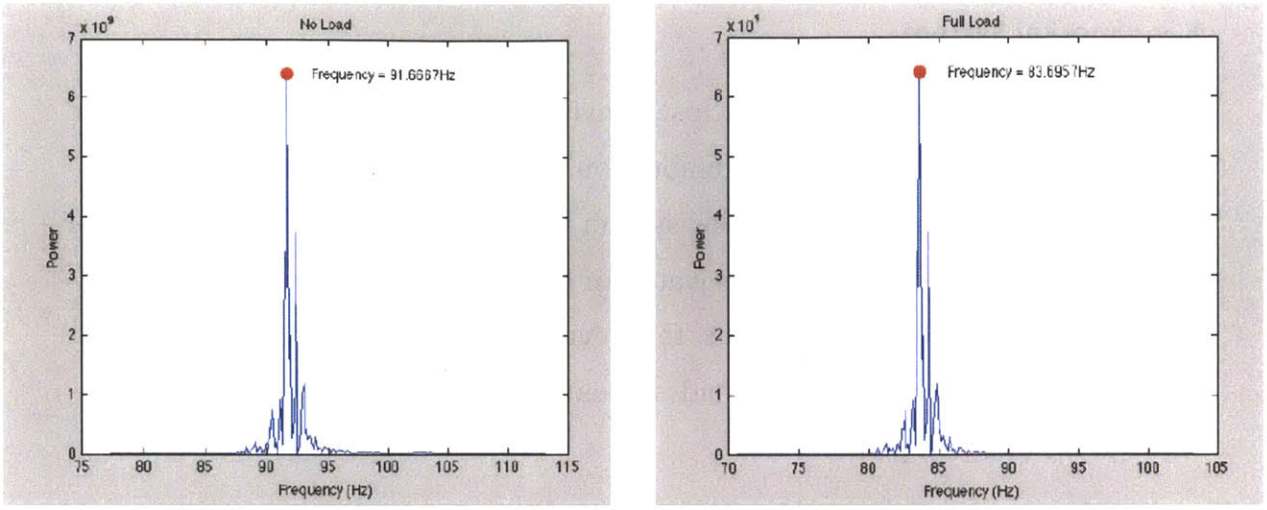

Figure 8.7: Engine Vibration Frequencies at No Load (Left) and Full Load (Right)

To dissipate this vibration, stud type mounts were utilized in the design. From the vibration tests, it was determined that mounts with a low spring response and a damping coefficient of less than 109 Ns/m was required. Silicone gel mounts from Advanced Antivibration Components were utilized for damping. Customized brackets were designed to ensure that the engine is properly connected to the mounts and then to the rail system that was designed to hold all the generator systems inside the AUV, as seen in figure 8.8.

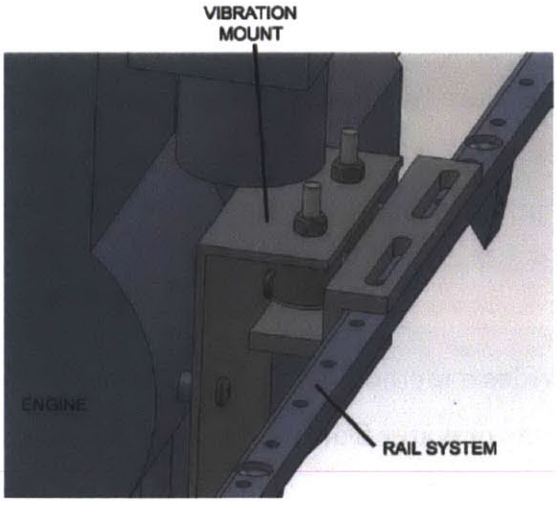

Figure 8.8: Vibration Mounting Layout

8.3 Snorkel System

Since the engine is located in an enclosed environment, there must be an avenue to allow air to flow to the engine for combustion. In this generator system, this is accomplished through a fixed snorkel system. This system not only provides air for engine combustion, it also provides water for buoyancy compensation in the fuel tanks and cooling, allows the exhaust to be evacuated from the AUV and provides extra buoyancy on the surface and aids in neutral buoyancy when submerging through the onboard plenum.

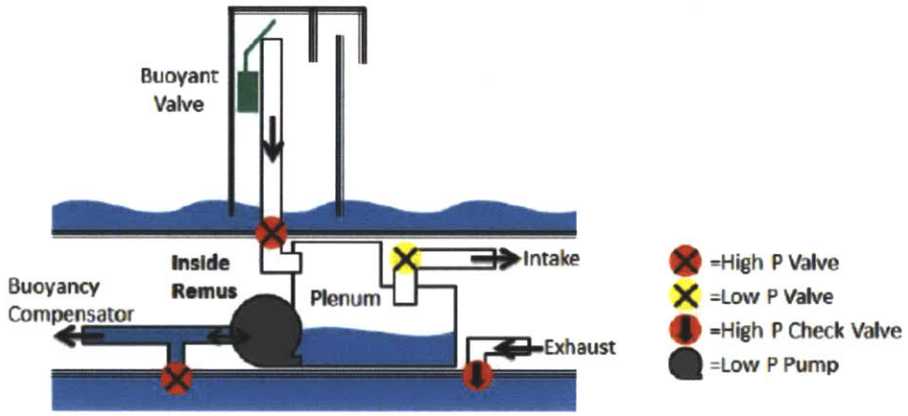

Figure 8.9: Snorkel System when operating at the surface

As seen in figure 8.9, there are two main sections to the snorkel system: the outer snorkel which provides air for combustion, and the inner portion that consists of the air plenum, a two way pump, exhaust system and a series of valves to maintain proper operation.

The outer snorkel provides a method of allowing air to enter the AUV, while preventing large amounts of water from accidentally entering the combustion air path. The outside of the outer snorkel contains a baffle, which provides a tortuous route for water to enter the inner portion of the snorkel. Holes around the base of the outer snorkel allow for any water collected in the outer shell to be released into the environment when the AUV surfaces. There is also a buoyant valve, which

provides a loose seal for the snorkel in the event the AUV is hit with a large wave. For pressure compensation reasons, this is not a tight valve and some water will pass into the plenum. The reason for this will be discussed later.

The inner portion of the snorkel system contains the plenum, as well as the valves and lines for proper operation. The plenum provides a reservoir of air for the engine in the event that the snorkel is temporarily submerged. A two-way pump is fitted in this section, which pumps water in and out of the plenum, as well as providing water to the fuel system buoyancy compensator. Finally, there is a line running from the plenum to the air intake of the engine, as well as a line for the engine exhaust to vacate the AUV.

The snorkel system operates in four different modes: at the surface when engine combustion takes place, when the snorkel is temporarily submerged while the engine is running, when the AUV is ascending or descending and when the AUV is submerged. The first mode of operation is illustrated in figure 8.9. In this mode, air from the atmosphere enters the plenum from the outer snorkel. From the plenum, the air enters the intake into the engine. At the same time, any water in the plenum is pumped out and water from the ocean is being pumped into the fuel system buoyancy compensator and the engine exhaust is vented to the ocean.

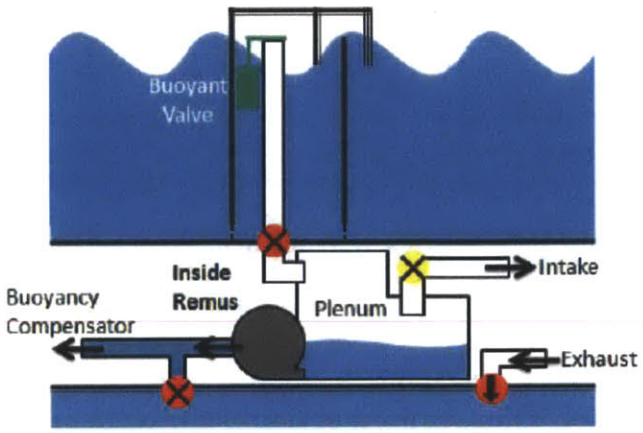

Figure 8.10: Snorkel System when Temporarily Submerged

Figure 8.10 illustrates the second mode, when the snorkel is temporarily submerged. In this mode, the outer snorkel is flooded, causing the buoyant valve to provide a loose seal on the snorkel. Any water accumulation in the plenum is pumped out and air is being provided to the engine from the plenum until this extra reservoir is used up. Since the engine is still running, water is being pumped into the buoyancy compensator and the engine exhaust is still being vented.

In the third mode, the AUV prepares for surfacing or diving. Figure 8.11 illustrates when the AUV is preparing for diving. In this diagram, the engine is no longer requiring air, so the intake valve is shut. The water pump begins to fill the plenum with water to provide extra ballast for the AUV. In this mode, there is no water being provided to the buoyancy compensator and the exhaust valve is shut. The reverse happens when the AUV surfaces. The pump removes water from the plenum and the correct valves open to allow air to enter the plenum and prepare for engine startup.

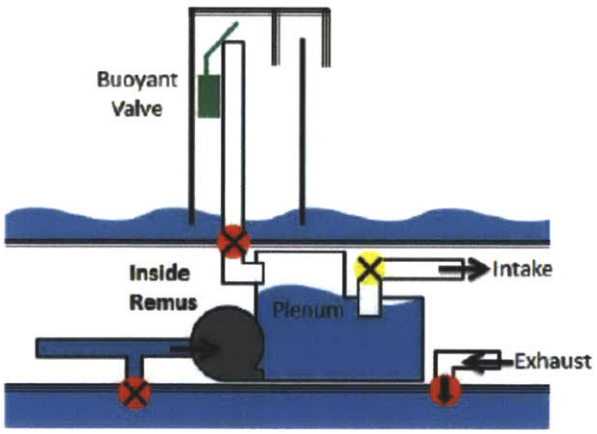

Figure 8.11: Snorkel System when Preparing to Dive

The final mode of operation is when the AUV is completely submerged. In this mode, the plenum is completely filled with water to provide extra ballast. The outer snorkel will be completely flooded, causing the buoyant valve to shut. As stated earlier, this valve does not provide a complete seal, which allows the inner snorkel

to also flood in this mode. This allows for pressure compensation and the ability to use lighter materials for snorkel construction, as water pressure will not be an issue. The pump and engine will be shut down and all the necessary valves will be closed.

Considerable discussion and analysis went into the determination of the height of the outer snorkel. A balance needed to be obtained between having the ability to withstand waves with a high snorkel and minimizing to height of the snorkel to minimize vehicle drag. To model the snorkel, a maximum wave height of 2 m was utilized. Without any form of plenum to increase the buoyancy, it was found that a snorkel of greater than 1 m would be required for snorkel operations. This was determined to be unacceptable. However, with the plenum installed, two advantages become apparent: extra buoyancy is provided to the AUV, allowing it to ride higher on the waves and the reservoir of air in the plenum means the snorkel does not have to be above the surface of the water 100% of the time. If the plenum is installed, only a 0.3 m snorkel is required to have the snorkel out of the water 50% of the time. The plenum is designed such that it can provide air to the engine for the other 50%.

8.4 Fuel System

To design the fuel system for the REMUS AUV generator, the group was given a large constraint on their design; that the fuel system must in no way impart any moment on the vehicle. This meant that as the fuel was being spent, the weight of the fuel must be replaced in some means. Since fuel is lighter than water, water alone could not be used. The solution was determined to be a water/air compensating fuel tank, where when fuel is burned by the engine, it is replaced with water and air in such a mixture that there would be no induced moment on the vehicle.

This water/air compensation is accomplished by using a series of bladders in two fuel tanks, one forward of the engine and one aft. Initially, the fuel bladder is full and encompasses the entire inner volume of both fuel tanks. As fuel is consumed, water

and air from the snorkel system is used to fill the other two bladders; water in the bladder below the fuel bladder and air fills the space above. This set up can be seen below in figure 8.12. In this figure, the fuel bladder is black and the water bladder is blue.

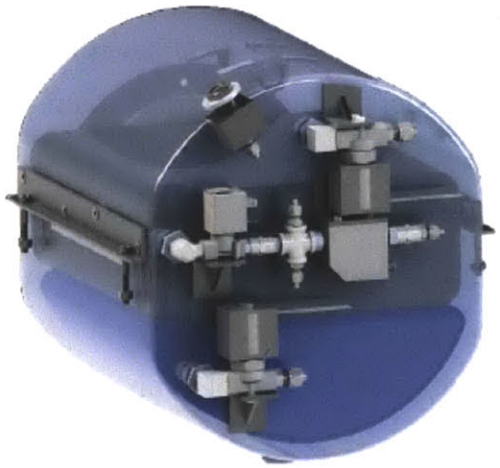

Figure 8.12: Fuel Tank System with Fuel and Water Bladders

To ensure proper weight distribution, a fluids analysis was conducted on the fuel system. It was determined that in order to not induce any moment, the lost weight of the fuel must be replaced by water and air in a 70/30 mixture. To accomplish this correct mixture, a series of valves are utilized which are timed by the control system, seen in figure 8.13.

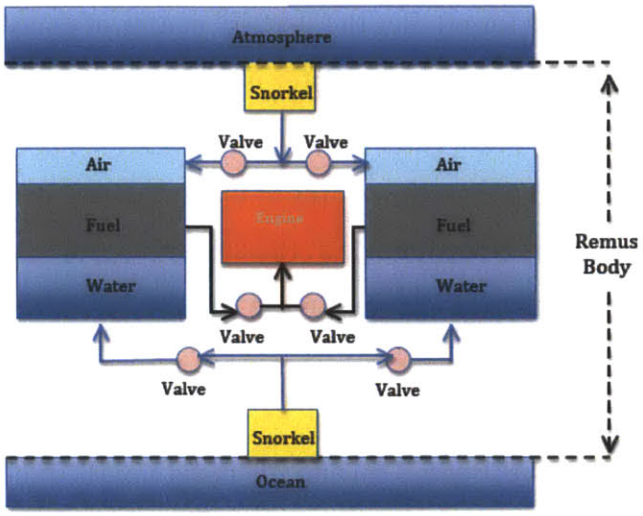

Figure 8.13: Fuel Tank and Valve Layout

Fuel will be taken from one tank at a time, and only 10 mL of fuel will be taken from a tank before switching. During this 10 mL of fuel draw, the first 3 mL will be replaced by air drawn from the snorkel. Once the 3 mL of fuel is consumed, the air valve closes, and the water valve opens. As the remaining 7 mL of fuel is consumed, water will fill the lower bladder of the system. Once this is complete, both the fuel and air valves will be closed and the whole operation will resume with the opposite fuel tank. This process is illustrated in figure 8.14.

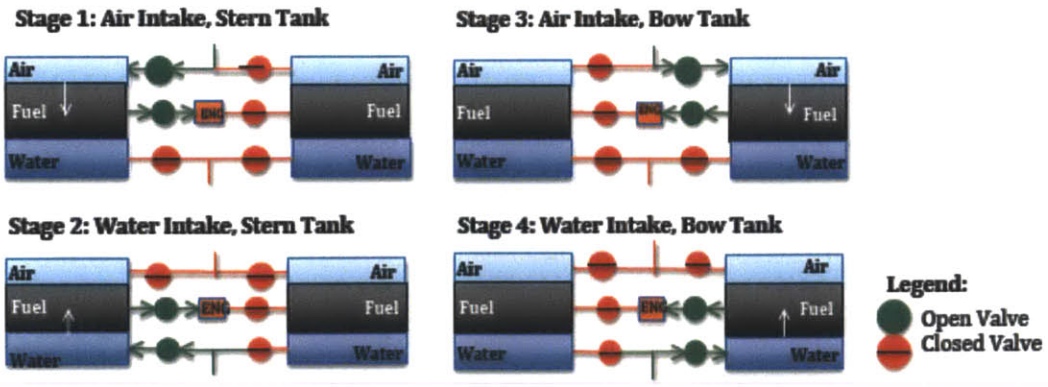

Figure 8.14: Fuel System Valve Timing

During this process, it was found that the vertical center of mass of the fuel tanks would lower due to the fact that heavy water is replacing lighter fuel low in the AUV. An investigation into the center of mass showed that at its worst point, the center of mass lowers 0.05 m. At all points the center of mass remains below the center of buoyancy, allowing for positive stability at the surface. Future studies will be conducted to determine further changes in the vehicle dynamics caused by this phenomenon.

Piping losses were also investigated during the design of the fuel system. The Honda GXH50 engine has its own onboard fuel pump, so the design team wanted to ensure that the designed piping would not lead to losses in excess of the fuel pump's capability. After the examination, it was found that with an approximate pipe length of 0.25 m, it was found that the losses equated about 1 Pa, low enough not to affect fuel flow into the engine. Finally, the effect of vehicle pitch on the fuel pressure was examined. It was found that with an increase in pitch of 15° would lead to a change of 0.1 Pa in head pressure in the fuel tanks, not enough to compromise fuel flow into the engine.

8.5 Control System

Since many different systems must work together seamlessly in order for the recharging system to operate correctly, a control system must be integrated into the recharger. This control system must also coordinate with the AUV's onboard systems in order to know when to charge as well as to monitor the environmental conditions that may hinder the recharging system performance.

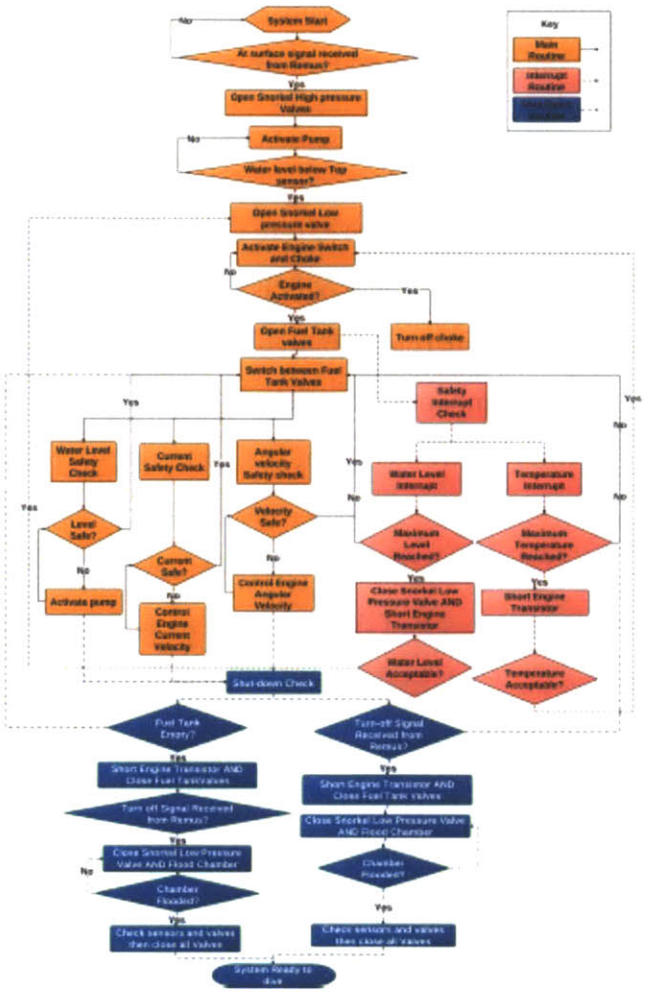

Figure 8.15: Control System Operational Flow Chart

Figure 8.15 above illustrates the operation of the control system during the recharge cycle. The operational cycle commences when the AUV sends a signal to the control system that indicates that the vehicle has surfaced. When this signal is received the control system preps the snorkel for operation by opening the water valves and using the water pump to empty to snorkel and plenum. Once the level sensors in the plenum indicate that the plenum is empty of water, the intake valve to the engine will open, allowing air to flow to the engine. At the same time, the engine will be prepped for combustion by using the fitted stepper motors to adjust the throttle and choke of the engine for ignition. The fuel system will also commence operation by opening and closing the correct valves as stated in section 8.4. Starting

of engine will then commence by back driving the generator to turn the crankshaft and commence ignition. Once the engine is running, the power generated will recharge the batteries.

When the generator is running, there are safety checks happening on a consistent basis. This includes a water safety check, which monitors the water level in the plenum. If the water level reaches the high level mark, then the engine will be shut down in order to protect it from water ingestion. A current safety check ensures that the generator produces the required current for optimum battery charging. If the current is out of range, a signal is sent to the throttle stepper motor to increase or decrease the engine speed to bring the current back into range. An angular velocity safety check certifies that the speed of the motor is within a specified range. The control system measures the back EMF of the generator, which corresponds to the engine speed. If the back EMF is out of range, the throttle will be altered to bring the engine back into range. There is a temperature safety check that ensures the engine does not overheat and cause damage to itself and other AUV components. If the air temperature in the engine compartment reaches 85°C, the control system will shut down the engine. Temperature sensors on and around the engine will be constantly monitoring the temperature and the throttle will be changed accordingly if the temperature is outside the required range. Finally, the fuel tanks are monitored and the control system will shut down the engine if the fuel tanks empty.

When the AUV signals to the control system that the batteries are fully charged, the ignition operation will happen in reverse. The engine will be shut down and all fuel tank valves will be closed. After this operation is confirmed, the plenum will be filled with water and the AUV will be ready to dive.

8.6 Power Management System

The power delivered from the generator is not what is required for battery charging. The generator produces three-phase AC power with 120 V and 8.3 Amps ("Honda EU1000i generator," n.d.). This must be converted into DC power with 12.6 V and 79 Amps for proper battery charging power. The output signal will be rectified and then passed through a transformer to ensure the proper output power. The MIT team also contracted out the design of a power regulator to ensure that the voltage remains at the level required for proper battery charging. This power is then fed into the Panacis battery system for charging, with the monitoring system ensuring an equal charge for each battery.

9 Integration and Evaluation

Now that all the major components of SPYROS' propulsion system have been chosen, they must now be integrated together to maximize vehicle range while reducing the overall length of the total system. To accomplish this, a MATLAB script was written to show how altering different variables in the propulsion system design would alter the range and size of the system. This script and its output are found in Appendix F.

9.1 Battery Integration

Before determining the correct number of batteries to place onboard SPYROS, the number of batteries that can fit inside the vehicle diameter must be determined. From Panacis, the battery has a width of 0.25 m and a height of 0.05 m. Using these dimensions and a hull diameter of 0.34 m, it can be seen in figure 9.1 that four batteries can be stacked at any one position within the mid-body section of SPYROS.

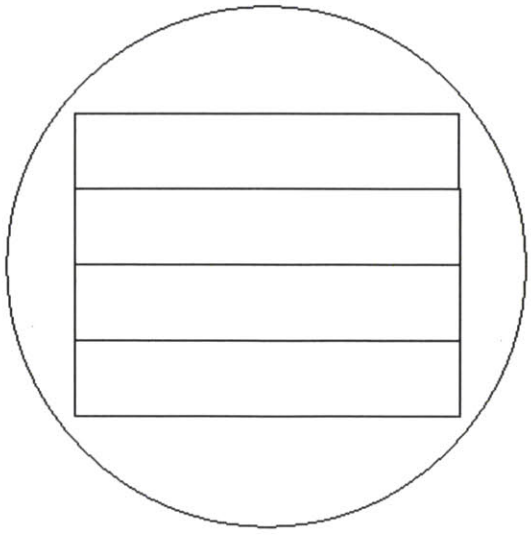

Figure 9.1: 2D slice of AUV mid-body showing four batteries stacked vertically

With this information, all possible battery configurations will be multiples of four in order to minimize the length of the propulsion system. Furthermore, in order to

reduce any moment on the AUV, it would be beneficial to balance the number of batteries forward and aft of the recharger, which would mean that a multiple of eight is required. Due to length constraints on SPYROS, this would limit the number of batteries to either 8 or 16.

Further investigation shows that using 16 batteries would cause the length of the AUV power system to be greater than the length of SPYROS' mid-body. Utilizing a Myring B form and a length to diameter ration of 10, the mid body length of SPYROS is 1.87 m (Myring, 1976). Utilizing SolidWorks drawings converted into IGES format for use in Rhino, it was determined that the generator system length minus fuel tanks is 0.7 m. The single battery has a length of 0.27 m, which would give a total battery length of 1.06 m if the batteries were stacked in groups of four. The batteries and generator would then have a length of 1.76 m without any fuel tanks, which is very close to the maximum length. Using eight batteries gives a total battery length of only 0.53 m, which means the power system length will be 1.23 m. This gives sufficient allowance for fuel tanks in order to obtain a sufficient vehicle range.

As stated in chapter 7, all batteries will be connected in parallel. Each battery has an onboard management system to connect the battery to the load and charger and ensures safe operation of the system. A sample diagram of how the batteries will be connected was provided by Panacis and can be seen in Figure 9.2. This example is for the 75 Ah battery, however the 90 Ah battery chemistry would be used for SPYROS.

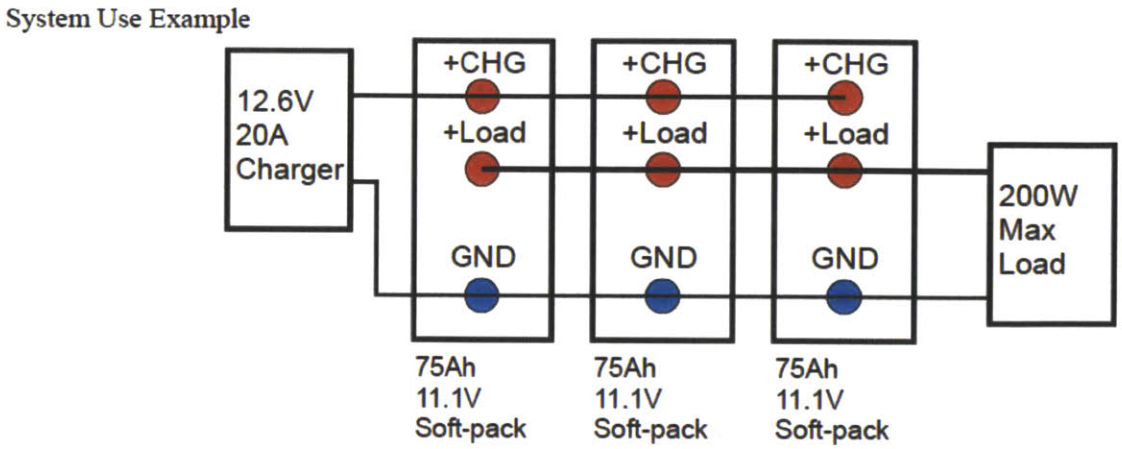

Figure 9.2: Example of Battery System Layout (*Modular Lithium Battery System*, 2012)

The MATLAB script also allows the user to input the depth of discharge (DOD) for each battery. This allows for some buffer in available battery power in the event that the sea conditions at the time of surfacing does not allow for the running of the generator. Running at a lower DOD also allows for extended overall life of the battery, as seen in figure 7.3.

9.2 Fuel Tank Integration

The one major change of the generator system design by the MIT Rapid Development Group (Dorsch et al., 2012) is the size of the fuel tank. Since SPYROS' missions and onboard systems are different, a different amount of fuel is required. To develop this, the same MATLAB script as described above was utilized. Firstly, the published full load fuel consumption of 0.01 L/s for the Honda GHX50 engine is utilized. Next, the length of engine runtime per charge needed to be calculated. It is assumed that a charge current of 12.6 V is required, therefore the maximum current from the 1 kW generator is 79.4 A. However, not all of this current will be used for charging the batteries. In order to continue to provide power for propulsion and hotel loads, the current available for charging will be equal to the following equation (assuming the bus voltage will be 12.6 V):

$$I_{charge} = I_{generator} - (I_{propulsion} + I_{hotel})$$

Using this value, the charge time can be calculated by using the battery capacity (720 Ah).

$$T_{charge} = \frac{C_{battery}}{I_{charge}}$$

The amount of fuel required per charge is then determined by multiplying the time per charge by the engine fuel consumption. Total fuel is determined by multiplying the fuel per charge by the number of charges. A buffer percentage (10% was used for the final design) was also added in the event of emergency.

Once the amount of fuel is determined, the length of the fuel tank must be calculated. Since the fuel volume was determined, the length of the fuel tank can be calculated by dividing the volume by the fuel tank's cross sectional area. This area is 0.058 m^2 and was found using the SolidWorks drawings.

The final piece of information for fuel tank sizing is to determine the number of charges per mission for SPYROS. This was determined by finding the total power system length for different numbers of charges and then choosing the charge number that comes the closest to the maximum mid-body length of 1.87 m. It was found that each charge of the eight-battery system with a DOD of 90% requires a fuel tank length of 0.1 m. With six charges, the total power system length (generator, batteries and fuel tank) is 1.82 m, very close to the maximum allowable length.

Once the fuel tank is correctly sized, the design of the propulsion system is complete. This propulsion system is outlined in figure 9.3.

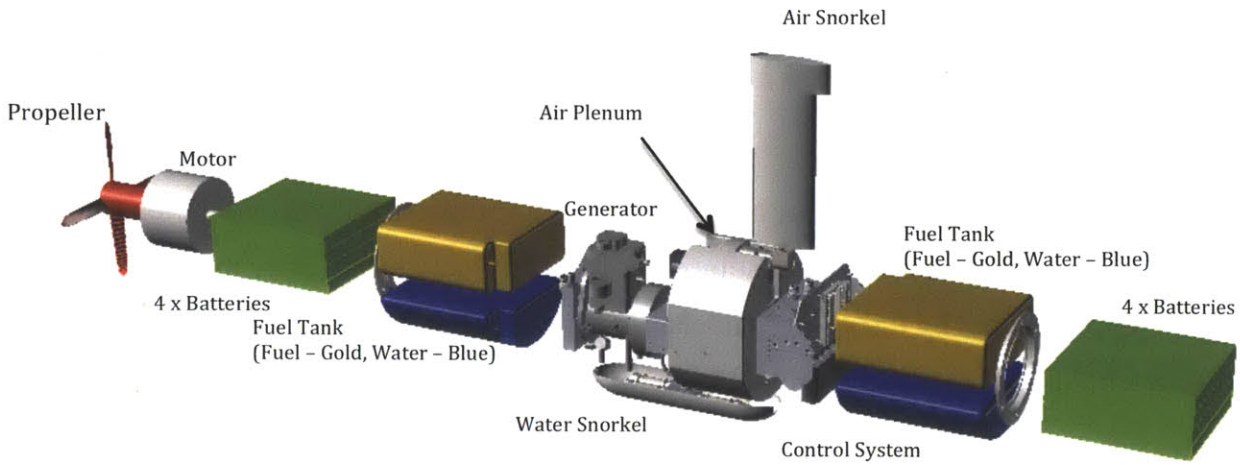

Figure 9.3: Illustration of Propulsion System

9.3 Distance Evaluation

SPYROS has been designed to travel through the water at 1 m/s (~2 kts) in a level, submerged condition. This kind of movement through the water occurs for the majority of a given mission, but do to the need to ascend to the surface for power generation, it is not the only locomotive state of SPYROS. To get a full account of the AUV's assignment, the resistance and speed while at the surface, and while diving and surfacing must be taken into account.

Current submersible hullforms are not ideal for surface transit. Burcher and Rydill note that the elliptical bow shape of current submarines lead to a large bow waves at the surface, increasing resistance for a given speed (Burcher & Rydill, 1994). Figure 6.5 in this text shows the difference between the submerged and surfaced power speed curves for submersibles. Since this text deals mainly with diesel submarines (especially the UPHOLDER Class developed by the Royal Navy), the power speed curve for SPYROS can be matched to the text using Froude similitude. At 1 m/s, SPYROS has a Froude number of 0.17. Using the published length of the

UPHOLDER Class submarine of 70.3 m, it would have a Froude number of 0.17 at a speed of 4.46 m/s (~ 9 kts) ("SSK Victoria Class Long-Range Patrol Submarines - Naval Technology," 2011). Using Burcher and Rydill's figure at 9 kts, approximately double the power would be required to maintain the speed at the surface than to maintain the speed submerged. Looking at the problem another way, if the power remained constant, than the speed reduces by approximately 1/8 (since power is proportional to speed cubed). To be conservative, the MATLAB model uses a surfaced speed of 0.75 m/s for SPYROS (or a speed reduction of 1/4).

Diving and surfacing operations were also considered during the development of the distance calculator. The overall horizontal distance and speed change due to the simple fact that SPYROS is travelling at an angle and not straight through the water. The horizontal speed and distance travelled by the AUV during diving and surfacing operations are therefore modified depending on the diving/surfacing angle. Extra forces such as lift must also be taken into account during these operations. Hoerner suggests using the following equation to determine the drag coefficient in these circumstances (Hoerner, 1965):

$$C_N = C_{D_{basic}} \sin^2 \alpha$$

where C_N is the overall drag coefficient taking both lift and drag into account, C_{Dbasic} is the original drag coefficient and α is the angle between the direction of flow and the horizontal. Hoerner states that this approximation is only good for subcritical Reynolds numbers, which means that it not appropriate for SPYROS as it's Reynolds number is in the supercritical region. Hoerner states that due to flow attachment in turbulent flow, the fluid flow is unpredictable. Therefore for SPYROS, the same doubling of power as seen in the surfaced state was used as a conservative estimate. A speed of 0.75 m/s was utilized as the forward speed of SPYROS before the diving/surfacing angle was taken into account.

Once the different conditions were analyzed the MATLAB script was run utilizing the conditions found in table 8-1. A hotel load of 8 W was utilized since this was the constraint imposed on the TETHYS AUV when travelling at 1 m/s. The other conditions were chosen after discussion with the Thesis Advisor.

Parameter	Value
Number of Batteries	8
Number of Charges	6
Hotel Load	8 W
Depth of Discharge	90%
Fuel Buffer	10%
Depth	1000 m
Diving/Surfacing Angle	15°

Table 9-1: Input Conditions for Distance Calculator

Using the above conditions, the distance calculator determines that SPYROS would travel a distance of 2363 nm. To put this into perspective, SPYROS can travel from Boston to the Azores in a single mission (2088 nm) ("Sea Distances - Voyage Calculator," n.d.). It must be noted that all distances mentioned do not take currents into account, only flat water.

The value in table 9-1 with the greatest chance of variability is the hotel load. This value can change substantially depending on mission requirements. Figure 9.4 shows how the hotel load affects the range of the vessel.

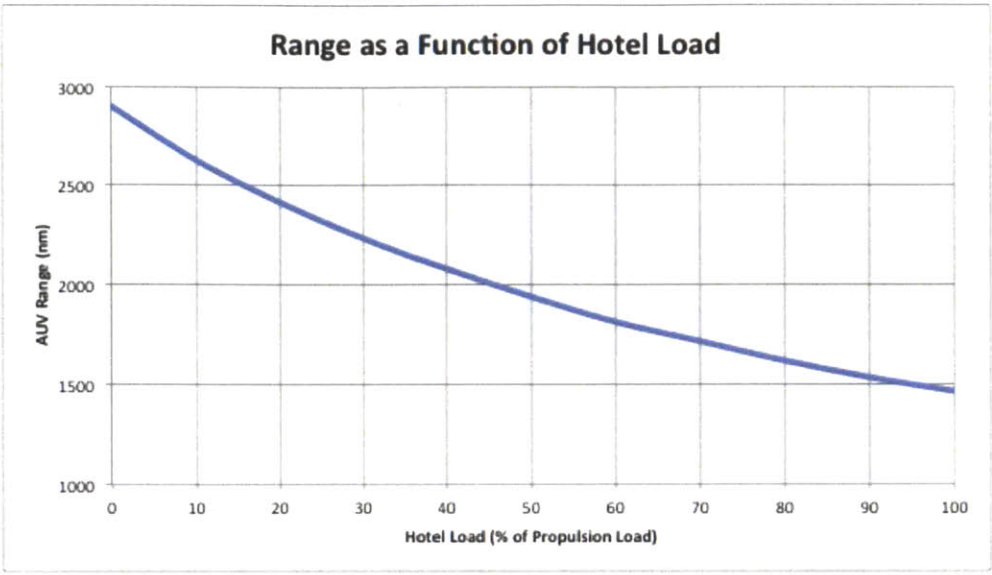

Figure 9.4: Range as a Function of Hotel Load

From this figure, it can be seen that if there were no hotel loads, then the range would be close to 3000 nm. This can be compared to when the hotel load is equal to the propulsion load (~35 W), then the range is closer to 1500 nm, or half the original range.

9.4 Recharger versus Battery Only System

One of the goals of this research was to determine if using the recharging system, and all the extra space and weight it requires, would be more efficient than an identical AUV with batteries filling the space used for the recharger. Utilizing the MATLAB script, the hull length used for the generator and fuel tanks can be determined for a particular condition. The script then uses the battery dimensions and layout detailed in section 9.1 to determine the number of batteries that can fit into this space. Finally, the distance calculator will calculate SPYROS' range with only the batteries onboard, with no charging cycles. For the conditions described in table 9-1, the battery only AUV will have a range of only 1098 nm, compared to 2363 nm for the AUV with a recharging system. This can be viewed graphically in figure 9.5.

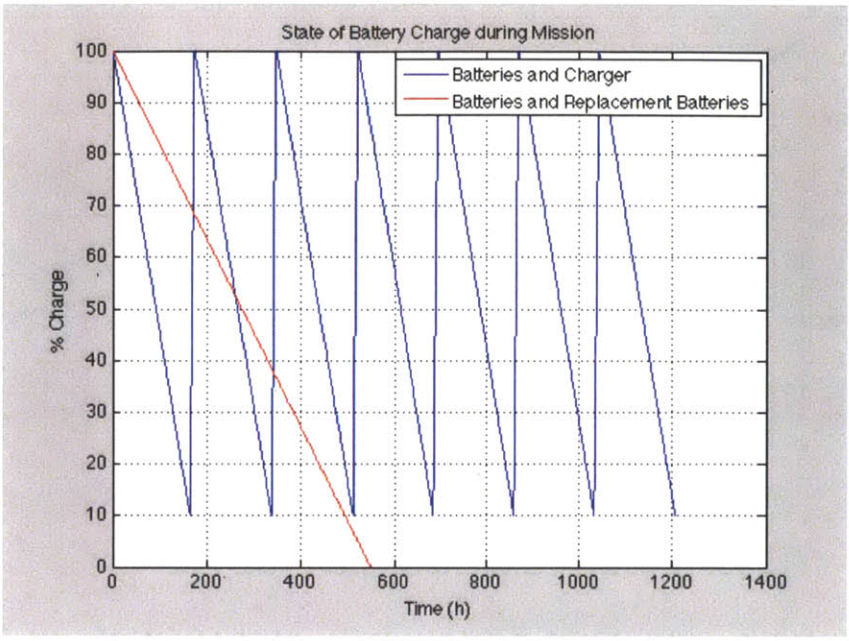

Figure 9.5: State of Battery Charge during Mission

In this figure, the percent charge for both AUV's is plotted against time. The sharp spikes in the blue curve indicate the recharging of the batteries and the blue line only goes down to 10% charge due to the fact that the input calls for a DOD of 90%. It was assumed that the battery only AUV would want to fully discharge its batteries in order to increase range and endurance. It can be seen that the battery only AUV has a much shorter endurance, which corresponds to a lower range than SPYROS.

9.5 Comparison with other AUVs

During the design process, two AUVs were used extensively for comparison purposes: the TETHYS AUV designed by the Monterey Bay Aquarium Research Institute (Bellingham et al., 2010) and the REMUS AUV designed primarily by the Woods Hole Oceanographic Institute (Allen et al., 2000). Though these two AUVs have different mission profiles (TETHYS is a long range AUV while REMUS is a standard research AUV), they give a good basis for comparison.

TETHYS has two different mission profiles depending on speed and hotel load. According to Bellingham, TETHYS can travel 1000 km (540 nm) at 1 m/s with a hotel load of 8 W and can travel 4000 km (2160 nm) at 0.5 m/s with a hotel load of 1 W (Bellingham et al., 2010). REMUS, on the other hand has a range of only 120 km (65 nm) at 1.5 m/s (Allen et al., 2000), but this is typical of most AUVs. The ranges can also be described in terms of an operational radius from a mothership, which is illustrated in figure 9.6.

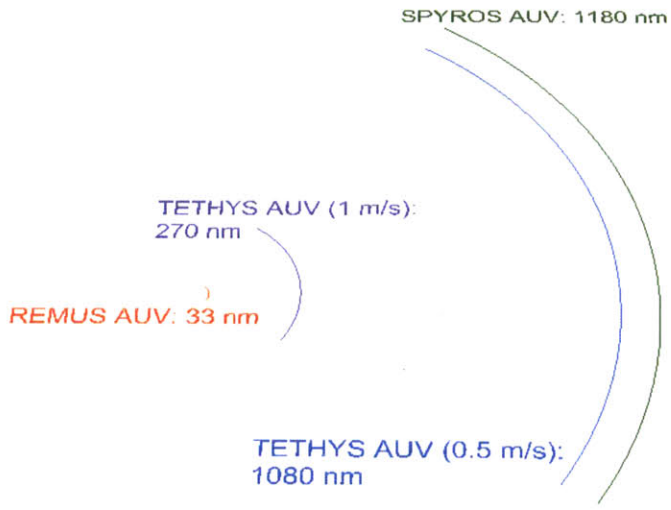

Figure 9.6: Operational Radii of different AUVs

The SPYROS system also compares well with many gliders. Gliders, as stated in Chapter 1, have much lower propulsion power, as they utilize the lift generated by hydrofoils for propulsion instead of a propeller. This allows for longer endurance than typical AUV designs. They do, however, travel at very low speeds and are very susceptible to ocean currents. The SCARLET KNIGHT glider developed by Rutgers University recently completed a voyage from New Jersey to Spain, travelling at total distance of 7400 km (4000 nm) at a speed of 0.25 m/s (Glenn, 2009). However, this voyage was greatly affected by the currents of the Atlantic Ocean. If only the straight line distance were taken into account, the voyage would have been only 5323 km (2874 nm), much closer to SPYROS' range of 2363 nm.

10 Conclusions and Recommendations

Throughout this thesis, the goal was to develop a concept design for a long distance AUV that utilizes an onboard electrical generator to increase the vehicle's range and endurance. Utilizing an AUV generator design developed by the MIT Rapid Development group, headed by Dan Dorsch and overseen by Dr. Doug Hart along with long-range AUV design principles, the SPYROS AUV was developed. SPYROS has a theoretical range of 2363 nm and can operate autonomously at sea for approximately 1200 hours or 50 days. From the outset, it was a goal to have an AUV that could travel from Boston to a European port autonomously. This was accomplished as SPYROS has the range to reach the Azores from Boston Harbor.

Despite this success, further work is recommended in order to develop SPYROS into a fully operational AUV. Currently, the drag equations are based off of approximate coefficients developed by Hoerner. Using the Myring B-form body, a model should be built and tow tank testing should be performed to determine the correct drag. These values can be used to update the propeller design and motor matching.

Since this is a novel design for an AUV, especially with the fixed snorkel protruding from the hull, a thorough analysis into SPYROS' dynamics must be conducted. In order for this design to be successful, SPYROS must have proper maneuvering and control characteristics. Once the snorkel and control surfaces are determined, this should be added to the model described above to ensure proper drag values are determined for the vessel.

To ensure all systems operate correctly, a design for a proper power bus should be developed. Many different types of power would be required between the propulsion and hotel loads. Simplified numbers were utilized in the current design, but a complete design would allow for accurate power consumption calculations, which would affect the range and endurance of the vessel.

Finally, a full working model of the propulsion system should be developed. The generator is currently being built by the MIT Rapid Development Group and could be connected to the battery and propulsion systems described in this thesis. With this model, further tests and evaluations could be conducted to confirm the viability of the design.

Bibliography

AUVAC. (2011). AUV System Fact Sheet: SPURV. Retrieved December 5, 2011, from http://archive.auvac.org/resources/browse/configuration/detail.php?configuration_id=121

Allen, B., Vorus, W. S., & Prestero, T. (2000). Propulsion system performance enhancements on REMUS AUVs. *OCEANS 2000 MTS/IEEE Conference and Exhibition* (Vol. 3, pp. 1869–1873). IEEE. Retrieved from http://ieeexplore.ieee.org/xpls/abs_all.jsp?arnumber=882209

Battery and Cell Chemistries. Battery primer. (2005).*The Electropaedia*. Retrieved March 20, 2012, from http://www.mpoweruk.com/chemistries.htm

Bellingham, J. G., Zhang, Y., Kerwin, J. E., Erikson, J., Hobson, B., Kieft, B., Godin, M., et al. (2010). Efficient propulsion for the Tethys long-range autonomous underwater vehicle. *Autonomous Underwater Vehicles (AUV), 2010 IEEE/OES* (pp. 1–7). IEEE. Retrieved from http://ieeexplore.ieee.org/xpls/abs_all.jsp?arnumber=5779645

Blidberg, D. R. (2001). The development of autonomous underwater vehicles (auvs); a brief summary. *IEEE ICRA* (Vol. 6500). Retrieved from http://ausi.org/publications/ICRA_01paper.pdf

Brege, E. D. (2011). *Design and Construction of a Low Cost , Modular Autonomous Underwater Vehicle. Mechanical Engineering*. Massachusetts Institute of Technology.

Brizzolara, S., Bovio, M., & Federici, A. (2011). Hydrodynamic Design of a Family of Hybrid SWATH Unmanned Surface Vehicles. *11th International Conference on Fast Sea Transportation*. Retrieved from http://esrdc.mit.edu/library/ESRDC_library/Brizzolara-Hydrodynamic-Sept-2011.pdf

Buchmann, I. (2012). Basic to Advanced Battery Information from Battery University. Retrieved March 22, 2012, from http://batteryuniversity.com/

Burcher, R., & Rydill, L. (1994). *Concepts in Submarine Design*. Cambridge, UK: Cambridge University Press.

Corvus Energy. (n.d.). Retrieved March 20, 2012, from http://corvus-energy.com/

CrustCrawler. (n.d.). *CrustCrawler " High Flow " 600HF UROV Thruster Technical Specifications.*

Debarros, E., Pascoal, a, & Desa, E. (2008). Investigation of a method for predicting AUV derivatives. *Ocean Engineering*, *35*(16), 1627-1636. doi:10.1016/j.oceaneng.2008.08.008

Dorsch, D., LaColla, J., Mooney, L., Shoemaker-Trejo, N., Brandeau, E., Saxton-Fox, T., Frankel, A., et al. (2012). *Internal Combustion Engine Hybrid Recharging System. Design*. Cambridge, MA, USA.

EV Works Pty Ltd. (n.d.). Retrieved March 15, 2012, from http://www.evworks.com.au/tech/?section=motors

Epps, B. (2010). *OpenProp v2.4 Theory Document* (Vol. 44). doi:10.1002/lsm.22009

Gertler, M. (1950). Resistance experiments on a systematic series of streamlined bodies of revolution-for application to the design of high-speed submarines. Retrieved from http://oai.dtic.mil/oai/oai?verb=getRecord&metadataPrefix=html&identifier=ADA800144

Gish, L. A. (2004). *Design of an AUV Recharging System. Ocean Engineering*. Massachusetts Institute of Technology.

Glenn, S. (2009). Flight Across the Atlantic - Scarlet Knight. Retrieved December 7, 2011, from http://rucool.marine.rutgers.edu/atlantic/

Hobby Depot - JetCat SPM5. (2010).*Hobby Depot*. Retrieved February 8, 2012, from http://www.hobbydepot.com.au/product_info.php?products_id=539

Hoerner, S. F. (1965). *Fluid-Dynamic Drag*. Published by Author.

Honda EU1000i generator. (n.d.). Retrieved February 9, 2012, from http://powerequipment.honda.com/generators/models/eu1000i

Honda Engines - Small Engines Models, Manuals, Parts & Resources. (n.d.). Retrieved March 27, 2012, from http://engines.honda.com/models/model-detail/gxh50

JET-ENGINE MAKER AIMS TO POWER THE FUTURE. (2011).*UK Trade and Investment*. Retrieved February 7, 2012, from http://www.bladonjets.com/news/jet-engine-maker-aims-to-power-the-future/

Jalbert, J., Baker, J., Duchesney, J., Pietryka, P., Dalton, W., Div, A., Scientific, F., et al. (2003). SOLAR-POWERED AUTONOMOUS UNDERWATER VEHICLE DEVELOPMENT Autonomous Undersea Systems Institute Robert Nitzel , Technology Systems , Inc . *Proceedings of the Thirteenth International Symposium on Unmanned Untethered Submersible Technology*.

Kimball, R. W., & Epps, B. P. (2010). OpenProp v2.4 propeller/turbine design code.

Kirtley, J. L. (Massachusetts I. of T. (2010). *Electric Power Principles: Sources, Conversion, Distribution and Use*. Chichester, West Sussex, United Kingdom: John Wiley & Sons Ltd.

Lamb, T. (2003). *Ship Design and Construction, Volume 1*. Society of Naval Architects and Marine Engineers.

Manley, J. E. (2006). *NOAA ' s AUV Vision : Status and Opportunities. Technology.*

Modular Lithium Battery System. (2012). Ottawa, Ontario.

Morash, J. P., Polidoro, V. C., & Hover, F. S. (2007). *A Modular High Voltage Lithium-Ion Battery for Unmanned Marine Vehicles. Small* (pp. 1-12).

Myring, D. F. (1976). A Theoretical Study of Body Drag in Subcritical Axisymmetric Flow. *Aeronautical Quarterly*, 186-194.

Newman, J. N. (1977). *Marine Hydrodynamics*. Cambridge, MA, USA: The MIT Press.

Oceaneering. (2011). Oceaneering » ROV Media. Retrieved December 6, 2011, from http://www.oceaneering.com/rovs/rov-media/

Properties of Bronze for Marine Propellers. (n.d.). Retrieved March 12, 2012, from http://www.propellerpages.com/?c=articles&f=2005-11-29_Properties_Bronze

Rotapower 27 Series Announcement. (2010). Retrieved February 10, 2012, from http://www.freedom-motors.com/index.php?option=com_content&view=article&id=97&Itemid=77

SL Montevideo Technology. (n.d.). Retrieved March 15, 2012, from http://www.slmti.com/default.asp

SSK Victoria Class Long-Range Patrol Submarines - Naval Technology. (2011). Retrieved April 5, 2012, from http://www.naval-technology.com/projects/ssk_victoria/

Sea Distances - Voyage Calculator. (n.d.). Retrieved from

Sherman, D. (2009). The Rotary Club. *Automobile Magazine*. Retrieved from http://en.wikipedia.org/wiki/Wankel_engine#cite_ref-a_0-2

Singer, D. J., Doerry, N., & Buckley, M. E. (2009). What is Set-Based Design ? *Naval Engineers Journal, 121*(4), 31–43. Wiley Online Library. Retrieved from http://onlinelibrary.wiley.com/doi/10.1111/j.1559-3584.2009.00226.x/full

Small, P. (2011). Lecture 12 : Design Space Exploration and Evaluation [Class Handouts]. *Spring*. Cambridge, MA, USA: Department of Mechanical Engineering, Massachusetts Institute of Technology.

Tichy, R., & Friel, D. (2012). The Future Of Lithium Ion Batteries. Micropower.

Vijay, S. (Dept of M. E. P. E. S. C. E. M. (n.d.). Topic Seminar on Autonomous Underwater Vehicles.

Woud, H. K., & Stapersma, D. (2008). *Design of Propulsion and Electric Power Generation Systems*. IMarEST.

Yamamoto, I., Aoki, T., Tsukioka, S., Yoshida, H., Hyakudome, T., Sawa, T., Ishibashi, S., et al. (2004). Fuel cell system of AUV "Urashima." *Oceans '04 MTS/IEEE Techno-Ocean '04 (IEEE Cat. No.04CH37600)* (Vol. 3, pp. 1732-1737). Ieee. doi:10.1109/OCEANS.2004.1406386

Appendix A – Myring Body Optimization MATLAB Script

Below is the script written to determine the optimum configuration of a Myring body using all the necessary variables as described in section 4.2.

```
clear all;
close all;
clc;

%Script to try to find minimum Drag Coefficient of Myring Body using
%Equations derived in de Barros et al, 2008


D=0.34;       %Max diameter of AUV
f=10;         %Finesse Ratio or Length/Diameter
L=f*D;        %Overall Length of AUV
b=1.87;       %Mid-body length

%Calculate friction drag coefficient
V=1;      %Speed in m/s
Re=(V*(D/2))/0.000001;
Cf=(0.075/(((log10(Re))-2)^2))+0.00025;

%initialize variables
val=struct;

alow=0.1;                          %set since 0 value will crash script
ahigh=L-b-0.1;
val.astep=linspace(alow,ahigh,10);   %c will be dependent on value of a

chigh=L-b-alow;
clow=L-b-ahigh;
val.cstep=linspace(chigh,clow,10);

val.nstep=linspace(1,3,10);        %may change range later, should be
at least 1

val.theta=linspace(0.5,50,10);

%Other needed variables for drag calculation
Sn=pi*(D^2/4);
db=0.25;          %Base diameter, diameter at aft of ship, setting to
prop hub diameter

for a=1:length(val.astep)
    for n=1:length(val.nstep)
        for theta=1:length(val.theta)

            step=zeros(1,L*1000);

            for x=1:round(val.astep(a)*1000)
                step(x)=x/1000;
```

```
                r(x)=0.5*D*(1-(((step(x))-
val.astep(a))/val.astep(a))^2)^(1/val.nstep(n));
            end
            for x=round(val.astep(a)*1000):round((val.astep(a)+b)*1000)
                r(x)=D/2;
                step(x)=x/1000;
            end
            for x=round((val.astep(a)+b)*1000):round(L*1000)
                step(x)=x/1000;
                r(x)=(0.5*D)-((((3*D)/(2*(val.cstep(a))^2))-...
                (tand(val.theta(theta))/val.cstep(a)))*(step(x)-
val.astep(a)-b)^2)+...
                (((D/val.cstep(a)^3)-
(tand(val.theta(theta))/val.cstep(a)^2))*...
                (step(x)-val.astep(a)-b)^3);
                if r(x-1)>=db && r(x)<=db
                    break
                end
            end
            Lvar=x/1000;
            for x=1:(Lvar*1000)
                Acyl(x)=2*pi*r(x)*(1/1000);
            end
            Ss=sum(Acyl);

            Cdstar=Cf*(1+(60*f^-3)+(0.0025*f))*(Ss/(L^2));
            Cdb=0.029*((db/D)^3)*(Cdstar^-0.5)*(Sn/(L^2));

            val.CD(a,n,theta)=Cdstar+Cdb;

        end
    end
end
[C,I]=min(val.CD(:,1,:));
[X,I]=min(C)
```

As can be seen, the output of the script is the value of the minimum drag coefficient and its index within the variable structure. It was found that if you minimize the variables, then the drag coefficient is at a minimum.

A second script was written specifically using the inputs as described in section 4.2 along with the variables as described for a Myring B-form (Myring, 1976), as seen in the following script. This script also outputs a figure of the body as constructed using Myring's equations.

```
clear all;
close all;
```

```
clc;

%Script to plot profile of Myring Body and determine surface area of
form


D=0.34;       %Max diameter of AUV
f=10;         %Finesse Ratio or Length/Diameter
L=f*D;       %Overall Length of AUV
n=1.25;         %affects slope of nose
theta=25;     %angle of tail degrees
TAN=tand(theta);
V=1;          %Speed in m/s

fa=0.15;
a=fa*L;
fb=0.55;
b=fb*L;
fc=0.30;
c=fc*L;

db=0.05;
Sn=pi*D^2/4;

step=zeros(1,L*1000);
r=zeros(1,L*1000);

for x=1:round(a*1000)
    step(x)=x/1000;
    r(x)=0.5*D*(1-(((step(x))-a)/a)^2)^(1/n);
end
for x=round(a*1000):round((a+b)*1000)
    r(x)=D/2;
    step(x)=x/1000;
end
for x=round((a+b)*1000):round(L*1000)
    step(x)=x/1000;
    r(x)=(0.5*D)-((((3*D)/(2*(c)^2))-(TAN/(c)))*(step(x)-a-b)^2)+...
        (((D/(c)^3)-(TAN/(c)^2))*(step(x)-a-b)^3);
    if r(x)<=db
        r(x)=0;
    end
end

plot(step,r);
axis equal;
grid on;

figure;
for x=1:(L*1000)
    rnorm(x)=r(x)/L;
end
[X,Y,Z]=cylinder(rnorm,100);
surf(Y,Z,X,'EdgeColor','none');
colormap bone;
axis equal;
```

```
for x=1:(L*1000)
    Acyl(x)=2*pi*r(x)*(1/1000);
end
Ss=sum(Acyl);
disp(['The Surface Area of Body is ' num2str(Ss) ' square meters']);


Re=(V*(D/2))/0.000001;
Cf=(0.075/(((log10(Re))-2)^2))+0.00025


Cdstar=Cf*(1+(60*f^-3)+(0.0025*f))*(Ss/(L^2))
Cdb=0.029*((db/D)^3)*(Cdstar^-0.5)*(Sn/(L^2))

CD=Cdstar+Cdb
```

Output:

The Surface Area of Body is 3.1622 square meters

Cf =

0.0074

Cdstar =

0.0022

Cdb =

1.5418e-05

CD =

0.0022

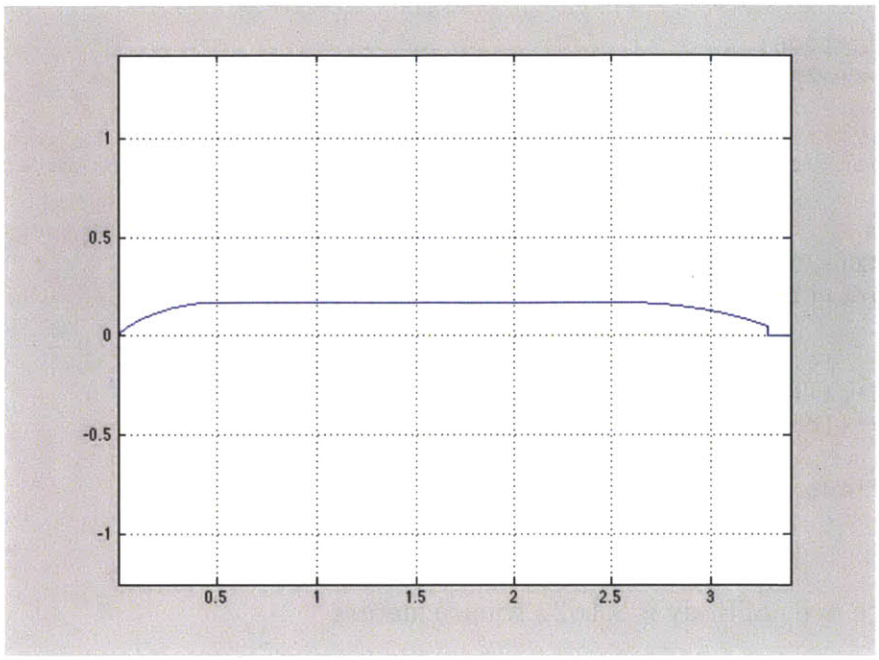

Figure A.1: Half Profile View of Hullform

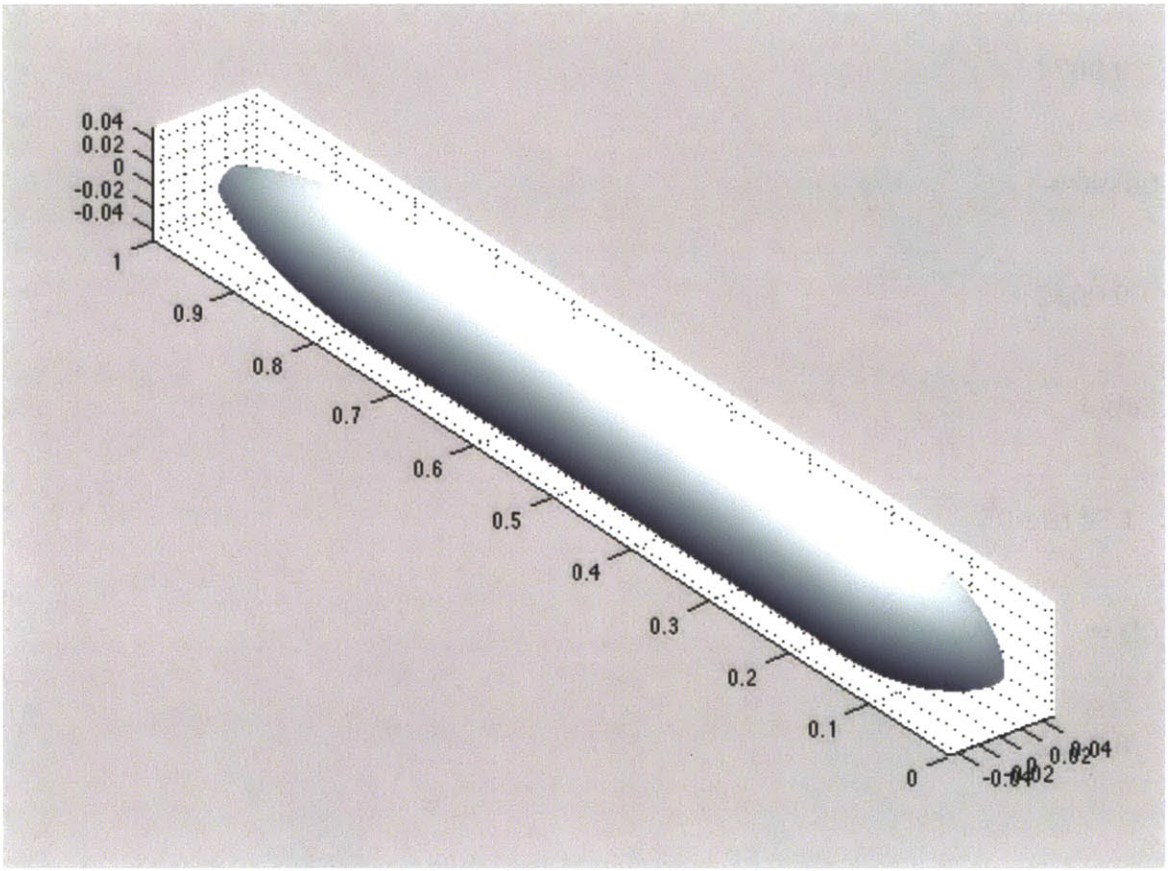

Figure A.2: Three Dimensional View of Hullform

Appendix B – OpenProp Single Design Output

After determining the proper characteristics for the propeller design, the User Interface was updated and can be seen in Figure B.1.

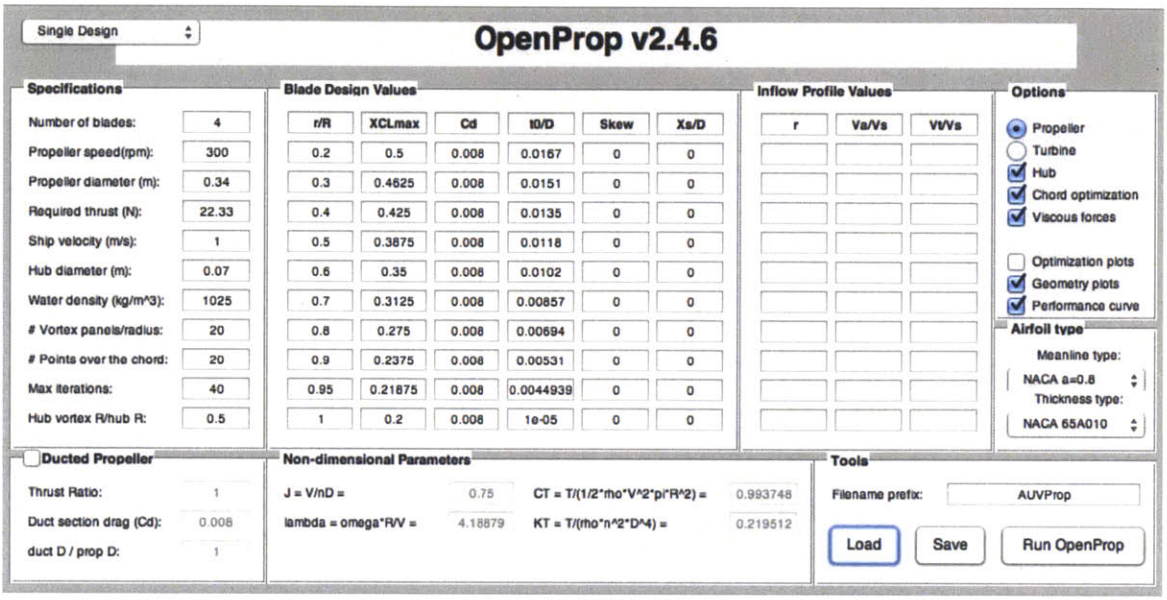

Figure B.1: OpenProp Single Design User Interface with Proper Inputs

Below are the OpenProp outputs when the program is completed.

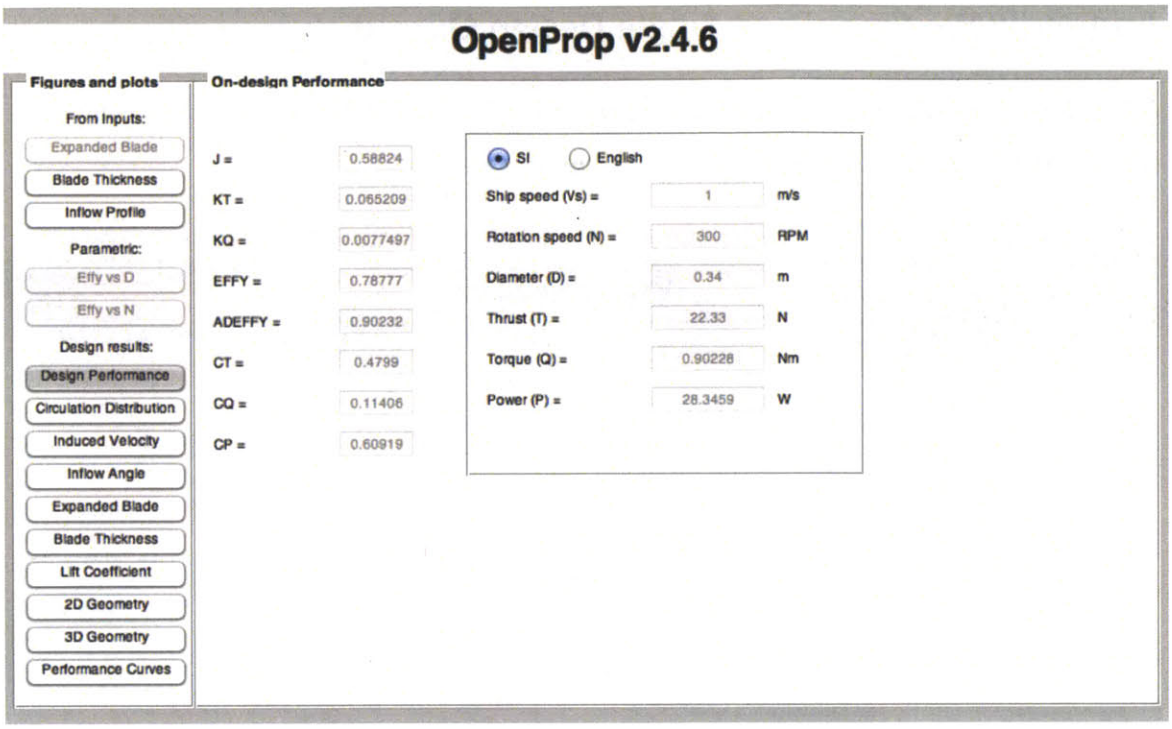

Figure B.2: On-Design Performance Output

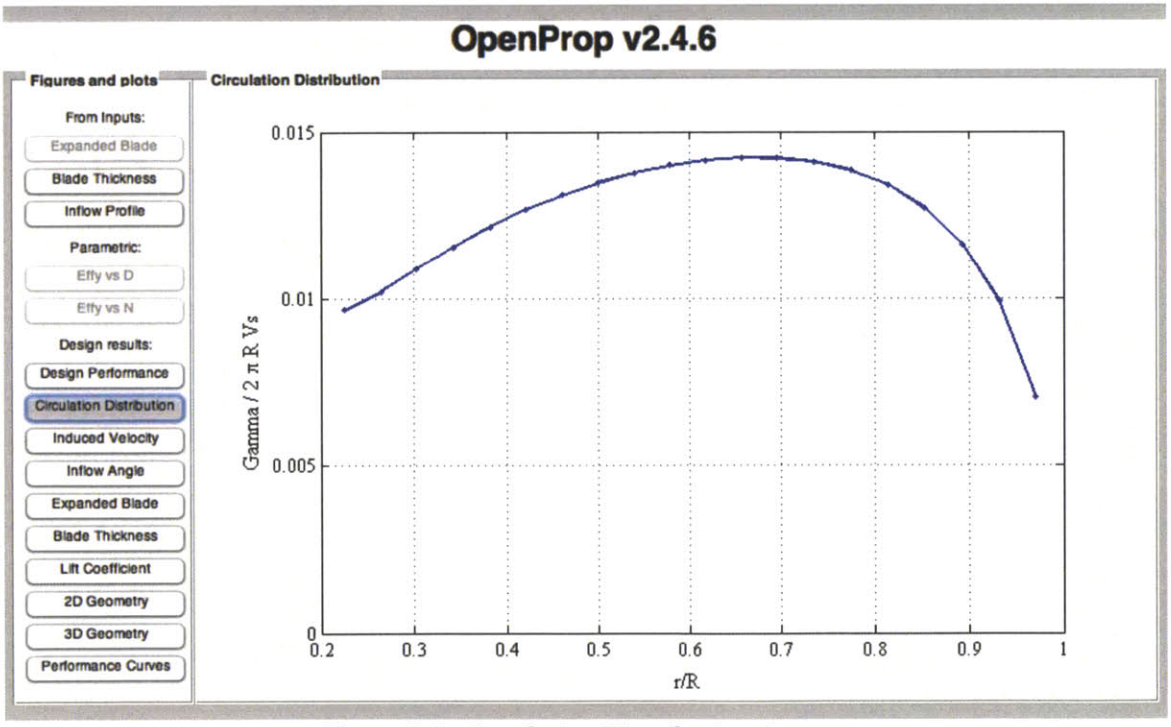

Figure B.3: Circulation Distribution Output

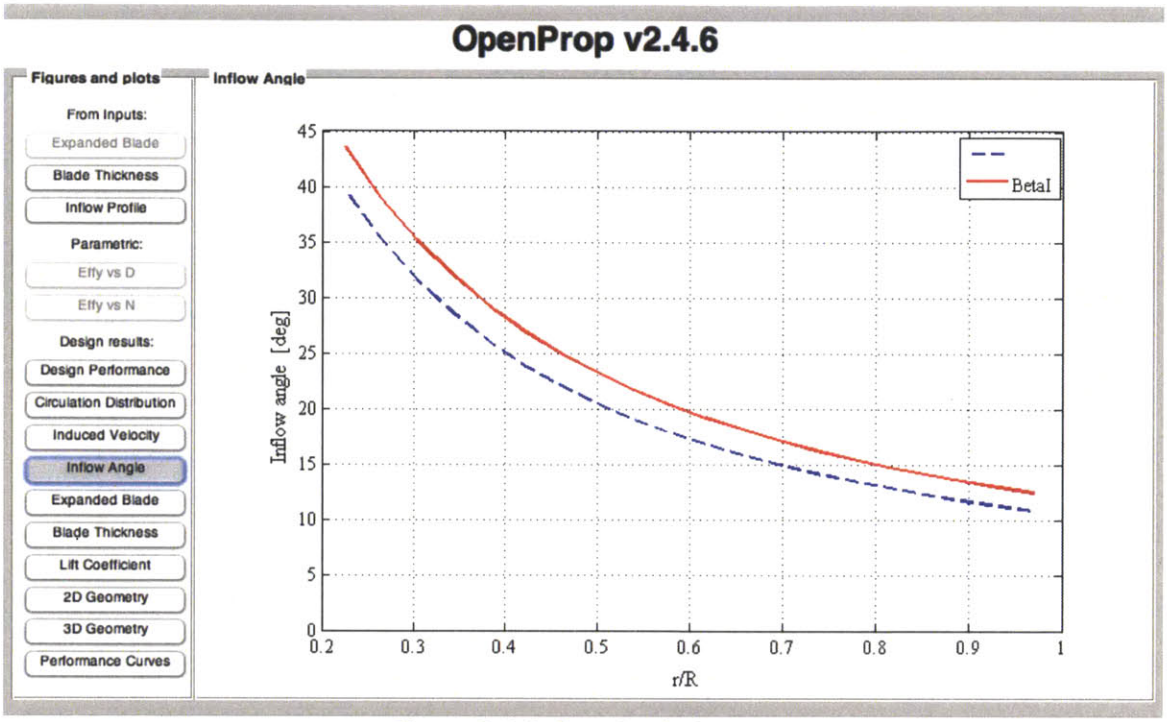

Figure B.4: Inflow Angle Output

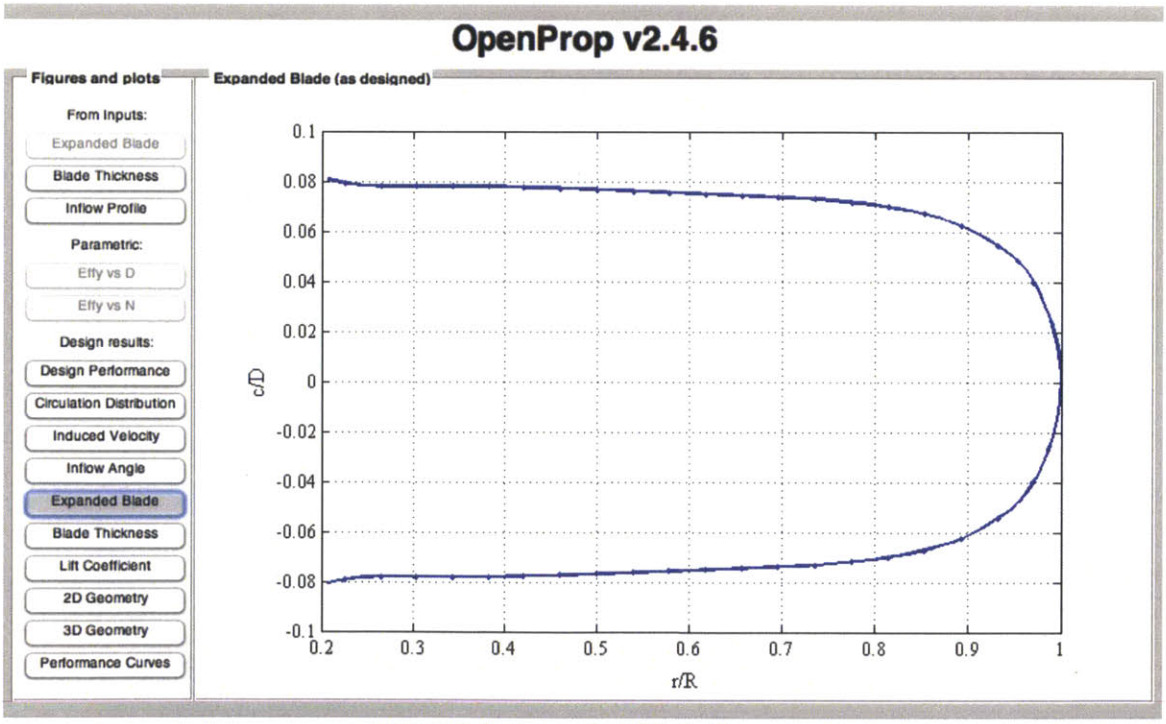

Figure B.5: Expanded Blade Output

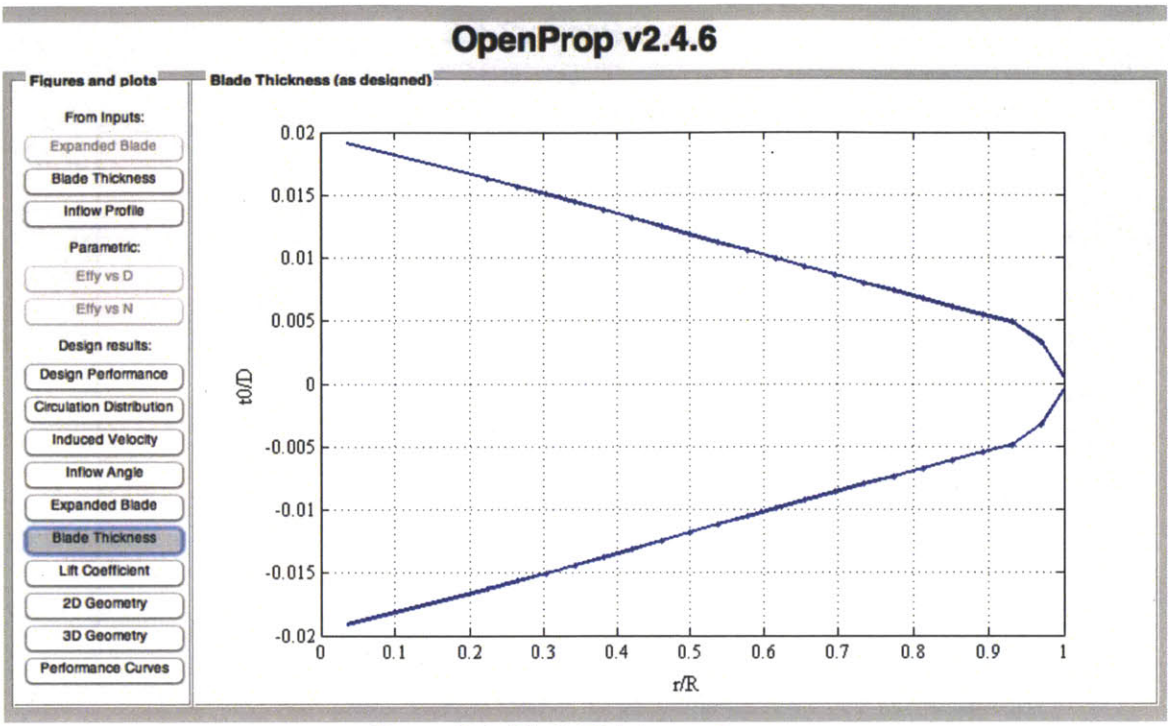

Figure B.6: Blade Thickness Output

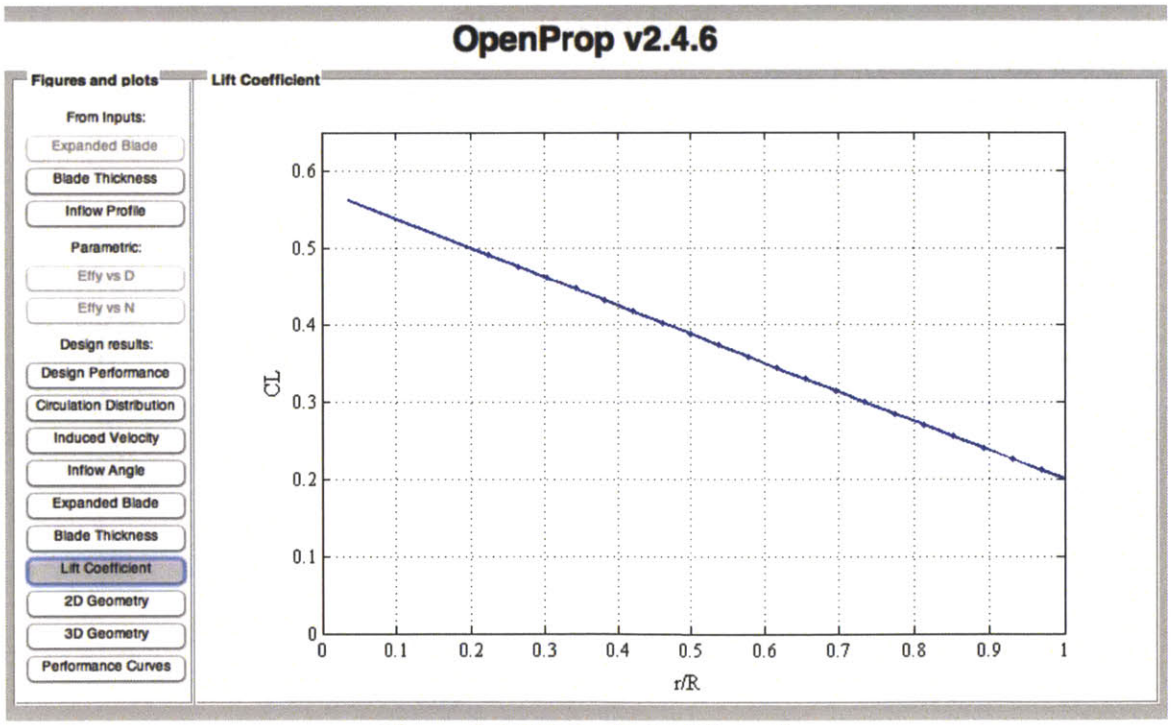

Figure B.7: Lift Coefficient Output

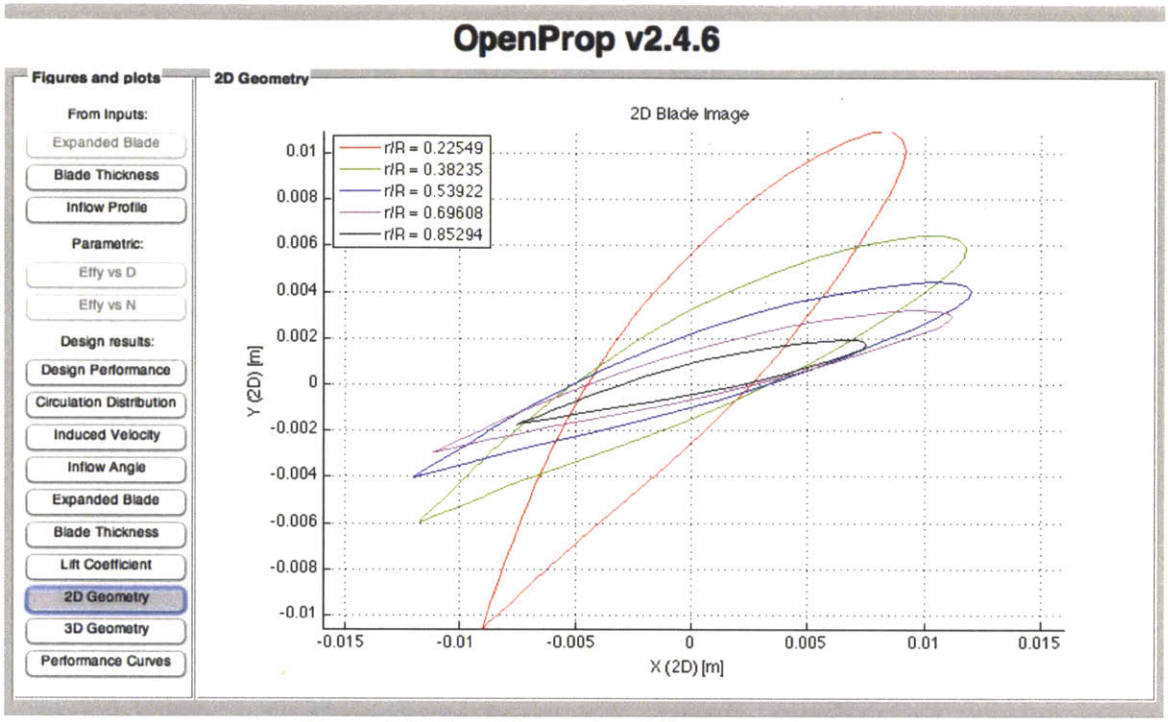

Figure B.8: Two Dimensional Geometry Output

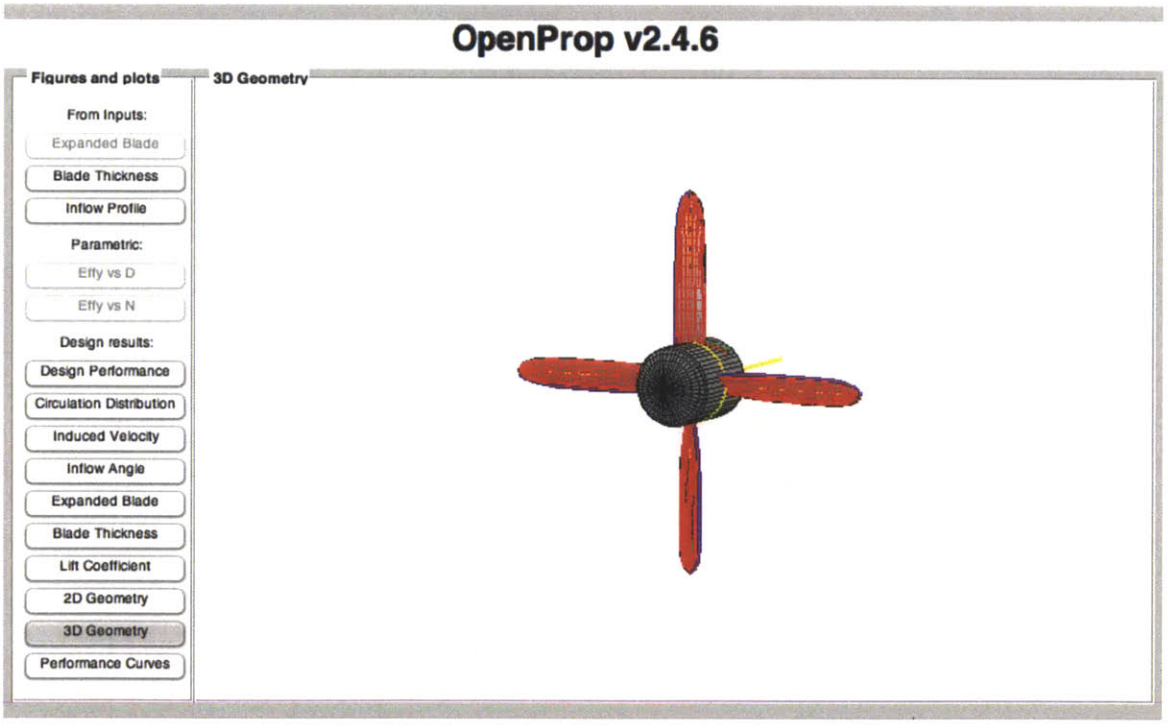

Figure B.9: Three Dimensional Geometry Output

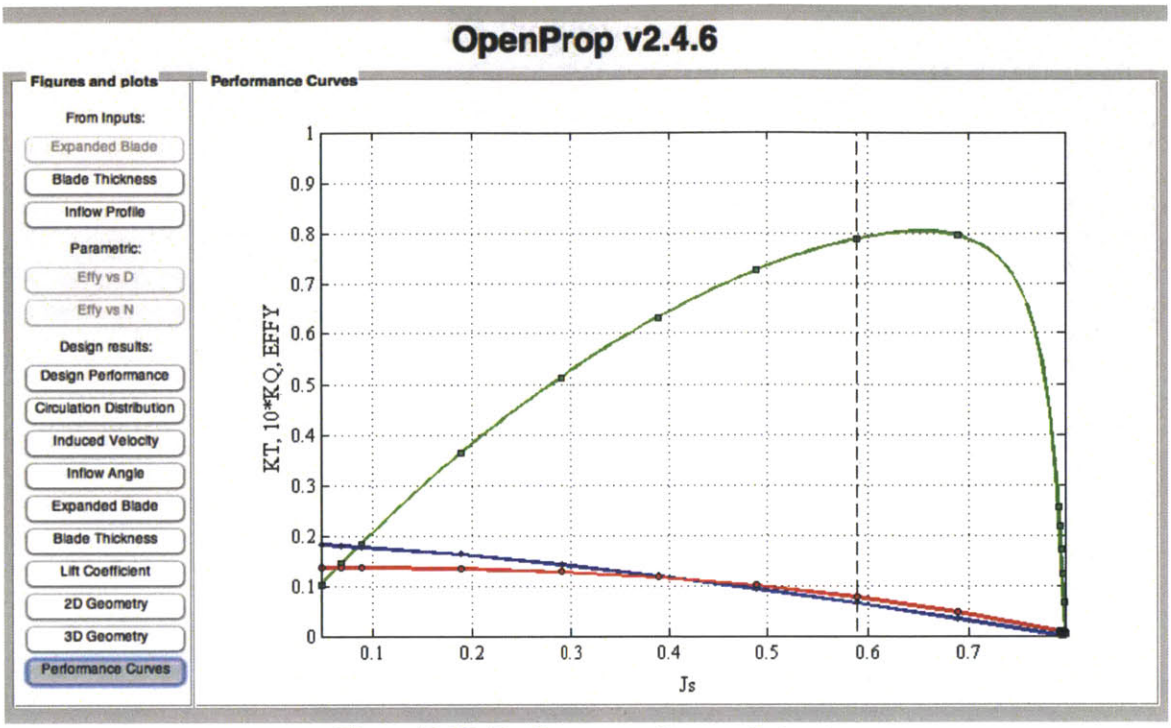

Figure B.10: Performance Curves Output

Appendix C – Motor/Propeller Matching

Below is the Engine Database developed using the information found on the website for SL Montevideo Technology ("SL Montevideo Technology," n.d.).

Motor Name	Slope	y-intercept	Torque Constant	Min RPM	Max RPM	Max Torque
BLOV-29-16-4P	-10.87	6600.93	167.24	355	607	2740.42
BLOV-29-16-4P	-10.71	5857.66	185.82	292	547	2730.72
BLOV-29-16-4P	-10.53	5234.96	204.4	240	497	2707.01
BLOV-29-16-4P	-10.66	4657.75	232.27	181	437	2728.57
BLOV-29-16-4P	-10.62	4153.38	260.15	134	391	2729.97
BLOV-29-16-4P	-10.48	3700.97	288.02	94	353	2715.44
BLOV-29-16-4P	-10.57	3299.28	325.18	54	312	2728.25
BLOV-29-14-4P	-9.21	5720.94	163.42	357	621	2432.09
BLOV-29-14-4P	-9.00	5082.89	179.77	297	565	2411
BLOV-29-14-4P	-9.14	4540.90	204.28	231	497	2430.34
BLOV-29-14-4P	-9.11	4043.29	228.79	177	444	2431.44
BLOV-29-14-4P	-8.99	3604.98	253.31	132	401	2418.3
BLOV-29-14-4P	-9.03	3206.47	285.99	86	355	2429.69
BLOV-29-14-4P	-9.20	2861.12	326.85	44	311	2456.33
BLOV-29-12-4P	-7.45	4901.89	154.47	374	658	2115.71
BLOV-29-12-4P	-7.54	4363.20	175.53	296	579	2132.62
BLOV-29-12-4P	-7.51	3884.14	196.59	233	517	2133.65
BLOV-29-12-4P	-7.42	3465.11	217.66	181	467	2122.1
BLOV-29-12-4P	-7.45	3086.02	245.74	128	414	2131.89
BLOV-29-12-4P	-7.59	2746.99	280.85	78	362	2155.1
BLOV-29-12-4P	-7.53	2184.15	351.06	4	290	2154.02
BLOV-29-10-4P	-5.96	3690.53	164.11	311	619	1836.32
BLOV-29-10-4P	-5.87	3282.70	181.69	248	559	1826.33
BLOV-29-10-4P	-5.92	2929.54	205.14	185	495	1834.66
BLOV-29-10-4P	-6.02	2607.17	234.44	125	433	1854.52
BLOV-29-10-4P	-5.89	2321.70	257.95	82	394	1838.5
BLOV-29-10-4P	-5.96	2067.70	293.05	36	347	1853.18
BLOV-29-08-4P	-4.41	2720.31	164.53	279	617	1490.22
BLOV-29-08-4P	-4.48	2420.90	188.04	204	540	1506.34
BLOV-29-08-4P	-4.39	2156.40	206.84	151	491	1493.23
BLOV-29-08-4P	-4.45	1923.61	235.05	94	432	1505.05
BLOV-29-08-4P	-4.43	1709.62	263.25	46	386	1505.88
BLOV-29-08-4P	-4.44	1523.58	296.16	3	343	1510.25
BLOV-29-06-4P	-2.97	1933.05	156.24	259	651	1163.99
BLOV-29-06-4P	-3.02	1725.03	177.55	183	572	1173.14
BLOV-29-06-4P	-3.01	1537.81	198.85	121	511	1173.67
BLOV-29-06-4P	-3.02	1370.06	223.71	64	454	1176.92

Motor Name	Slope	y-intercept	Torque Constant	Min RPM	Max RPM	Max Torque
BLOV-29-06-4P	-3.02	1217.59	252.12	12	403	1181.33
BLOV-29-17-12P	-18.32	10387.78	185.35	352	567	3938.93
BLOV-29-17-12P	-17.54	8276.92	222.42	250	472	3892.96
BLOV-29-17-12P	-18.22	7378.81	259.49	185	405	4008.24
BLOV-29-17-12P	-18.54	6562.87	296.56	134	354	4078.62
BLOV-29-17-12P	-18.41	5209.93	370.7	59	283	4123.76
BLOV-29-17-12P	-17.96	4633.00	407.76	29	258	4112.24
BLOV-29-13-12P	-12.73	7959.03	168.17	389	625	3005.33
BLOV-29-13-12P	-13.27	7099.84	196.19	302	535	3092.08
BLOV-29-13-12P	-12.02	5627.63	224.22	221	468	2970.14
BLOV-29-13-12P	-12.03	5003.66	252.25	167	416	2994.98
BLOV-29-13-12P	-11.91	4464.39	280.28	123	375	3000.07
BLOV-29-13-12P	-8.33	2398.57	364.36	36	288	2098.75
BLOV-29-09-12P	-8.07	5307.30	159.75	381	658	2234.23
BLOV-29-09-12P	-8.13	4747.84	179.72	307	584	2251.97
BLOV-29-09-12P	-8.83	4220.14	219.65	209	478	2374.93
BLOV-29-09-12P	-8.59	3762.23	239.62	164	438	2353.54
BLOV-29-09-12P	-8.27	3349.91	259.59	124	405	2324.26
BLOV-29-09-12P	-8.52	2988.86	299.53	72	351	2375.76
BLOV-29-09-12P	-8.59	2654.89	339.47	29	309	2405.73
BLOV-29-07-12P	-6.15	4003.32	161.43	353	651	1832.55
BLOV-29-07-12P	-6.60	3575.99	193.71	252	542	1913.35
BLOV-29-07-12P	-6.34	3175.47	209.86	203	501	1888.8
BLOV-29-07-12P	-6.52	2829.77	242.14	138	434	1929.98
BLOV-29-07-12P	-6.58	2518.88	274.43	86	383	1953.28
BLOV-29-07-12P	-6.56	2245.00	306.71	43	342	1962.73
BLOV-29-07-12P	-6.45	2000.16	339	6	310	1961.45
BLOV-29-06-12P	-4.94	3002.64	172.83	282	608	1609.97
BLOV-29-06-12P	-4.76	2683.00	186.13	231	564	1584.11
BLOV-29-06-12P	-4.84	2388.71	212.72	161	494	1610.2
BLOV-29-06-12P	-4.85	2127.01	239.31	104	439	1623.12
BLOV-29-06-12P	-4.80	1894.37	265.9	56	395	1625.8
BLOV-29-06-12P	-4.92	1689.07	305.78	6	343	1659.52
BLOV-29-05-12P	-3.95	2251.53	184.28	223	570	1370.67
BLOV-29-05-12P	-3.93	2005.15	205.96	160	510	1376.08
BLOV-29-05-12P	-3.88	1788.81	227.64	107	461	1373.62
BLOV-29-05-12P	-3.78	1591.90	249.33	60	421	1365.03
BLOV-29-05-12P	-3.80	1418.34	281.85	10	373	1380.31
BLOV-29-04-12P	-2.56	1624.95	165.41	234	635	1026.15
BLOV-29-04-12P	-2.62	1447.79	190.22	153	552	1046.5
BLOV-29-04-12P	-2.64	1290.32	215.03	88	488	1057.64
BLOV-29-04-12P	-2.62	1148.17	239.85	33	438	1061.66
BLOV-29-02-12P	-1.48	965.03	161.5	169	650	714.12

Motor Name	Slope	y-intercept	Torque Constant	Min RPM	Max RPM	Max Torque
BLOV-29-02-12P	-1.50	858.30	183.78	90	572	723.25
BLOV-29-02-12P	-1.50	765.97	206.06	26	510	726.92
BLHP-38-18-12P	-60.28	31886.79	198.62	406	529	7414.13
BLHP-38-18-12P	-63.63	25260.75	264.83	275	397	7762.75
BLHP-38-18-12P	-56.37	17870.38	331.04	186	317	7384.92
BLHP-38-18-12P	-53.92	14234.59	397.25	129	264	7279.05
BLHP-38-18-12P	-57.14	11314.52	529.67	65	198	7600.16
BLHP-38-18-12P	-56.39	8965.37	662.08	23	159	7668.49
BLHP-38-12-12P	-39.43	23301.37	177.64	453	591	5440.93
BLHP-38-12-12P	-34.75	16436.24	222.05	324	473	5177.59
BLHP-38-12-12P	-37.02	14587.47	266.46	248	394	5405.51
BLHP-38-12-12P	-34.80	10301.01	355.27	143	296	5324.51
BLHP-38-12-12P	-35.04	9216.52	399.68	110	263	5361.7
BLHP-38-12-12P	-34.00	7310.27	488.5	58	215	5338.2
BLHP-38-09-12P	-24.17	15176.53	167.39	465	628	3939.13
BLHP-38-09-12P	-22.98	12018.91	200.87	354	523	3883.74
BLHP-38-09-12P	-24.43	9576.87	267.83	226	392	4055.51
BLHP-38-09-12P	-24.45	8533.91	301.3	182	349	4083.56
BLHP-38-09-12P	-24.17	7588.21	334.78	145	314	4084.1
BLHP-38-09-12P	-23.00	6025.84	401.74	87	262	4024.89
BLHP-38-09-12P	-24.43	4787.73	535.65	24	196	4201.48
BLHP-38-08-12P	-20.02	12510.81	168.23	451	625	3483.01
BLHP-38-08-12P	-18.67	9985.94	196.27	354	535	3378.42
BLHP-38-08-12P	-18.96	8874.73	224.31	287	468	3432.32
BLHP-38-08-12P	-18.99	7899.70	252.35	234	416	3456.12
BLHP-38-08-12P	-18.78	7044.17	280.39	191	375	3456.34
BLHP-38-08-12P	-19.43	5594.52	364.5	105	288	3554.85
BLHP-38-08-12P	-18.60	4985.10	392.54	80	268	3497.01
BLHP-38-08-12P	-19.04	3960.20	504.69	20	208	3579.41
BLHP-38-06-12P	-13.90	9227.89	158.09	462	664	2807.28
BLHP-38-06-12P	-14.12	8203.98	180.68	379	581	2852.33
BLHP-38-06-12P	-14.15	7314.53	203.26	314	517	2872.05
BLHP-38-06-12P	-14.01	6514.33	225.85	260	465	2871.91
BLHP-38-06-12P	-14.97	5807.76	271.02	188	388	2993.69
BLHP-38-06-12P	-14.47	5181.65	293.6	154	358	2952.67
BLHP-38-06-12P	-13.89	4612.42	316.19	123	332	2903.6
BLHP-38-06-12P	-14.21	3665.62	406.53	49	258	2969.44
BLHP-38-04-12P	-9.45	5801.32	171.03	381	614	2201.48
BLHP-38-04-12P	-9.28	5176.56	188.14	322	558	2189.37
BLHP-38-04-12P	-8.99	4604.96	205.24	271	512	2167.57
BLHP-38-04-12P	-8.69	4102.43	222.35	226	472	2138.13
BLHP-38-04-12P	-8.94	3658.30	256.55	165	409	2182.46
BLHP-38-04-12P	-9.04	3264.30	290.76	117	361	2206.34

Motor Name	Slope	y-intercept	Torque Constant	Min RPM	Max RPM	Max Torque
BLHP-38-04-12P	-8.87	2591.47	359.17	43	292	2209.85
BLHP-38-04-12P	-9.02	2309.01	410.48	7	256	2245.87
BLHP-38-03-12P	-4.71	3045.74	162.64	319	646	1541.73
BLHP-38-03-12P	-4.81	2717.34	185.87	240	565	1563.07
BLHP-38-03-12P	-4.82	2420.06	209.11	176	502	1571.59
BLHP-38-03-12P	-4.77	2157.06	232.34	123	452	1570.07
BLHP-38-03-12P	-4.89	1919.88	267.19	66	393	1597.46
BLHP-38-03-12P	-4.91	1709.36	302.04	20	348	1611.12
BLHP-38-01-12P	-1.67	960.14	182.98	42	574	889.89
BLHP-29-13-12P	-15.23	8252.63	193.6	350	542	2923.44
BLHP-29-13-12P	-16.26	7349.18	232.33	264	452	3056.74
BLHP-29-13-12P	-16.90	6541.32	271.05	201	387	3143.89
BLHP-29-13-12P	-17.18	5825.08	309.77	153	339	3196.06
BLHP-29-13-12P	-17.07	4624.69	387.21	82	271	3225.34
BLHP-29-13-12P	-16.82	4138.22	425.93	55	246	3213.01
BLHP-29-13-12P	-15.76	3279.11	503.37	8	208	3152.99
BLHP-29-09-12P	-10.68	6813.96	164.33	429	638	2232.16
BLHP-29-09-12P	-11.10	6069.19	191.72	340	547	2296.75
BLHP-29-09-12P	-11.28	5403.10	219.11	272	479	2334.95
BLHP-29-09-12P	-11.31	4818.61	246.5	218	426	2352.75
BLHP-29-09-12P	-11.21	4294.32	273.89	173	383	2354.59
BLHP-29-09-12P	-11.00	3829.50	301.28	135	348	2343.92
BLHP-29-09-12P	-10.66	3399.88	328.66	101	319	2323.43
BLHP-29-09-12P	-11.30	2700.99	438.22	24	239	2429.76
BLHP-29-07-12P	-8.37	4931.62	178.35	362	589	1900.64
BLHP-29-07-12P	-8.44	4412.53	200.65	296	523	1915.19
BLHP-29-07-12P	-8.33	3924.70	222.94	241	471	1916.52
BLHP-29-07-12P	-7.94	3113.32	267.53	154	392	1890.23
BLHP-29-07-12P	-8.27	2778.13	312.12	101	336	1943.04
BLHP-29-07-12P	-8.41	2471.35	356.71	59	294	1975.4
BLHP-29-06-12P	-5.86	3705.19	166.09	367	632	1553.6
BLHP-29-06-12P	-6.38	3295.99	203	260	517	1638.43
BLHP-29-06-12P	-6.20	2936.50	221.45	212	474	1623.13
BLHP-29-06-12P	-5.98	2618.62	239.9	170	438	1602.26
BLHP-29-06-12P	-6.15	2332.46	276.81	113	379	1637.03
BLHP-29-06-12P	-6.20	2078.63	313.72	68	335	1656.7
BLHP-29-06-12P	-6.19	1850.35	350.63	30	299	1664.7
BLHP-29-05-12P	-5.03	3205.11	164.95	362	637	1383.68
BLHP-29-05-12P	-4.88	2848.03	179.94	303	584	1370.37
BLHP-29-05-12P	-4.71	2539.54	194.94	252	539	1352.22
BLHP-29-05-12P	-4.85	2262.92	224.93	182	467	1381.01
BLHP-29-05-12P	-4.90	2019.29	254.92	127	412	1396.84
BLHP-29-05-12P	-4.87	1797.08	284.91	81	369	1402.6

Motor Name	Slope	y-intercept	Torque Constant	Min RPM	Max RPM	Max Torque
BLHP-29-05-12P	-4.88	1424.29	359.89	0	292	1424.29
BLHP-29-04-12P	-3.12	1916.44	171.49	267	614	1083.07
BLHP-29-04-12P	-3.17	1712.58	194.36	195	541	1095.29
BLHP-29-04-12P	-3.15	1524.84	217.23	135	484	1099.52
BLHP-29-04-12P	-3.10	1357.96	240.09	84	438	1097.53
BLHP-29-04-12P	-3.16	1210.55	274.39	30	383	1115.73
BLHP-29-02-12P	-1.68	1092.00	162.02	188	649	775.67
BLHP-29-02-12P	-1.71	973.43	185.17	109	568	786.63
BLHP-29-02-12P	-1.72	867.33	208.32	44	505	791.76
BLHP-24-11-12P	-6.09	3564.09	179.36	333	585	1535.3
BLHP-24-11-12P	-5.62	2819.16	209.26	236	502	1493.82
BLHP-24-11-12P	-5.72	2510.42	239.15	173	439	1521.12
BLHP-24-11-12P	-5.75	2243.04	269.05	123	390	1535.62
BLHP-24-11-12P	-5.68	1994.87	298.94	80	351	1540.2
BLHP-24-11-12P	-5.57	1776.58	328.83	43	319	1537.1
BLHP-24-08-12P	-3.92	2399.00	171.53	314	612	1168.14
BLHP-24-08-12P	-3.93	2136.52	192.97	244	544	1178.23
BLHP-24-08-12P	-3.88	1902.63	214.41	186	490	1180.41
BLHP-24-08-12P	-3.82	1699.67	235.86	137	445	1176.4
BLHP-24-08-12P	-3.71	1512.31	257.3	93	408	1167.59
BLHP-24-08-12P	-3.84	1344.70	300.18	37	350	1202.55
BLHP-24-06-12P	-2.62	1693.72	161.91	301	647	905.76
BLHP-24-06-12P	-2.56	1507.32	178.1	236	588	902.34
BLHP-24-06-12P	-2.49	1343.91	194.29	180	539	895.11
BLHP-24-06-12P	-2.59	1195.81	226.68	106	462	921.45
BLHP-24-06-12P	-2.64	1064.68	259.06	48	404	938.18
BLHP-24-05-12P	-2.12	1321.49	169.48	240	622	811.59
BLHP-24-05-12P	-2.05	1177.26	183.6	183	574	801.93
BLHP-24-05-12P	-2.10	1047.63	211.85	108	498	820.43
BLHP-24-05-12P	-2.13	933.53	240.09	48	439	831.46
BLHP-24-04-12P	-1.44	920.51	164.49	187	639	651.13
BLHP-24-04-12P	-1.45	819.46	186.42	110	564	659.64
BLHP-24-04-12P	-1.45	729.99	208.36	46	505	663.5
BLHP-20-12-8P	-2.87	1850.31	163.06	314	644	948.14
BLHP-20-12-8P	-2.82	1649.60	179.36	250	585	944.64
BLHP-20-12-8P	-2.75	1472.96	195.67	195	536	937.09
BLHP-20-12-8P	-2.85	1309.10	228.28	121	460	964.75
BLHP-20-12-8P	-2.91	1168.23	260.89	64	402	982.24
BLHP-20-12-8P	-2.74	1038.45	277.2	28	379	961.73
BLHP-20-08-8P	-1.55	986.21	173.82	199	638	678.6
BLHP-20-08-8P	-1.55	877.29	195.55	124	567	685.43
BLHP-20-08-8P	-1.61	782.12	228.14	47	486	706.48

Table C-1: Selected Motor Database

This database was imported into a MATLAB Script to find a motor that matches the input propeller speed and torque. The script with the output for the desired propeller (300 rpm, 902.28 mNm torque) is found below.

```
clear all;
close all;
clc;

[ndata, text, alldata]=xlsread('Motor Selection 98.xls','11V');

Torque=902.28;  %Input Torque in mNm
RPM=300;        %Input Speed in rpm

y=1;
for x=2:209
    if Torque<=alldata{x,12}
        if alldata{x,10}<=RPM<=alldata{x,11}
            TorqueTest=(alldata{x,7}*RPM)+alldata{x,8};
            error=(abs(TorqueTest-Torque)/Torque)*100;
            if error<=5
                fitdata(y,1)=x;
                fitdata(y,2)=alldata{x,2};
                fitdata(y,3)=TorqueTest;
                fitdata(y,4)=TorqueTest/alldata{x,9};
                y=y+1;
            end
        end
    end
end

for x=1:y-1
    fprintf('Motor %s will work with a no load speed of %d and current
of %4.2f Amps\n',...
        alldata{fitdata(x,1),1},fitdata(x,2),fitdata(x,4));
end
```

Output:

Motor BLOV-29-14-4P will work with a no load speed of 401 and current of 3.58 Amps

Motor BLOV-29-13-12P will work with a no load speed of 375 and current of 3.19 Amps

Motor BLOV-29-09-12P will work with a no load speed of 405 and current of 3.35 Amps

Motor BLOV-29-07-12P will work with a no load speed of 434 and current of 3.61 Amps

Motor BLOV-29-06-12P will work with a no load speed of 494 and current of 4.41 Amps

Motor BLOV-29-04-12P will work with a no load speed of 635 and current of 5.18 Amps

Motor BLHP-29-09-12P will work with a no load speed of 383 and current of 3.40 Amps

Motor BLHP-24-06-12P will work with a no load speed of 647 and current of 5.61 Amps

Appendix D – Selected Motor Information

The tables and figures below were taken directly from the SL Montevideo Technology Inc. website ("SL Montevideo Technology," n.d.). The selected motor is the BLOV-29-13-12P Motor with a no load speed of 375 rpm and a running voltage of 11 VDC.

Size Parameters (Approximate)

PARAMETER	UNITS	VALUE
Number of Poles	P	**12**
Thermal Resistance, t_r	°C/W	**1.2**
Max. Continuous Stall Torque, T_{cs}	mN-m	**3078.5**
Motor Constant, K_m	mN-m/$W^{1/2}$	**397.59**
Hysteresis Drag Torque, T_f	mN-m	**87.56**
Viscous Damping	mN-m/RPM X 10^{-5}	**64.26**
Detent Torque, T_{fmax}	mN-m	**220.32**
Inertia, Sensorless, J_m	g-cm^2	**2081.27**
Inertia, w/halls, J_m	g-cm^2	**2174.79**
Weight, housed, W	g	**3115.61**
Weight, frameless, W	g	**2636.51**

Table D-1: Size Parameters for Selected Motor

Winding Data at 11 VDC (Approximate)

PARAMETER	UNITS	VALUE
Torque Constant, K_t	mN-m/A	280.28
Voltage Constant, K_e	V/kRPM	29.35
No Load Speed, NLS	RPM	375
Electrical Time Constant, t_e	mS	2.3
Mechanical Time Constant, Sensorless, t_m	mS	1.28
Mechanical Time Constant, w/Halls, t_m	mS	1.38
Resistance at 25°C, R_m	Ohm	0.5
Inductance, L_m	mH	1.14
Max. Continuous Power Output at 100°C Rise	W	38.6
Max. Continuous Torque Output at 100°C Rise	mN-m	3000.07
Max. Continuous Speed Output at 100°C Rise	RPM	123

Table D-2: Winding Data for Selected Motor

Continuous Duty Capability (Approximate)

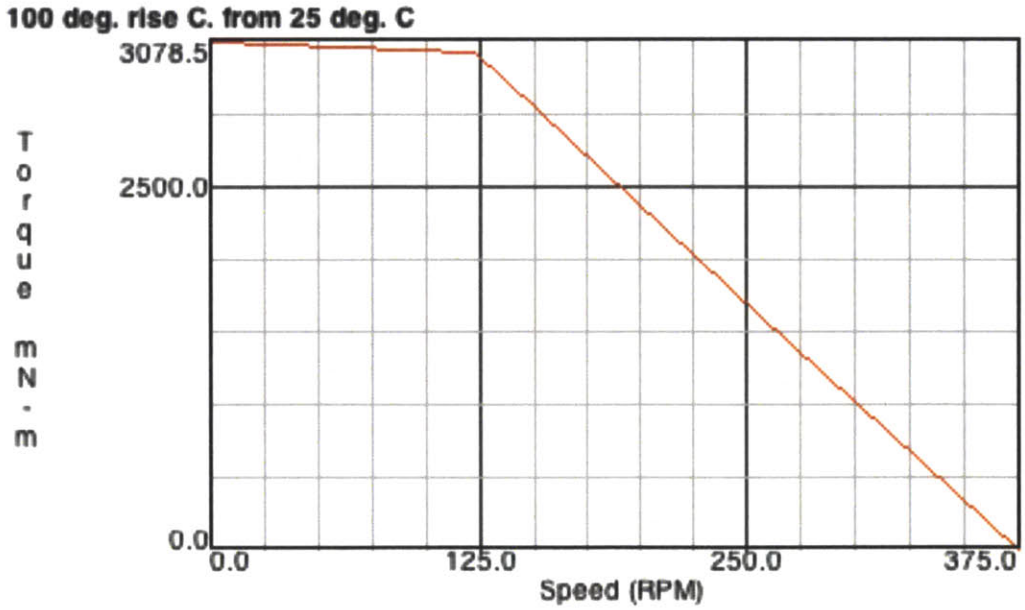

Figure D.1: Speed Torque Curve for Selected Motor

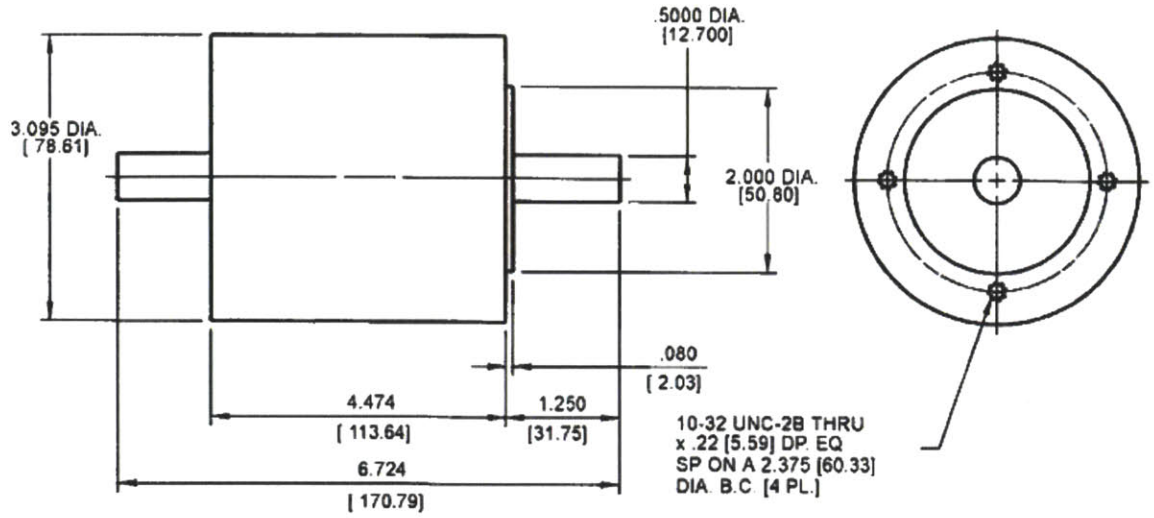

Figure D.2: Selected Motor Technical Drawing

Appendix E – Battery Information

Below is the information provided by Panacis Inc. on their Modular Lithium Battery System. It must be noted that this information is for the NCM -111 Cathode, as opposed to the NCM -622 as described in Chapter 7. The sizes and dimensions of the battery stay the same, but the capacity increases from 75 Ah per battery to 90 Ah per battery.

Feature	Value	Comment
Capacity	75Ah	
Voltage (range)	11.1V (9.6 – 12.6V)	Battery will tolerate higher voltage on terminals without damage
Energy	832Wh	
Cycle Life (100% DOD)	1500 cycles	Room temperature, 0.5C charge, 0.1C discharge, 20% acceptable capacity degradation at end of test.
Weight	6kg	Approximate value +/- 20%
Connections	+Charge, +Load, Ground	Charger and Load must be connected to separate terminals
Parallel Expandability	Infinite	Packs can be wired in parallel to increase system capacity
Serial Expandability	None	Packs cannot be wired in series to increase voltage
Maximum Discharge Current	20 amps	Pack includes circuitry to switch off output for various over-current and time combinations
Maximum Charge Current	20 amps recommended, 40 amps max (system)	When used in a system configuration, total current on the charge bus should be limited to 40 amps
Temperature Range (Discharge)	-20 to +50C	Higher temperatures will affect cycle life, system will operate at lower temperatures, consult factory for details
Temperature Range (Charge)	0 to +50C	Battery includes circuitry to automatically disable charging when too hot or cold. Battery will simply cease to accept a charge. Charging to -20C is available on request under certain use conditions.

Table E-1: Characteristics of Panacis Inc. Modular Lithium Battery System (Each Battery)

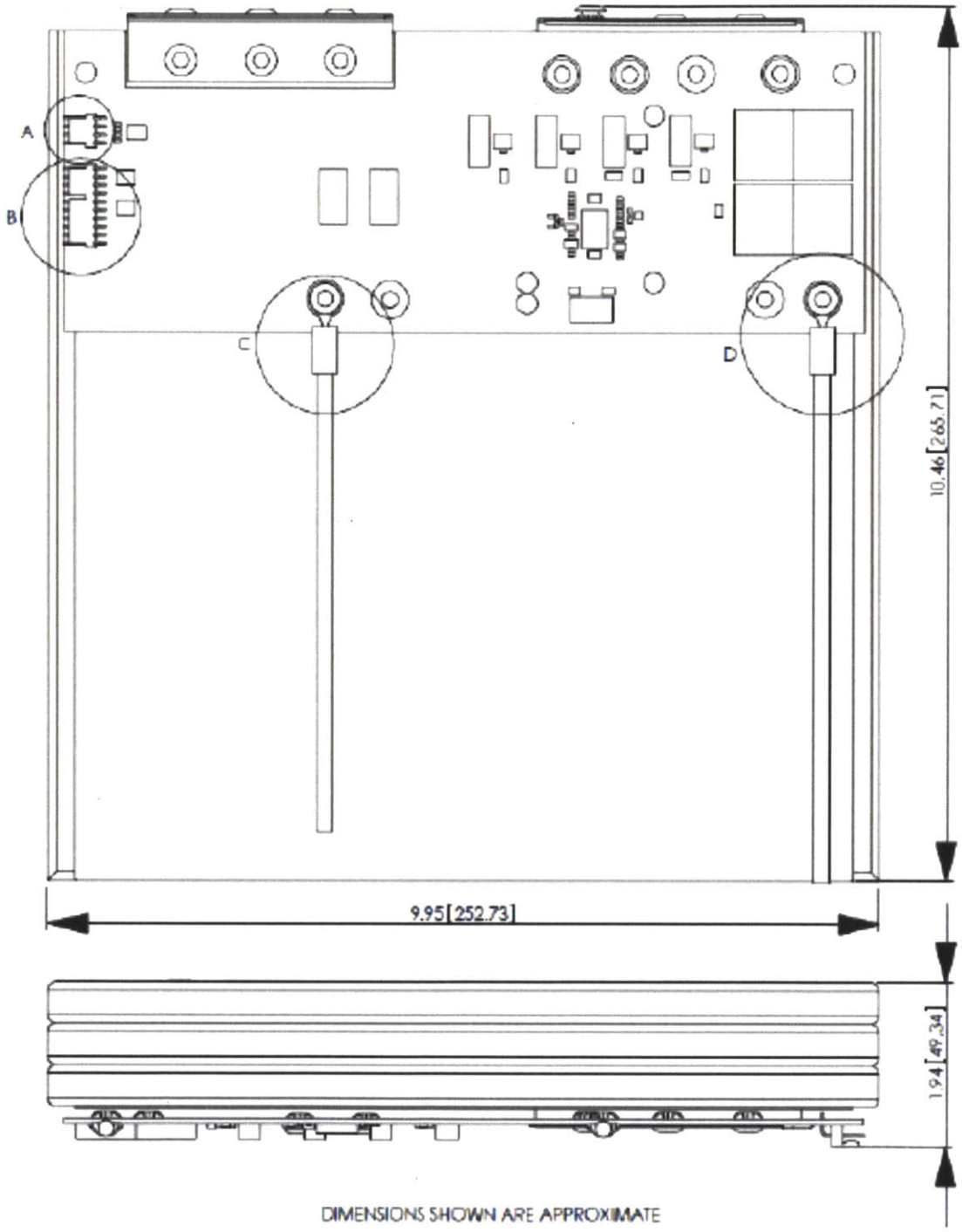

Figure E.1: Dimensions of Panacis Inc. Modular Lithium Battery System

Appendix F – MATLAB Distance Calculator

Below is the script written to determine the distance travelled by SPYROS depending on the number of batteries, number of charging cycles and hotel load. This script will also output the sizing of the power generation system and will determine the distance travelled by SPYROS if the generator and fuel tanks were replaced with more batteries.

```
clear all;
close all;
clc;

%User Inputs
nbatt=8;                    %Number of Batteries, should be multiple of
4
hotload=8;                %Hotel Load, in Watts
ncharge=6;                  %Number of Battery charges during voyage
DOD=90;                     %Battery Depth of Discharge
FuelBuf=10;                 %Fuel Buffer, in percent
depth=1000;                 %AUV Operating Depth, in m
angle=15;                   %Angle of Dive and Ascent, in degrees

%Constants
speed=2;                                    %AUV Speed, in kts
battC=90;                                   %Capacity of each battery, in
Ah
propI=3.19;                                 %Current required for
propulsion, in Amps
V=11;                                       %System voltage
FuelCons=0.01;                              %Fuel Consumption in L/min
GenL=0.7;                                   %Length of Generator (currently
assumed), in m
BatLength=0.26571;                          %Length of single battery, in m
FuelXArea=0.058;                            %Cross Sectional Area of Fuel
Tank in m^2
Icharge=1000/12.6;                          %Charging Current, in Amps

%Time Calculations

Itot=propI+(hotload/V);                 %Total Current (Prop plus hotel)
Ctot=battC*nbatt;                       %Total Capacity, in Ah

%Initial Discharge Calcs
SingleTime=(Ctot/Itot)*(DOD/100);           %Time for selected DOD of
battery, in h

%Charging Calcs
Tcharge=(Ctot/(Icharge-Itot))*(DOD/100);                    %Time for
single charge, in h
Tchargetot=Tcharge*ncharge;                                 %Total
```

```
Charging Time, in h
Fueltot=(1+(FuelBuf/100))*FuelCons*(Tchargetot*60);       %Total Fuel
consumed, in L, with buffer

%Hull Length Calcs
FuelL=(Fueltot/1000)/FuelXArea;     %Length of Fuel Tank, in m
BattL=(nbatt/4)*BatLength;          %Length of Battery required, in m
Ltot=FuelL+BattL+GenL;              %Total Hull Length required, in m

%Battery replacement Calcs
nRepBat=floor((FuelL+GenL)/BatLength)*4;    %Num of replacement
batteries
TimeRepBat=((battC*(nbatt+nRepBat))/Itot);  %Time w just batteries


%Required Graphs
runtime=floor(SingleTime);
chargetime=ceil(Tcharge);

mdis=(100-(100-DOD))/(0-runtime);
mcharge=((100-DOD)-100)/(0-chargetime);

for x=1:(ncharge+1)
    if x==1
        b=100;
        for y=1:runtime
            hour(y)=y-1;
            charge(y)=(mdis*hour(y))+b;
        end
    else
        bcharge=(100-DOD)-(mcharge*(((x-1)*runtime)+((x-
2)*chargetime)));
        for y=(((x-1)*runtime)+((x-2)*chargetime)):...
                (((x-1)*runtime)+((x-1)*chargetime))
            hour(y)=y;
            charge(y)=(mcharge*hour(y))+bcharge;
        end
        bdis=100-(mdis*(((x-1)*runtime)+((x-1)*chargetime)));
        for y=((((x-1)*runtime)+((x-1)*chargetime))+1):...
                ((x*runtime)+((x-1)*chargetime))
            hour(y)=y;
            charge(y)=(mdis*hour(y))+bdis;
        end
    end
end

singleruntime=floor(TimeRepBat);
msingle=(100)/(0-floor(TimeRepBat));
for y=1:floor(TimeRepBat)
    hoursingle(y)=y-1;
    chargesingle(y)=(msingle*hoursingle(y))+100;
end

plot(hour,charge);
hold on;
grid on;
plot(hoursingle,chargesingle, 'red');
```

```
title('State of Battery Charge during Mission');
xlabel('Time (h)');
ylabel('% Charge');
ylim([0 100]);
legend('Batteries and Charger', 'Batteries and Replacement Batteries')

%Distance Calculations

angleDist=(depth*tand(90-angle))*0.00054;
angleSpeed=(0.75*speed)*cosd(angle);
angleTime=ceil(angleDist/angleSpeed);

surfaceSpeed=0.75*speed;
surfaceDist=surfaceSpeed*chargetime;

depthTime=runtime-(2*angleTime);
depthDist=speed*depthTime;

angleDistTotal=angleDist*((2*ncharge)+2);
surfaceDistTotal=surfaceDist*ncharge;
depthDistTotal=depthDist*(ncharge+1);

DistTotal=angleDistTotal+surfaceDistTotal+depthDistTotal;

%Distance Calculations - No charger

angleDistSingle=2*angleDist;

depthTimeSingle=singleruntime-(2*angleTime);
depthDistSingle=speed*depthTimeSingle;

DistTotalSingle=angleDistSingle+depthDistSingle;


%OUTPUTS
fprintf('Total Number of batteries: %1.0f\n', nbatt);
fprintf('Hotel Load: %4.2f W\n', hotload);
fprintf('Total Distance Travelled with %2.0f percent DOD and %2.0f
charges: %4.2f nm\n', ...
    DOD, ncharge, DistTotal);
fprintf('\nTotal Fuel Tank Length: %4.2f m\n', FuelL);
fprintf('Total Battery Length: %4.2f m\n', BattL);
fprintf('Total Power Section Length: %4.2f m\n', Ltot);
fprintf('\nReplace Generator and Fuel Tank with Batteries\n');
fprintf('Total number of replacement batteries: %2.0f\n', nRepBat);
fprintf('Total distance with only batteries: %4.2f nm\n',
DistTotalSingle);
```

Output:

Total Number of batteries: 8

Hotel Load: 8.00 W

Total Distance Travelled with 90 percent DOD and 6 charges: 2363.21 nm

Total Fuel Tank Length: 0.59 m

Total Battery Length: 0.53 m

Total Power Section Length: 1.82 m

Replace Generator and Fuel Tank with Batteries

Total number of replacement batteries: 16

Total distance with only batteries: 1098.03 nm

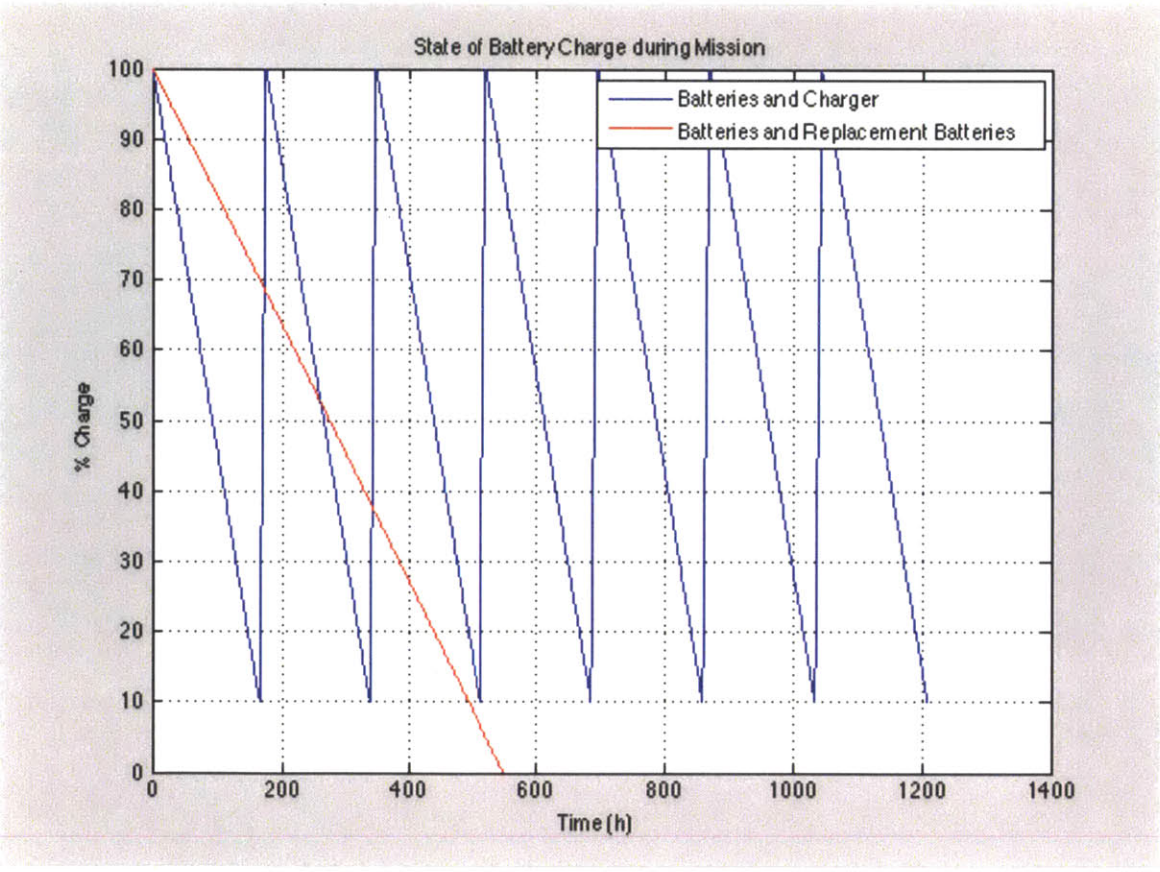

Figure F.1: State of Battery Charge during Mission